Strength Properties of Wood and Wood-Based Materials

9

Peter Niemz, Walter Sonderegger, Per Johan Gustafsson, Bohumil Kasal, and Tiberiu Polocoşer

Contents

Per Johan Gustafsson: deceased.

P. Niemz (✉)
ETH Zürich, Wood Physics (today Wood Material Science), Institute for Building Materials, Zurich, Switzerland
e-mail: niemzp@retired.ethz.ch

W. Sonderegger
Swiss Wood Solutions AG, Altdorf, Switzerland
e-mail: sonderegger@swisswoodsolutions.ch

P. J. Gustafsson
Deceased, former Division of Structural Mechanics, Lund University, Lund, Sweden

B. Kasal
Fraunhofer Institute for Wood Research, Wilhelm-Klauditz-Institut WKI, Braunschweig, Germany
e-mail: kasalb@tu-bs.de; bohumil.kasal@wki.fraunhofer.de

T. Polocoşer
Magnusson Klemencic Associates, Seattle, WA, USA
e-mail: polocose@gmail.com

Abstract

Knowledge of the strength of wood and wood-based materials is an important basis for the calculation and dimensioning of wooden products. This chapter describes the basics of the strength properties, test methods, important influencing parameters (e.g., moisture content, load direction, type of load, duration of load, speed of loading). Phenomenological aspects of failure on various structural levels, fracture mechanical properties as well as essential test methods such as tension, compression, shear strength, bending, torsion, and cleavage are also described. An overview is given of test specifications, strength properties of wood, and wood-based materials depending on the type of load and the direction of loading. Hardness, wear resistance, and other methods are also described. In addition to static

P. Niemz et al. (eds.), *Springer Handbook of Wood Science and Technology*,
https://doi.org/10.1007/978-3-030-81315-4_9

load in short-term tests, impact resistance and fatigue as well as the influence of load duration in the static long-term test are described. In addition, selected results of the first studies to determine the properties of the molecular structure are briefly described.

Keywords

Bending strength · Compression strength · Fatigue · Fracture mechanics · Hardness · Impact bending · Shear strength · Tensile strength

9.1 Overview

The strength is the stress that is calculated from the maximum force at failure or from another defined strain (e.g., at 2% strain by pressure perpendicular to the fiber).

Depending on the load speed, a distinction is made between:

- Static strength (the failure of the test specimen is caused by a slowly rising load)
- Dynamic strength (the fracture is induced by a transient load, e.g., impact bending, or an alternating, accelerate cycling, load, e.g., Wöhler test)

Depending on the direction (longitudinal, radial, tangential) or type of force, strength is distinguished in:

- Tensile strength (and breaking length)
- Compressive strength
- Bending strength
- Shear strength
- Splitting strength (cleavage)
- Torsional strength

The strength properties further include nail and screw pull-out resistance as well as hardness and abrasion resistance.

The properties of wood and wood-based materials are subject to great variability (for example, the influence of growth conditions and the climate). Therefore, in practical use, e.g., in timber construction, safety factors S (old concept) or, in particular, characteristic properties are calculated (e.g., EN 1995-1-1, Eurocode 5). The following applies:

$$S = \frac{\text{ultimate stress}}{\text{existing stress}} \leq \frac{\text{ultimate stress}}{\text{allowed max .stress}} \qquad (9.1)$$

For wood in general, safety factors of 2–10 are expected; for visually or mechanically sorted wood a safety factor of 4 is sufficient. In contrast, in the relevant literature on wood physics only mean values are calculated including standard deviation and/or the coefficient of variation where appropriate. In the literature regarding timber construction, characteristic values are commonly listed. Usually, the existence of a normal distribution is assumed, although other distributions, such as the Pearson distribution, may be present under special loads [1]. A listing of different distributions is shown in Table 9.1.

In timber construction, characteristic values determined on boards or squared timber are calculated (see, for example, EN 408). Owing to knots, fiber shape, density fluctuations, etc., the properties are not comparable with those determined on small clear samples. The evaluation of these characteristics is a specific field of research in civil engineering (see, for example, Glos, Finkler, Denzler, and Neuhaus [3–6]).

Tables 9.7 and 9.8 show the characteristic values for wood and wood-based materials when used in building construction (EN 1995, Eurocode 5). In furniture-making, however, furniture elements and furniture collections are dimensioned according to their permissible deformation.

Characteristic Values

In construction, the so-called 5% fractile (or characteristic value) is usually used (Fig. 9.1). With the additional use of safety factors, so-called design values are calculated (see, for example, EN 1995-1-1, Eurocode 5).

Table 9.1 Distribution functions for wood properties [2], supplemented for vibration tests and fracture toughness by Scheffler [1]

Attribute	Distribution
Moisture content	Normal (Gauss)
Density	Normal (Gauss)
Module of elasticity	Normal (Gauss)
Module of elasticity (vibration test)	Pearson
Sound velocity	Normal (Gauss)
Strength	Log-normal (two-dimensional)
Volume	Weibull
Fracture toughness	Weibull

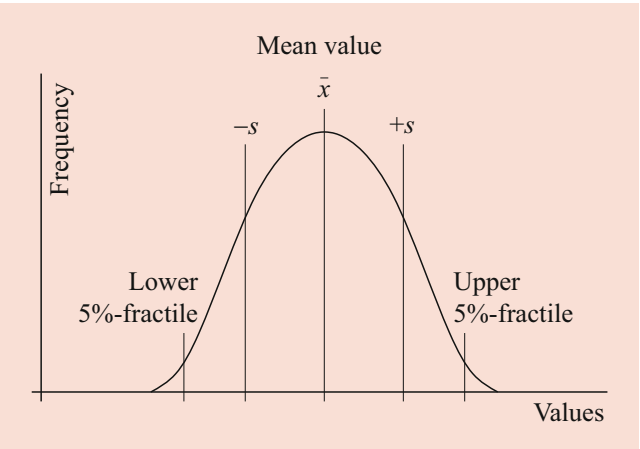

Fig. 9.1 Mean value, standard deviations s, and 5% fractiles

For the coefficient of variation of the properties, the following reference values apply (for tensile loads):

- Small clear specimens, without defect, 20%
- Visually graded wood, 40%
- Plywood, 18%
- Particle boards (oriented strand board, OSB), 12%
- Medium-density fiberboard (MDF), 8%

Symbols
Different symbols are used for strength:

- f: primarily in timber construction, e.g., f_c – compression, f_m – bending, f_t – tension, f_V – shearing [6]
- R: primarily for metals
- σ: common in mechanics, where the load type (b – bending, t – tension, c – compression) is used as the first index and the state (U – ultimate load or breaking load, P – proportionality limit) as the second index
- τ: for shear strengths in mechanics

Subsequently, σ and τ are used. When citing characteristic values according to the timber construction standards, the usually applied f is used.

9.2 Important Influencing Factors

The main factors influencing the strength of wood and wood-based materials are (analogous to those of the elastic properties, ▶ Chap. 8):

- Wood structure
- Climatic conditions
- Aging
- Load prehistory (mechanical and climatic)
- Testing method

The influence is almost the same, regardless of the type of strength.

9.2.1 Wood Structure

Grain and Growth-Ring Orientation

Wood is an orthotropic material (see ▶ Chap. 6). Similar to the elastic properties, the strength properties are direction dependent both for solid wood and for wood-based materials. The strength σ of solid wood acts in the three main axes (L – in fiber direction (longitudinal), R – radial, T – tangential) as follows:

$$\sigma_L \gg \sigma_R > \sigma_T \tag{9.2}$$

Therefore, grain and growth-ring orientation decisively influence the strength properties and also the elasto-mechanical and rheological properties of wood. High loads can be absorbed in the case of solid wood only parallel to the fiber. As the grain angle increases, the strength and modulus of elasticity decreases. Even slight deviations from the fiber orientation cause a significant decrease in wood strength (Fig. 9.2a).

Figure 9.2b shows the influence of the growth-ring orientation (angle between the radial and tangential directions). Radial strength is greater than tangential strength, the

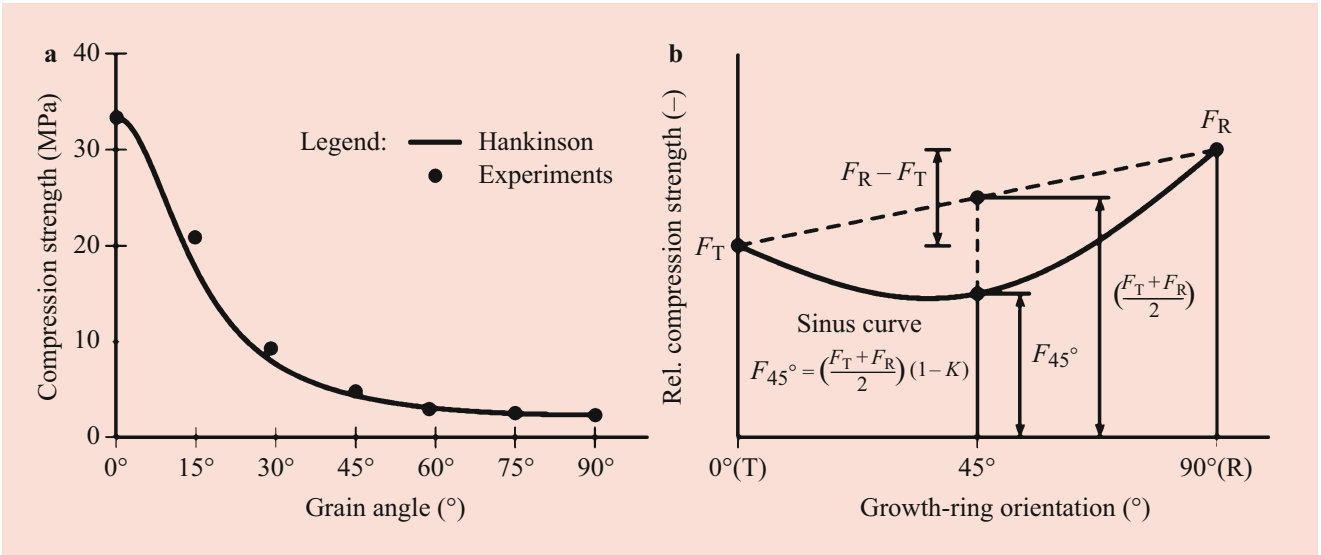

Fig. 9.2 Influence of (**a**) grain angle (LR: Longitudinal (0°) to radial (90°), LT: Longitudinal (0°) to tangential (90°)) and (**b**) growth-ring orientation (TR: Tangential (0°) to radial (90°)) on wood strength [7]

minimum is at about 45°. The growth-ring orientation should also be taken into account in bending tests on small, defect-free samples (for example, load in the case of bending is usually carried out in a tangential or radial direction, ISO 13061-3:2014).

Strength properties of wood-based materials are distinguished in properties parallel to the plane (sometimes further distinguished in properties parallel and perpendicular to the production direction) and perpendicular to the plane and are influenced by the fiber orientation of the elements (layers, particles).

Generally, uniaxial stress is still used in practice. But the characteristic values of wood and wood-based materials in all main axes are increasingly required for finite element calculations of elasticity as well as strength.

Density and Growth Rings

The density of wood and wood-based materials has a dominant influence on strength properties. The density allows a first, rough estimate of the strength (Figs. 9.3, 9.4, and 9.5). As the density increases, the strength increases linearly. This is because the applied force is transferred with increasing density to an effectively larger, supporting cross section (void fraction decreases). The density correlation with strength applies both within one type of wood and between the types of wood. The influence of the average density of 103 wood species on selected properties is compiled in Niemz and Sonderegger [8].

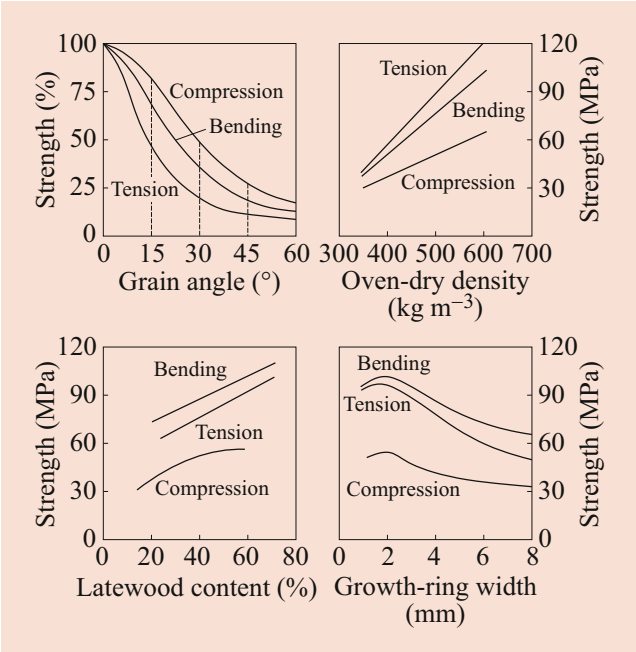

Fig. 9.3 Main structural factors influencing various properties of Douglas fir [9]

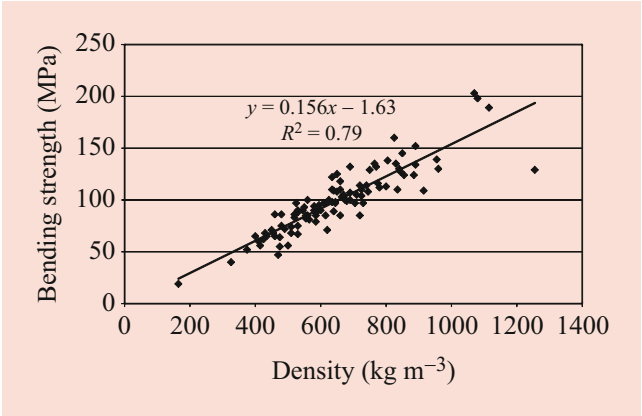

Fig. 9.4 Relationship between density and bending strength using material parameters from the literature on 103 wood species [8]

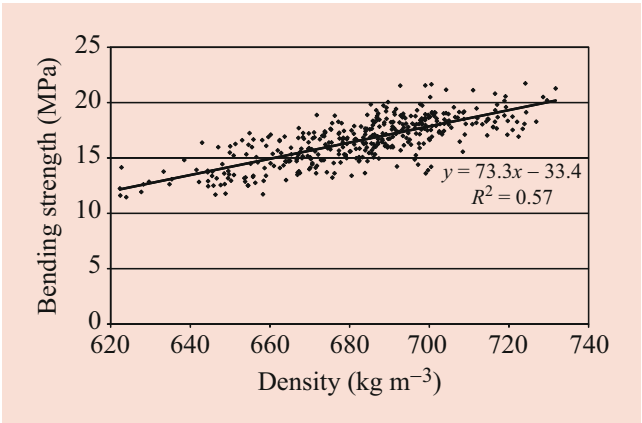

Fig. 9.5 Correlation between density and bending strength of particle board. (Measurements: ETH Zurich)

Wood strength increases with increasing latewood content. For softwood, there is a good correlation between latewood content and strength (Fig. 9.3). Growth-ring width is a less reliable benchmark, especially for softwood. Growth factors such as soil, exposition, and sea level are superimposed on the growth-ring width.

Knots/Notches/Compression Wood/Chemical Composition

Knots have a higher bulk density than the surrounding wood (in hardwood 5–6% higher, in softwood by investigations of [10] up to 150% higher) and cause a change in fiber orientation close to the knots. Owing to occurring stress peaks, wood failure mostly takes place near branches. As the knot-area ratio (KAR value) increases, the tensile strength of the wood decreases (Fig. 9.6); in the same way the compressive and bending strength and the modulus of elasticity of the wood are influenced.

Defects as well as notches (or breakthroughs in beams) affect strength. Investigations are described in Kollmann [11]

for solid wood and in Niemz and Bekhta [12] for wood-based materials. The following applies for the notch strength under tensile load [11, 13]:

$$\sigma_N = \frac{F_{max}}{A_N} = \alpha_N \cdot \sigma_{tb} \quad (9.3)$$

σ_N – Notch strength (ultimate tensile stress of a notched specimen) (Pa)
F_{max} – Maximum load (N)
A_N – Area of the cross-section without notches (m^2)
α_N – Notch factor (−)
σ_{tb} – Tensile strength of the intact cross-section (without notches) (Pa)

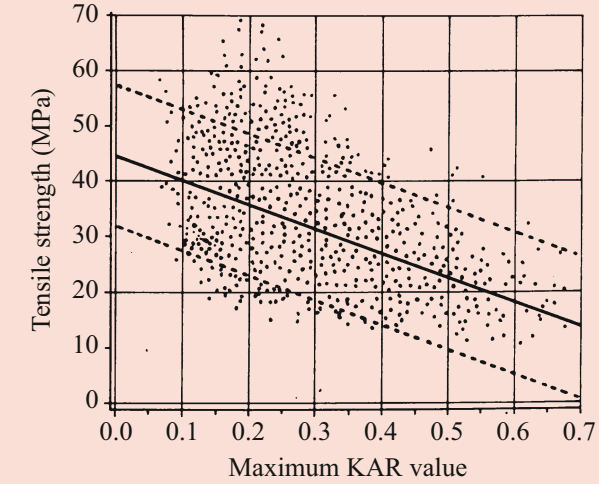

Fig. 9.6 Influence of the knot area ratio (KAR value) on the tensile strength of softwood [10]

Trendelenburg [14] has shown that the quality factor $\frac{\sigma_{cb}}{100 \times R}$ (σ_{cb} – compression strength in grain direction, R – specific gravity) increases linearly with the lignin content (Fig. 9.7). Resin pockets do not influence the crushing strength [13].

Compression wood has higher compressive and flexural strength than normal wood owing to its changed structural design, which induces considerably higher density (Table 9.2). But flexural strength in relation to density decreases with increasing percentage of compression wood [15]. The breakage at bending load for compression wood is short-fibered.

Like solid wood, the strength properties of wood-based materials are influenced by their structural design. The important structural parameters for particle boards are density, density profile, particle geometry, and solid resin content. The coefficient of variation of the properties of wood-based materials is much lower than that of solid wood. This is due to homogenization, which occurs in the production of wood-

Table 9.2 Properties of compression wood and normal wood (*Pinus ponderosa*) according to Timell [16]

Property	Normal wood	Compression wood
Density (kg m^{-3})	370	500
Bending strength (MPa)	68.9	82.0
Compression strength (MPa)	36.5	41.8

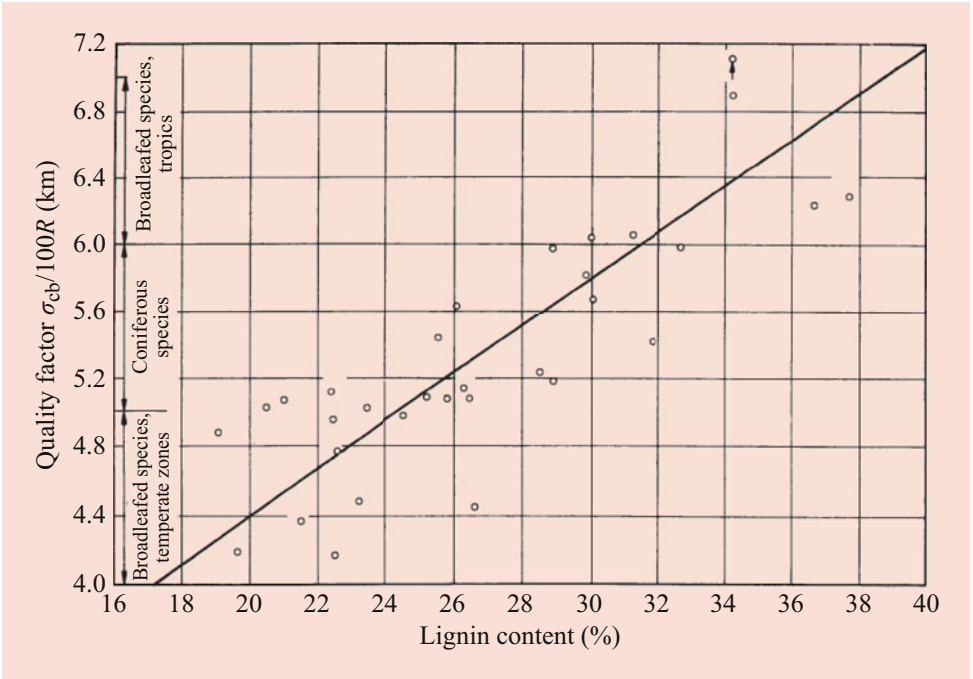

Fig. 9.7 Crushing strength to specific gravity (quality factor) in relation to lignin content for coniferous and broad-leafed wood grown in the temperate zones and in the tropics [14]

Table 9.3 Coefficient of variation *V* of some properties of wood and wood-based materials[a]

Tensile strength	*V* (%)	Bending strength	*V* (%)	Density	*V* (%)
Wood, small clear specimens	20	Wood, small clear specimens	6. . .21	Wood, small clear specimens	5. . .14
Wood, visually graded	40	Wood, visually graded	14.2	Wood, visually graded	9.7
Plywood	18	Plywood	9.3	Plywood	6.0
Particleboard (OSB)	12	Particleboard (OSB)	17.3	Particleboard (OSB)	9.0
MDF	8	MDF	8. . .10	MDF	2. . .6

OSB oriented strand board, *MDF* medium-density fiberboard
[a]See DIN 68364

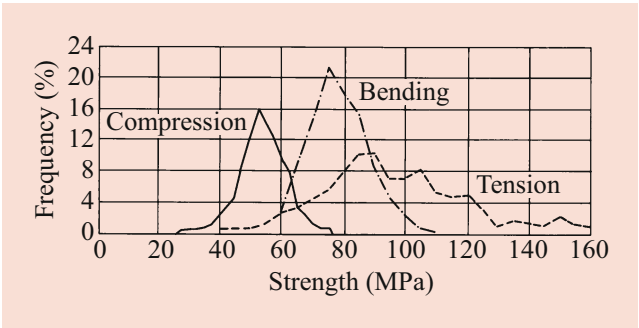

Fig. 9.8 Frequency distribution of the bending, compressive, and tensile strength of spruce. (H. Klemm cited in Kollmann [11])

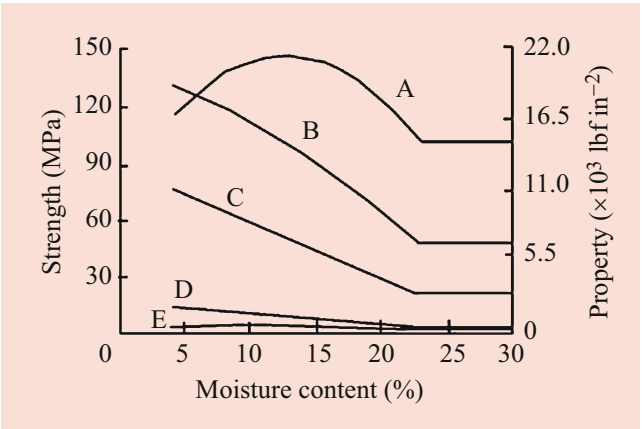

Fig. 9.9 Influence of moisture content on wood strength [17]. (**A**) Tension parallel to grain. (**B**) Bending. (**C**) Compression parallel to grain. (**D**) Compression perpendicular to grain. (**E**) Tension perpendicular to grain

based materials (Table 9.3). Also, the variation depends on the load type. Figure 9.8 shows the distribution of the strength properties of solid wood at different load types for small clear specimens. In static calculations, the property variations of wood and wood-based materials are taken into account by safety factors and increasingly by characteristic values (5% fractiles; Tables 9.1 and 9.3).

9.2.2 Climatic Conditions

As the moisture content of wood increases, the modulus of elasticity and strength decrease up to the fiber-saturation range. Above that range, the strengths are almost constant (Fig. 9.9). The fracture energy increases as the wood moisture increases. Wood in the so-called green state (moisture above fiber saturation) has significantly lower strengths than in a normal climate (Table 9.4). An overview is given in the Wood Handbook for most North American wood species [17].

Tensile and shear strength of wood initially increase within the moisture range 0 . . . 6% to 10% and then decrease until they reach fiber saturation. This effect can be attributed among others to a reduction of tensions between the cellulose molecules that occurs within the range of chemisorption. For wood-based materials, e.g., particle board, tensile strength and modulus of elasticity also decrease with increasing moisture content (Fig. 9.10). Hoffmeyer (cited in Neuhaus [6]) indicates, for example, following a change in the strength of solid wood per 1% change of moisture content (moisture range between 8 and 20%):

- Compression strength in fiber direction: 6%
- Compression strength perpendicular to the grain: 5%
- Bending strength: 4%
- Tensile strength parallel to the fiber: 2.5%
- Tensile strength perpendicular to the fiber: 2%
- Shear strength: 2.5%

Above 20% wood moisture, the relationship is no longer strictly linear. Property changes of European beech as a function of moisture content are listed in Table 9.4 [18].

An increase in temperature generally causes a decrease in strength and of the modulus of elasticity for both wood and wood-based materials (Figs. 9.11 and 9.12). For softwood in timber dimensions, Glos (cited in Neuhaus [6]) gives the following values of strength reduction per 10 °C temperature change, starting at +20 °C (moisture content 10–15%):

- Bending: 5%
- Compression: 5%
- Tension: 1%

In addition, the interaction between temperature and moisture content must be considered. As the moisture content increases, the temperature influence also increases. On the other hand, very low temperatures (within the negative range) lead to considerable embrittlement of the wood. This effect is

Table 9.4 Relative change (%) in Young's modulus and strength at different moisture levels of small clear samples of European beech compared with normal climate [18]

Property	Load	Relative property changes compared with normal climate (ω = 12%) at the three main directions for different moisture ranges					
		ω = 0–6%			Fiber saturation (ω = approx. 30%)		
		L	R	T	L	R	T
Modulus of elasticity	Tension	+37.6	+24.5	+13.7	−16.6	−59.6	−57.2
	Compression	+19.9	+42.1	+40.0	−29.8	−42.6	−38.3
	Bending	+8.0			−19.6		
Strength	Tension	+19.2	+13.8	+43.8	−25.4	−25.1	−31.0
	Compression	+91.5	+50.0	+41.4	−44.4	−45.5	−44.6
	Bending	+37.8			−36.1		

L longitudinal, *R* radial, *T* tangential

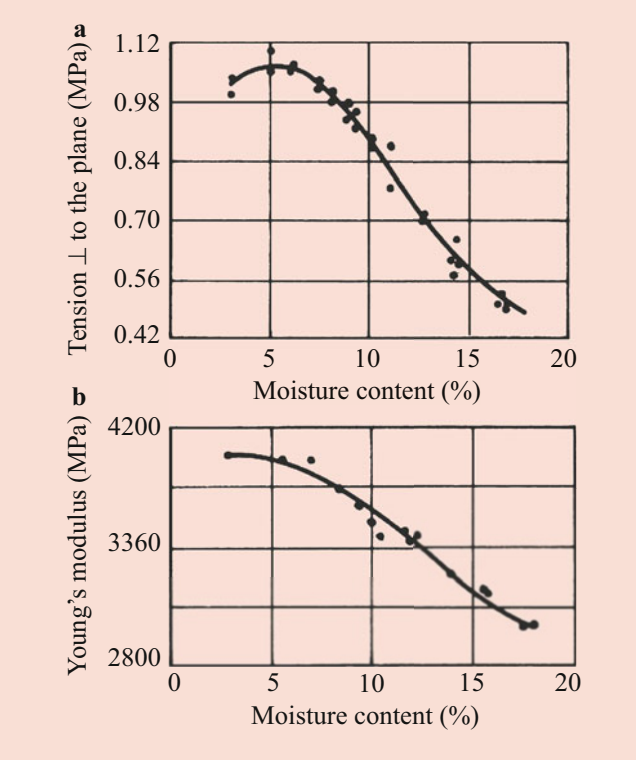

Fig. 9.10 Influence of moisture content on Young's modulus and tensile strength perpendicular to the plane of particle boards [19]

used, for example, in wood chipping (cutting force, chip geometry). The usual temperature fluctuations in practical use, especially indoors, are normally not considered for static calculations.

9.2.3 Aging

Under dry climatic conditions in the interior, properties of wood do not change or hardly change over the years (see Lexikon der Holztechnik and Sonderegger et al. [22, 23]). Nevertheless, a certain reduction in impact bending strength is to be found. For glued wood (glulam), the moisture resistance and the durability of the bond are important. Especially in a dry indoor climate, inappropriate bonds can lead to severe cracking but also to delamination of adhesive joints, in particular, if the average wood moisture is changed significantly by a strong change in humidity. For hardwood, this problem is more pronounced than for coniferous wood [24].

9.2.4 Previous History (Mechanical and Climatic)

The properties of wood and wood-based materials are significantly influenced by previous mechanical and climatic stress. Also, fungal or insect infestation affect the properties to some degree or other.

Fungus and Insect Damage

- The bending and compressive strength of spruce wood with horntail (wood wasp) or black spruce beetle decreases independently of other infestation features with the hole density (number of boreholes, based on the sample cross-section). The compressive strength is reduced by about 10% and the bending strength by up to 30% (Fig. 9.13)
- Blue-stain and red-striped wood do not affect the bending and tensile strength
- Wood-destroying fungi such as brown rot, white rot, and soft rot cause a significant loss of strength, whereby the fracture pattern changes:
  - Brown rot (degradation of polysaccharides, increase in relative lignin content): both strength and density decrease, the break is cubical
  - White rot (degradation of polysaccharides and lignin, thereby increasing the proportion of cellulose): the break is clean (short-fibered), and strength and density decrease
  - Soft rot (degradation of polysaccharides in the cell wall): impact strength is reduced, and there is little mass loss

Mass loss and loss of strength correlate at the first two types of fungus.

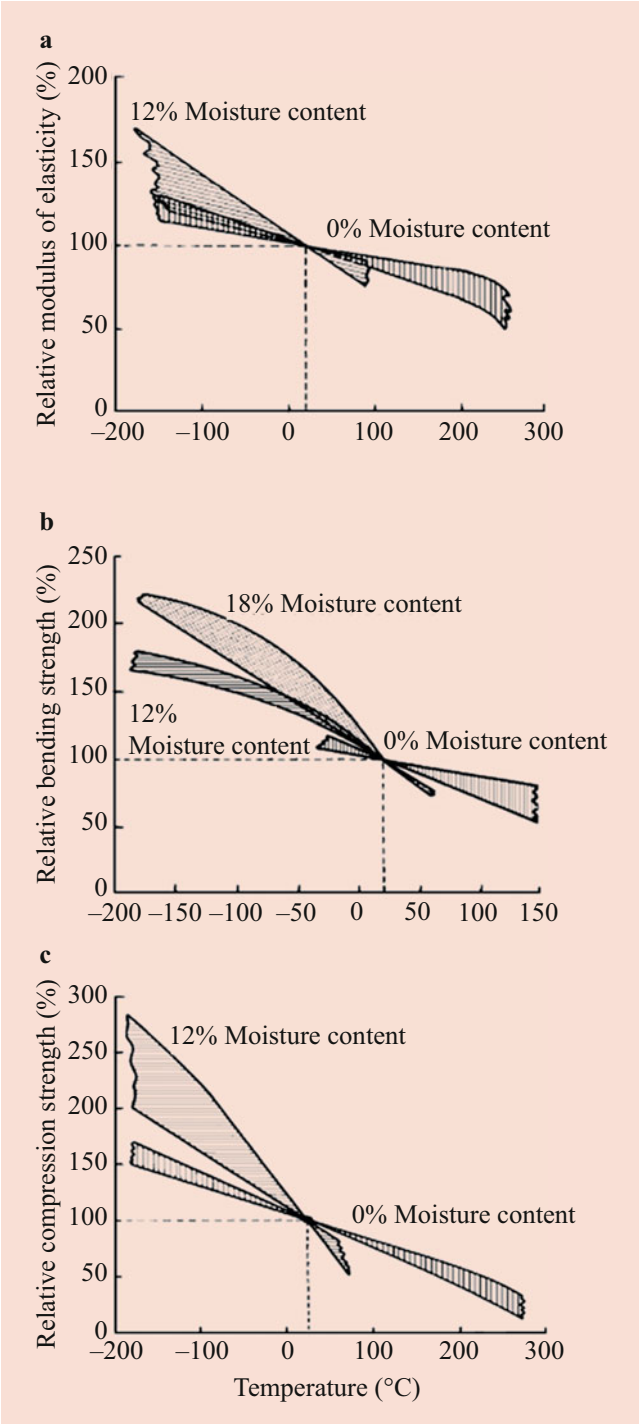

Fig. 9.11 Influence of temperature on selected properties of wood [17]

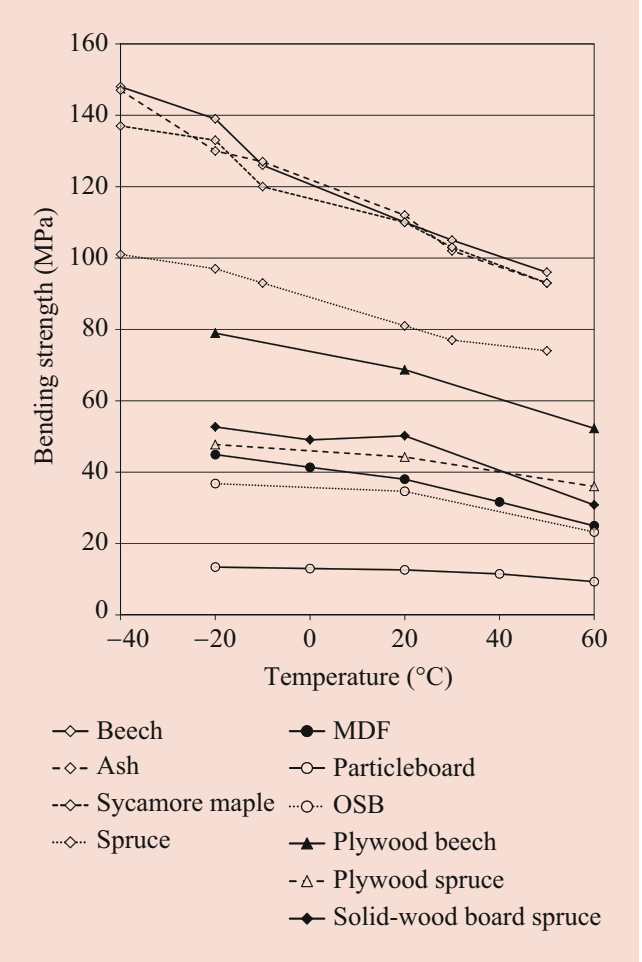

Fig. 9.12 Influence of temperature on the bending strength of wood and wood-based materials [20, 21]

Steaming and Thermal Treatment

The elasto-mechanical wood properties change during steaming. Modulus of elasticity, proportional limit, and strength are reduced; ductility, in particular, plastic stretching, is strongly increased [25]. Higher steaming temperatures combined with mass loss can lead to a reduction in the modulus of elasticity and the impact bending strength and also in the compressive strength after wood redrying [22, 25].

Thermal wood treatment partially results, depending on the process and the intensity of the treatment, in a significant reduction in hardness and strength, in particular, of impact bending strength (Sect. ▶ 6.3).

Compression Failures

Strong storms lead to compression failures (upsets, transverse or thunder shakes) in the standing tree, which cause damage or reduction of the mechanical properties. This wood cannot be used for statically highly stressed elements. Figure 9.14 shows the bending strength of small clear samples as a function of the width of visible compression lines on the planed sample sides. Similar results were obtained for spruce wood in timber dimensions [26].

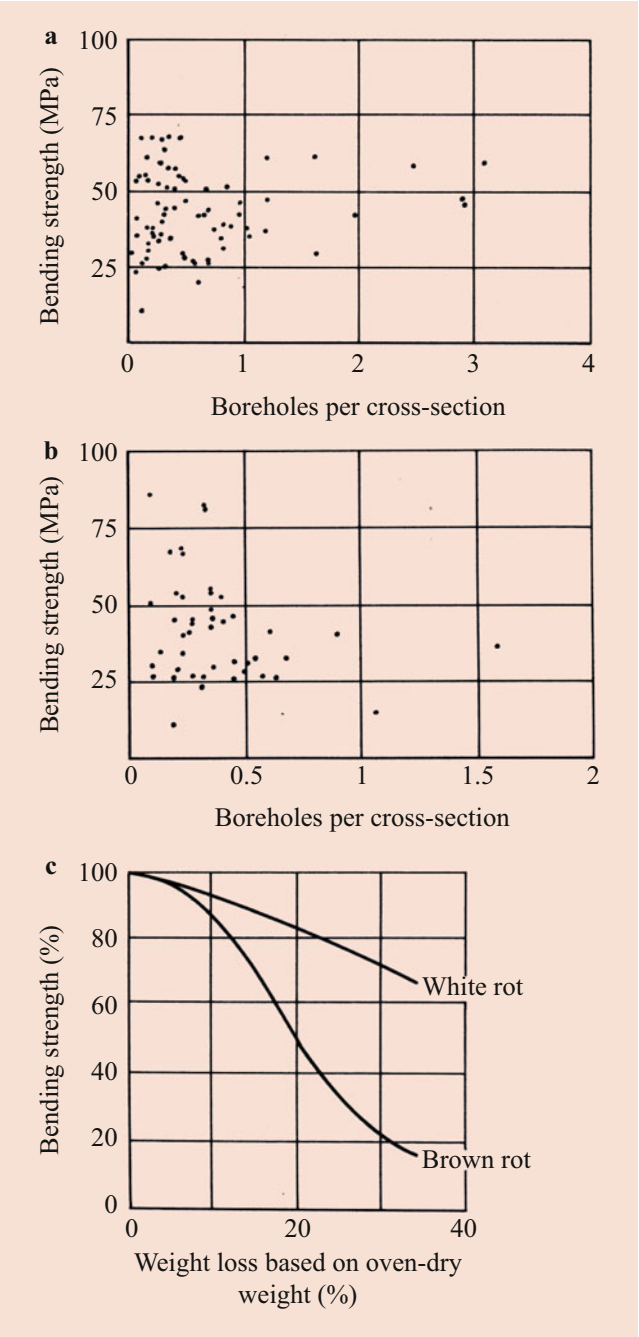

Fig. 9.13 Bending strength of spruce depending on hole density from insect infestation and on mass loss from fungal infestation. (**a**) Bark-beetle infestation. (**b**) Wood wasp/black spruce beetle infestation. (**c**) White and brown rot attack

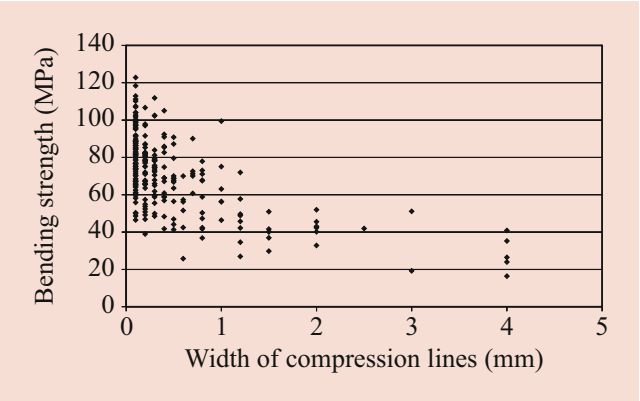

Fig. 9.14 Influence of compression failure (depending on the width of compression lines) on the bending strength of spruce wood [27]

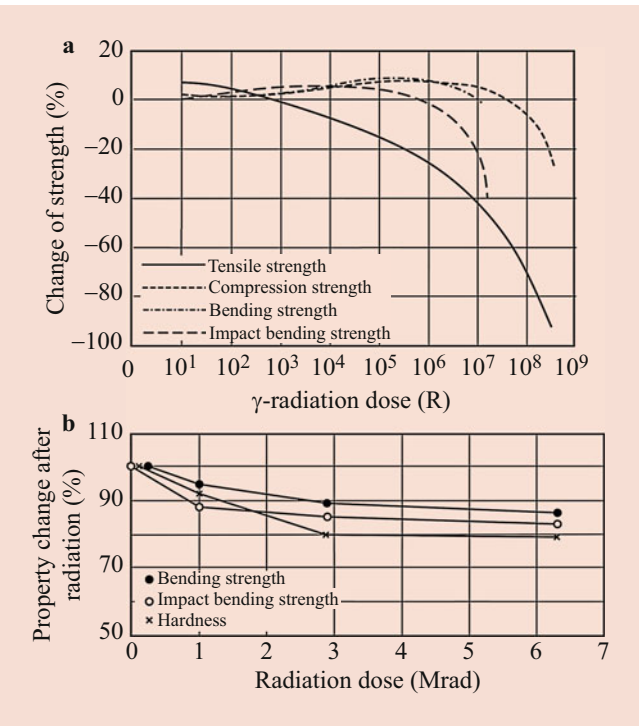

Fig. 9.15 Influence of gamma radiation on the properties of (**a**) pine wood [28] and (**b**) particleboard [29]

9.2.5 Influence of Gamma and X-Ray Radiation

Gamma rays cause damage depending on the radiation dose. Figure 9.15 shows the examples of solid wood and particle board. Further work on the effects of gamma rays can be found in Bodig and Jayne, Ross, Burmester, and Lawniczak et al. [7, 17, 28, 29].

Previously, gamma rays, for example, were used for the polymerization of wood-impregnated plastics [28]. In the case of X-ray or synchrotron imaging, according to the current state of knowledge, no damage occurs at the radiated power used.

9.2.6 Testing Method

The properties are significantly influenced by the testing method. Important influencing factors are the load speed and duration, the type of load, and the sample geometry.

Load Duration and Loading Rate

Figure 9.16 shows schematically the influence of the load duration and Table 9.5 the influence of the loading rate. The loading rate significantly affects the properties. During the test, therefore, the time to break must comply with the standard (for example, 60–90 s), otherwise values that are too high or too low will be determined (Fig. 9.16). Very high loading speeds lead to higher values, very low to lower values.

The effect was also proven in timber testing and it was found that this influence also depends on the quality of the wood. For example, Madsen [30] found that, with constant long-term stress, lumber of lesser strength had a longer loading time until stress to break than lumber of higher strength. The influence of the loading speed increases with wood moisture [30, 31]. Extensive investigations on the dynamic load of spruce wood were carried out by Eisenacher [32]. This wood was used for energy absorption in containers in case of their free fall (crash test of containers).

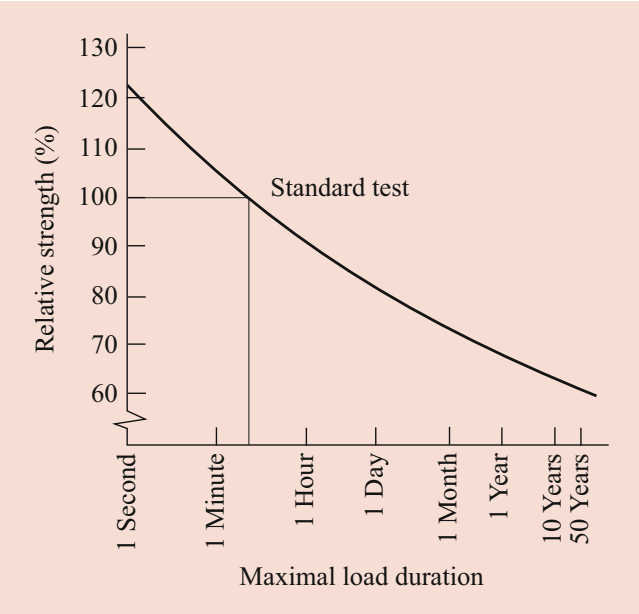

Fig. 9.16 Influence of load duration on strength [7]

Table 9.5 Influence of loading rate on the properties of wood and wood-based materials

Loading rate	Impact
Very slow	Undetectable, at long-term exposure: creep and relaxation phenomena
Moderate	Significant influence
Abrupt (e.g., pendulum impact)	Strong influence

According to Langendorf et al. [33], changed

Influence of Load Type

Strength properties are significantly influenced by the type of load. Thus, tensile strength in fiber direction in solid wood is about twice as high as compression strength, and bending strength lies between tensile and compression strength. For particle-based materials, compression strength is equal to or greater than tensile strength in board direction, and bending strength is greater than tensile and compression strength, which is due to plastic deformation during loading.

In the case of bending, the type of load (e.g., three-point or four-point bending) also influences the test result. For example, in the case of a bending beam with three-point loading, the ratio of span to thickness of the sample has a significant effect on the modulus of elasticity because the shear loss is neglected.

Sample Geometry

Solid Wood

Data on material parameters in wood physics relate almost exclusively to small clear specimens. But the strength decreases with increasing knots. In addition, the properties are highly dependent on growing conditions and also vary within a tree. The strength properties of lumber are therefore lower than those of small, defect-free samples. Round wood has about 10% higher strength properties than sawn timber. This depends on the fact that the fibers are cut during the production of sawn timber, which generates a certain fiber angle for lumbers (slope of grain, see equation by Hankinson [34]).

In solid wood, therefore, boards and beams are graded and characteristic values are determined. The test is carried out according to EN 408. For industrial grading of wood, various test machines are currently used, which are based on the deformation measurement, the measured natural frequency, or ultrasound velocity, and which determine the modulus of elasticity (see ▶ Chaps. 19 and ▶ 20).

Extensive work has been carried out on wood sorting by Steiger, Fink, Burger and Glos, and Glos and Schulz [2, 4, 35, 36]. Hübner [37] carried out extensive investigations into the grading of hardwood (beech and ash) and recently Khaloian Sarnaghi and van de Kuilen [38] tested spruce, Douglas fir, and beech wood to that effect (Fig. 9.17).

The wood properties are volume dependent because of existing defects and property fluctuations. Madson and

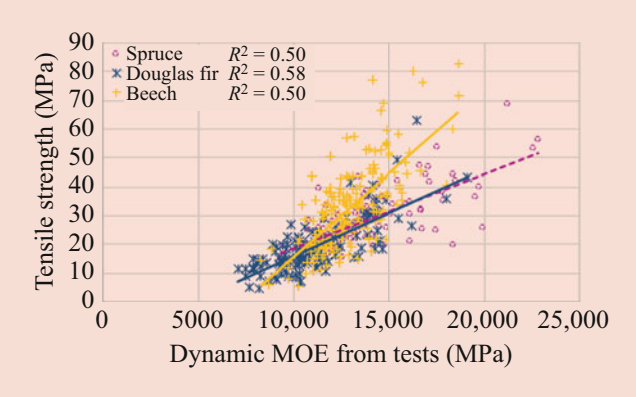

Fig. 9.17 Correlation between tensile strength and dynamic Young's modulus calculated on the basis of longitudinal vibration [38]

Buchanan (cited in Dunky and Niemz [39]) give the following relationship for the component size of wood:

$$\frac{\sigma_2}{\sigma_1} = \left(\frac{V_1}{V_2}\right)^m \cong \left(\frac{l_1}{l_2}\right)^{m_l} \cdot \left(\frac{b_1}{b_2}\right)^{m_b} \cdot \left(\frac{d_1}{d_2}\right)^{m_d} \qquad (9.4)$$

V – Volume of the specimens (m^3)
σ – Measured stress (Pa)
l – Specimen length (m)
b – Specimen width (m)
d – Specimen thickness (m)

For the coefficients m, e.g., (assuming a 10% fractile):

$m_l = 0.15$
$m_b = 0.10$

Therefore, the strength of timber decreases as the length of the samples increases. As samples with a larger width have a smaller branch share, the strength increases with increasing width. According to Weibull's (theory of the weakest link) results:

$$\frac{\sigma_2}{\sigma_1} = \left(\frac{V_1}{V_2}\right)^{1/k} = \left(\frac{V_1}{V_2}\right)^m \qquad (9.5)$$

σ – Measured stress (Pa)
V – Volume of the specimens (m^3)
k – Parameter of the Weibull distribution
m – Exponent

For the calculation and dimensioning of glued wooden elements, various models have been developed, e.g., Fink, Görlacher, Ehlbeck, Colling, and Blass [4, 10, 40–42]. With these, by using the finite element method, the strength of glulam beams can be calculated from the properties of the lamellas considering the wood part (density, knot area ratio, modulus of elasticity, length of the lamellas) and the finger jointing. Timber sorting is a standard feature in large glulam companies today (Table 9.6).

Table 9.6 Correlation of the bending strength of sawn timber with different sorting criteria [3]

Parameter	Correlation coefficient
Density	0.5
Growth-ring width	0.4
Knots	0.5
Fiber deviation	0.2
Modulus of elasticity	0.7. . .0.8

Wood-Based Materials

The properties of wood-based materials also depend on the size of the test specimen. Single large particles (e.g., OSB) have a significant impact on strength when testing small samples. Investigations by McNatt et al. [43] have shown that Young's modulus of panels from plywood and OSB is higher and bending strength is lower than those of small, defect-free specimens of these materials (Fig. 9.18).

A proposal for testing "medium-sized components" of wood-based panels is available in EN 789:2004. Böhme [44] determined the following changes in the properties of medium-sized samples (sample geometry approximately within the range 1 m in bending and tension) compared with small samples (400 mm in tension):

- Reduction in bending strength: 10%
- Increase in the bending Young's modulus: 11–12%
- Reduction in tensile strength: 1%
- Increase in pressure resistance: 18%
- Reduction in shear strength parallel to the board plane: 24%
- Reduction in shear strength perpendicular to the board plane: 4%

Table 9.7 shows the characteristic strength values of solid wood (structural timber), Table 9.8 of wood-based materials.

9.3 Phenomenological Description of the Fracture Behavior of Wood and Wood-Based Materials

9.3.1 Solid Wood

Extensive work has been carried out on the fracture behavior of wood and on the influence of structural elements such as wood rays. The first works were published in the 1950s [45–49]. In summary, the fracture behavior of wood is described in Smith et al. [50]. The following breakage phases were determined [46]:

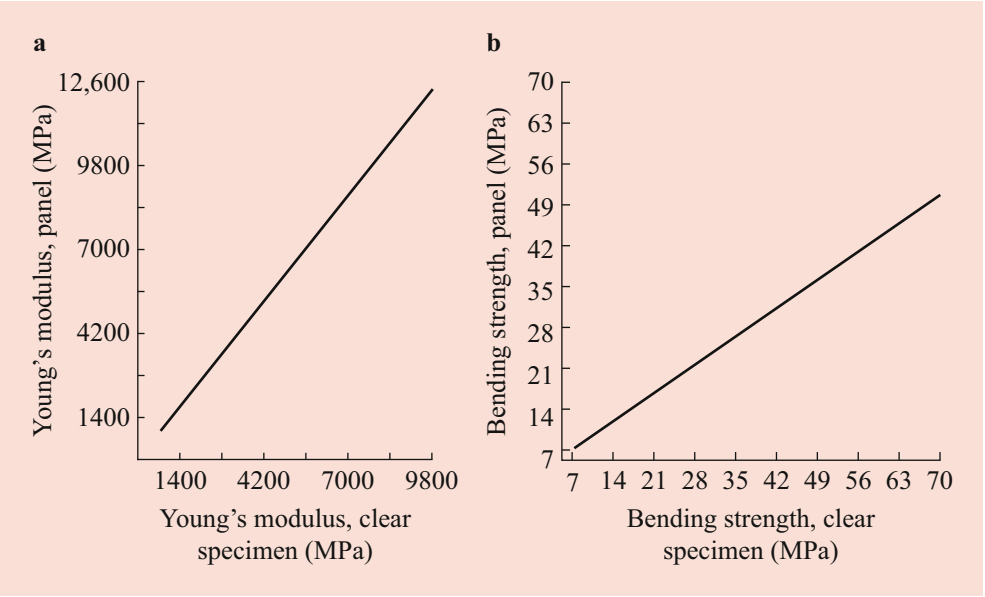

Fig. 9.18 Correlation of (**a**) Young's modulus and (**b**) bending strength of small specimens with panels (300 mm × 1000 mm) of wood-based materials (OSB, plywood) [43]; applicable to all types of wood-based materials

Table 9.7 Characteristic strength values (MPa) of structural timber according to EN 338:2016

	Softwood			Hardwood		
Class	C18	C24	C30	D30	D40	D50
Bending ∥	18	24	30	30	40	50
Tension ∥	10	14.5	19	18	24	30
Tension ⊥	0.4	0.4	0.4	0.6	0.6	0.6
Compression ∥	18	21	24	24	27	30
Compression ⊥	2.2	2.5	2.7	5.3	5.5	6.2
Shear strength (shearing, torsion)	3.4	4	4	3.9	4.2	4.5

∥ in fiber direction, ⊥ perpendicular to the fiber

Table 9.8 Characteristic strength values (MPa) of wood-based materials according to EN 12369

	Density	Bending	Tension	Compression	Shearing	
Material	(kg m^{-3})	f_m (f_p)	f_t	f_c	f_v	f_r
CLT $_{\parallel}$	410	12. . .35 (10. . .25)	6. . .16	10. . .16	2.5. . .4.0	1.2. . .1.6
CLT$_{\perp}$	410	5. . .9 (12)	6	10. . .16	2. . .5	1.4
Plywood $_{\parallel,\perp}$	350. . .750	3. . .80	1.2. . .40	1.2. . .40	1.8. . .7.5	0.4. . .1.2
OSB/2$_{\parallel}$, OSB/3$_{\parallel}$	550	14.8. . .18.0	9.0. . .9.9	14.8. . .15.9	6.8	1.0
OSB/2$_{\perp}$, OSB/3$_{\perp}$	550	7.4. . .9.0	6.8. . .7.2	12.4. . .12.9	6.8	1.0
OSB/4$_{\parallel}$	550	21.0. . .24.5	10.9. . .11.9	17.0. . .18.1	6.9	1.1
OSB/4$_{\perp}$	550	11.4. . .13.0	8.0. . .8.5	13.7. . .14.3	6.9	1.1
Particleboard, type P4	500. . .650	5.8. . .14.2	4.4. . .8.9	6.1. . .12.0	4.2. . .6.6	1.0. . .1.8
Particleboard type P5	500. . .650	7.5. . .15.0	5.6. . .9.4	7.8. . .12.7	4.4. . .7.0	1.0. . .1.9
Particleboard type P6	500. . .650	10.0. . .16.5	7.5. . .10.5	10.4. . .14.1	5.5. . .7.8	1.7. . .1.9
Particleboard type P7	500. . .650	12.5. . .18.3	8.0. . .11.5	13.0. . .15.5	7.0. . .8.6	1.8. . .2.4
Fiberboard, HB.HLA2	800. . .900	32. . .37	23. . .27	24. . .28	16. . .19	2.5. . .3.0
Fiberboard, MBH.LA2	600. . .650	15. . .17	8. . .9	8. . .9	4.5. . .5.5	0.25. . .0.3
MDF.LA	500. . .650	19. . .21	10. . .13	10. . .13	5.0. . .6.5	–
MDF.HLS	500. . .650	18. . .22	13. . .18	13. . .18	7.0. . .8.5	–

CLT cross-laminated timber, *OSB* oriented strand board, *HB.HLA2* hardboard for heavy duty load bearing in humid conditions, *MBH.LA2* medium board for heavy duty load bearing in dry conditions, *MDF* medium-density fiberboard, ∥ in the direction of the main axis or fiber direction of the cover layer, ⊥ in the direction of the minor axis or perpendicular to the fiber direction of the cover layer, f_m bending strength perpendicular to the plane, f_p bending strength in the plane, f_t, f_c tensile and compressive strength in the plane, f_v shearing perpendicular to the plane, f_r sharing in the plane

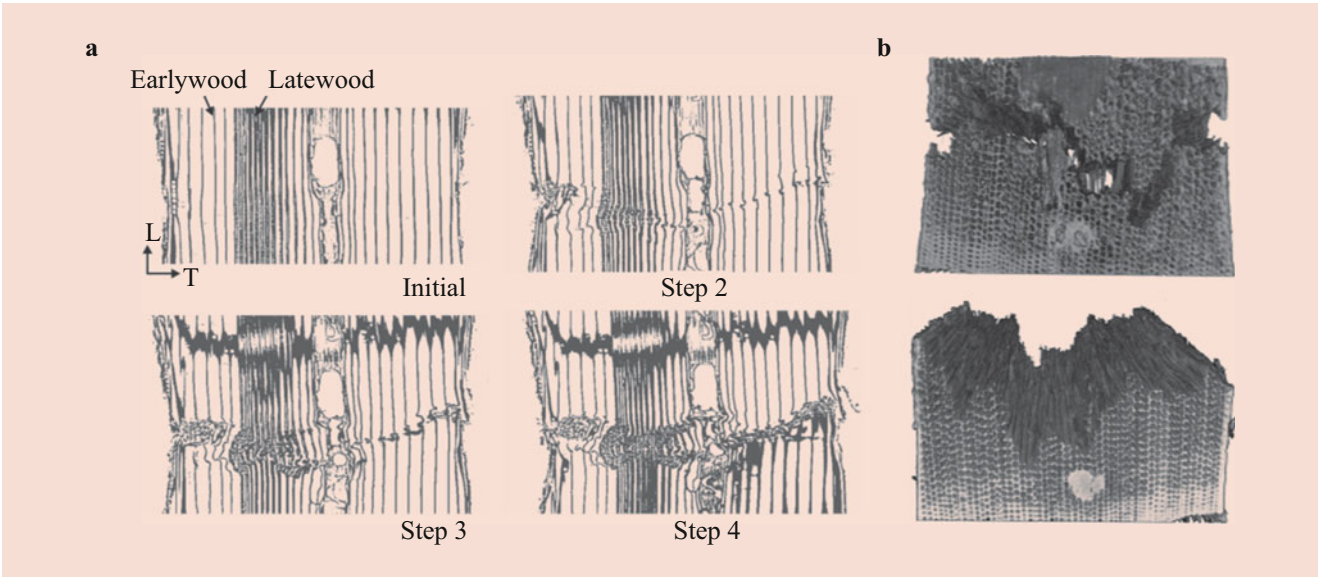

Fig. 9.19 Synchrotron images of the failure of spruce [52]. (**a**) Compression load in fiber direction. (**b**) Tensile stress perpendicular to the fiber

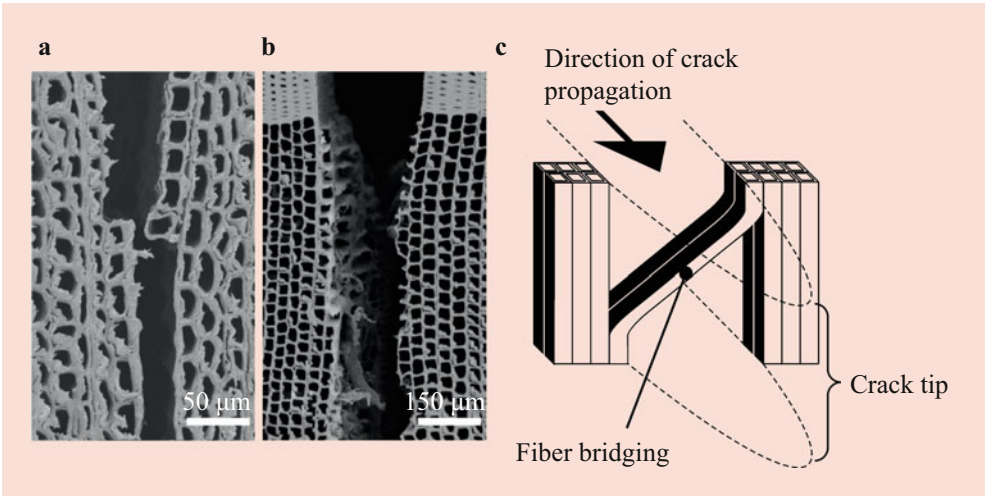

Fig. 9.20 Fractures of solid wood [54]. (**a**) Predominant intercellular fracture of yew. (**b**) Predominant cell wall fracture of spruce in TR (tangential-radial) direction. (**c**) Fiber bridging

- Start of cracking
- Crack growth
- Unstable failure

For their detection, increasingly, methods such as X-ray micro-CT or synchrotron tomography (partly in combination with acoustic emission) are used (Fig. 9.19) [51–53]. Depending on the sample geometry in the synchrotron, the maximum resolution is currently 0.3 µm. Also, in-situ measurements in the electron microscope are possible.

Crack formation begins during wood growth, during the felling of the wood, or during the technical wood drying. The first micro fractures in the cell walls are therefore already detectable in the standing tree. These fractions are reflected in the form of sliding lines (failure lines).

Crack growth begins even at stresses between 5% and 20% of the ultimate load, as evidenced by acoustic emission analysis or suitable optical methods (e.g., chlor-zinc-iodine staining and microscopic observation). However, these micro-cracks do not lead to a reduction of the load-bearing capacity of the wood. A failure of the structure in the case of overstress or shear is characterized by two types of fractures, namely:

- Internal wall fracture with a fracture behavior within the middle lamella to primary wall region (Fig. 9.20a)
- External wall fracture with a crack propagation perpendicular to the cell-wall layers (Fig. 9.20b)

A slow, even load leads rather to a break within the cell wall, whereas an impact load results more in an external wall

break [49]. These macroscopic cracks are the result of a multitude of micro fractures.

The failure process depends significantly on:

- The type of load
- The grain angle
- The wood structure (including any structural defects)
- The climatic factors (moisture content, temperature)
- The properties of adhesive joints at glued wood

The ultimate strain (strain at fracture) amounts to 0.6–1.7% for wood and 0.6–1.0% for wood-based materials, e.g., particle board. There is a strong influence of moisture content, temperature, and cutting direction. The microfibril angle in the cell wall S_2 has a significant effect on the ultimate strain, but also on the properties such as modulus of elasticity and strength. For example, juvenile wood and also compression wood have a much larger microfibril angle than normal wood. This affects the ultimate strain, which increases, and also the modulus of elasticity, which is reduced. Crack propagation can be superimposed by fiber bridging [54] (Fig. 9.20c) or adhesive bridging in glued elements [55].

Extensive work has further been published in the past 20 years on the influence of wood rays [56] as well as concerning fracture mechanical approaches to the influence of special tissue such as compression wood [57].

9.3.2 Wood-Based Materials

Cross-Laminated Timber, Plywood

Laminated wood-based materials such as plywood or cross-laminated timber (CLT) with layers that are perpendicular to each other are characterized by the shear failure of the transverse layers, the so-called rolling shear (Fig. 9.21). This is due to the low shear modulus and the low shear strength (especially in coniferous wood such as spruce and pine) in the RT (radial-tangential) plane.

Curved glulam beams (free formed, twisted, curved) can also fail owing to transverse tensile stresses. On the other hand, rolling shear failure is less pronounced in the testing of entire boards than in the bending of beams or small clear specimens [58, 59]. Shear failure may also occur on particle board and MDF, and in particular on lightweight honeycomb panels, when the density of the middle layer is very low or the bond is insufficient.

The proportion of wood failure (as opposed to adhesive failure) is an important criterion of the bond quality and moisture resistance of glued-laminated timber. The bond quality is tested by tensile shear strength according to different treatments before testing (EN 302-1) and by the delamination resistance of glued-laminated timber (EN 302-2).

Inadequate bonding quality, no moisture-resistant adhesives, and strong changes in humidity can lead to delamination of adhesive joints, even after several years or decades [55]. These processes can be calculated to some extent at present taking into account moisture-dependent properties such as mechano-sorption, rheology, and plasticity [24].

Factors influencing the fracture behavior of solid wood-based materials (e.g., CLT) include:

- Wood properties (modulus of elasticity, strength, growth-ring orientation, swelling, and shrinkage)
- Thickness of the lamellas
- Orientation of the lamellas
- Growth-ring orientation in the RT direction
- Humidity differences between the lamellas during gluing
- Humidity changes in service
- Adhesive quality

Particle-Based Materials

The group of particle-based materials includes particleboard and fiberboard. In contrast to homogeneous solids, these materials consist of a network of intersecting and overlapping particles interlinked by adhesive joints. Macroscopic cavities

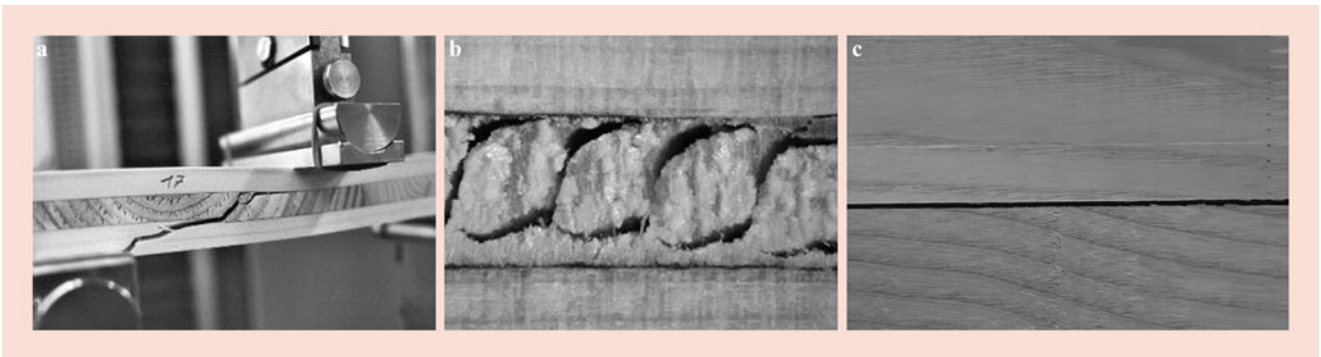

Fig. 9.21 Failure of glued wooden elements. (**a**) Bending of three-layer CLT. (**b**) Rolling shear in the RT plane of a three-layer CLT. (**c**) Delamination of a glulam adhesive joint. (Photo: Niemz, ETH)

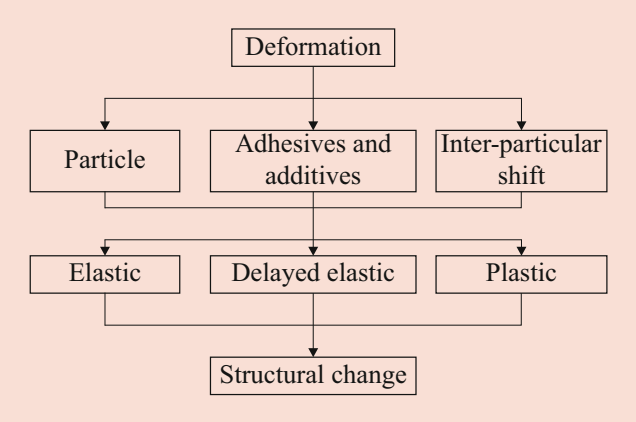

Fig. 9.22 Components of deformation and fracture of particle-based materials

are located between the particles. The proportion of the cavities is up to 30% by volume, for example, in particle boards.

The deformation and the macroscopic fracture of particle-based materials is a sum of (Fig. 9.22):

- Elastic and plastic deformation of the particles
- Elastic and plastic deformation of the inter-particle connections (adhesive joints)
- Micro fractures of particles, adhesive joints, and their interfaces
- Inter-particle shifts

The proportion of individual deformations and fractures is mainly determined by the structural composition of the particle material (morphology of the particles, type and content of adhesive, degree of particle orientation, layer structure). However, moisture content also has a big influence.

The fracture process begins even at low stress levels of about 20% of maximum bending strength in the form of local microcracks and local displacement of particles. This can be detected by acoustic emission analysis. Figure 9.23 shows scanning electron microscopic (SEM) images of failure in particleboards. The shifts stop at zones of higher packing density, thus creating a mechanism for constant formation and re-closure of inter-particle voids. The crack width at 20–30% of bending strength is 2–25 µm [60].

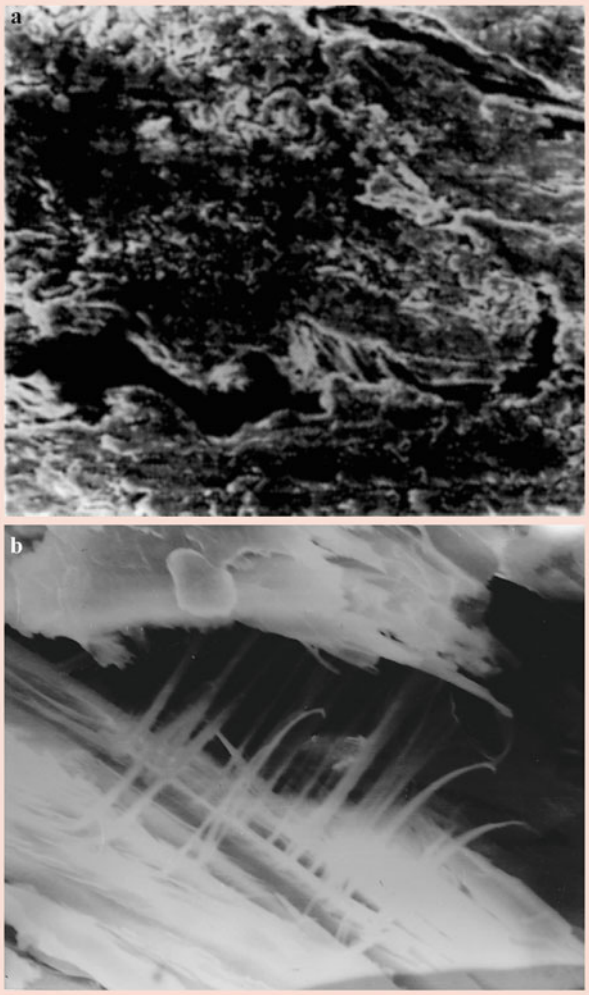

Fig. 9.23 Scanning electron microscopic images of (**a**) an inter-particle fracture and (**b**) an intra-particle fracture with fiber bridging in particle board. (Photo: Niemz)

9.4 Basics of Fracture Mechanics

9.4.1 What are Fracture and Fracture Mechanics?

Failure of a structural element is caused by some *failure mechanism* such as a fracture causing material instability or large strains or large displacements causing geometrical instability. *Fracture* means that any two points of material that originally were adjacent lose their contact. This gives a discontinuity of the displacements corresponding to an opening or sliding separation of material. The separation of material can in terms of continuum mechanics be regarded as a result of *strain instability* that gives *strain localization* to a local region where the strain becomes very large corresponding to finite relative displacement between points that originally were adjacent. Strain instability is a state of bifurcation where the material is stressed and strained to a limit at which subsequent performance is statically undetermined and may result in either an increase or a decrease in the strain corresponding to fracture or unloading, respectively, of the point of material.

Fracture mechanics [50, 61–67] may generally be defined as an analysis of fracture: observations, tests,

theories, modeling, and calculations. An alternative and more limited definition of fracture mechanics, not adopted here, is the analysis of fracture starting from the tip of a pre-existing sharp crack. The prediction of *load-carrying capacity* of structural elements as limited by fracture is from the engineering point of view a most important part of fracture mechanics. This prediction can be carried out by empirical–statistical and/or rational models. Material properties in rational models are defined by values of parameters defined within the model used and determined by experimental tests.

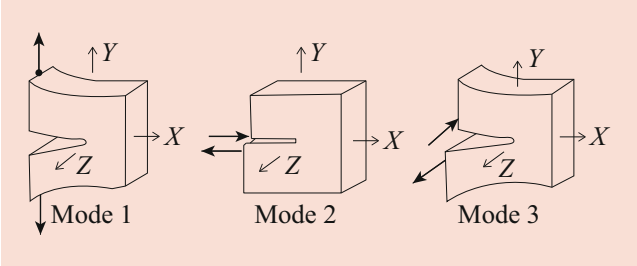

Fig. 9.24 Modes of loading of a crack. Mode 1: opening, displacement discontinuity in u_y. Mode 2: sliding toward the crack front, displacement discontinuity in u_x. Mode 3: sliding along the crack front, displacement discontinuity in u_z

9.4.2 Modelling of Material Structure

The material structure of wood shows an intrinsic *structural hierarchy* with several levels. The levels of clear wood and timber are of prime interest in relation to structural engineering. Fracture at lower levels is of interest in relation to industrial processes dealing with the decomposition of wood. For each level, the material may be modeled either as a continuum or as a heterogeneous structure in which the elements in turn may consist of a continuum. Here, the *clear wood* level will be highlighted and the material at this level being regarded as a *continuous* material with statistically *homogeneous* or gradually varying properties and orientation. Homogenization at this level is reasonable if the size of the heterogeneities such as growth-ring width and fiber length is small compared with the relevant dimensions of the element. In fracture analysis, clear wood is commonly regarded either as *orthotropic* or as *transversely isotropic* in the radial-tangential (RT) plane. Fracture analysis of *timber* as a homogeneous material is more difficult owing to the large size of heterogeneities such as knots. Rational analysis of timber may therefore require the material to be analyzed as a structure made up of different parts with different properties and orientation.

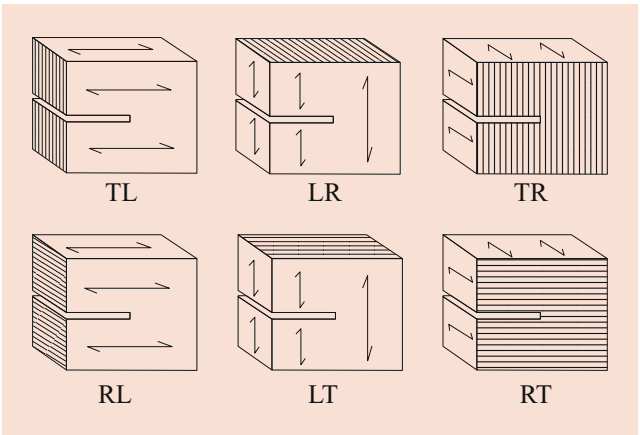

Fig. 9.25 Basic orientations of crack plane and crack front in wood

The six basic orientations of a crack in orthotropic materials are shown in Fig. 9.25. The first notation letter indicates the orientation of the normal to the crack plane and the second indicates the orientation within the crack plan that is perpendicular to the crack front. The letters T, L and R, denote the tangential, longitudinal and radial direction of the material, respectively.

9.4.3 Modes of Loading and Crack Orientations

Three modes of loading and six basic crack orientations can be defined for the case of loading of a pre-existing crack in an orthotropic material [63]. The three modes of loading are illustrated in Fig. 9.24 and they are defined based on the direction of the displacement discontinuity across the crack in the vicinity of the crack front. Different points along the crack front may have different magnitudes of the three modes of loading. The modes of loading for isotropic materials and for cracks in orthotropic materials oriented according to the material directions can also be defined based on the state of stress straight ahead of the crack tip: modes 1, 2, and 3 corresponding to $\sigma_y \neq 0$, $\tau_{xy} \neq 0$, and $\tau_{yz} \neq 0$ respectively.

9.4.4 Fracture Process Zone, Self-Similarity, and Size-Effect

Fracture involves the development of a local *fracture process zone*, FPZ, in the material structure. This region is characterized by damage and mechanical degradation of the material structure resulting in decreasing stress as the deformation is increasing. Figure 9.26 shows a schematic outline of the FPZ at the tip of a propagating crack and it also shows the other regions that typically develop during fracture. The strains are large in regions 3, 4, and 5b, commonly less in the two unloading regions denoted 6, and basically infinite in region 2. Figure 9.27 shows corresponding experimental observations of the normal strain perpendicular to grain at a specimen

surface, in the vicinity of a mode 1 crack in Scots pine wood, propagating along the grain, starting from a TL-oriented notch in a compact tension test specimen [68].

Pictures showing the failure of wood at the structural level where clear wood is observed as a structure made up of growth rings and fibers can be found in Niemz and Sonderegger, Vasic and Smith, Holmberg, Stefansson, and Persson et al. [67, 69–73].

The shape, the absolute size, and relative size of the different regions indicated in Fig. 9.26 can be very different for different kinds of materials. For wood the length of a fully developed FPZ can by theoretical estimations be found to be in the order of a centimeter, with a variation from a few millimeters to several centimeters dependent on mode of loading, orientation of the fracture, and material properties [68, 69, 74, 75]. If the fully developed FPZ is small compared with the length of the initial crack and other relevant lengths of the structural element, then the absolute size, performance, and fracture toughness of the FPZ is essentially governed only by the intrinsic properties of the material and is thus invariant with respect to the size of the structural element, given the mode of loading and crack orientation. This *self-similarity* of an FPZ can give a *size-effect in load capacity* of a structural element different than the conventional size-effect rule according to which the load capacity for equally shaped bodies is proportional to the size squared, and where the size can be any length measure of the body. After the maximum load is reached, then the development and propagation of the FPZ becomes unstable at controlled loading. For a very large element with a long initial crack this happens at the instant when the FPZ is fully developed or when the fully developed FPZ has propagated some length. For smaller elements the FPZ commonly becomes unstable before it is fully developed and for large elements without any stress concentration the FPZ commonly becomes unstable at the load of the initiation of fracture zone development.

The load capacity is determined in the case of a fully developed FPZ by the material's fracture toughness and in the case of the start of FPZ development by some stress or strain-based criterion. Commonly, both material toughness and material strength matter. The two extreme cases give different size effects, for a linear elastic body the load capacity in terms of force being proportional to the length measure to the power of 1.5 and 2, respectively.

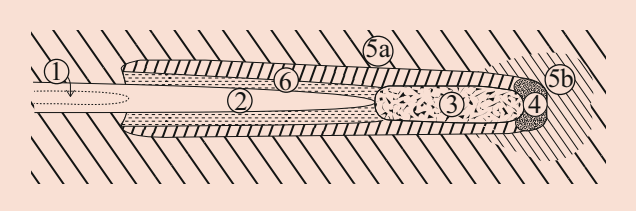

Fig. 9.26 Schematic outline showing material performance regions at the tip of a propagating crack

9.4.5 Wood Fracture Models: An Overview

An overview of rational models for wood engineering fracture strength analysis is shown in Table 9.9. Linear elastic stress analysis combined with some *conventional stress-based criterion* is the most commonly used framework for

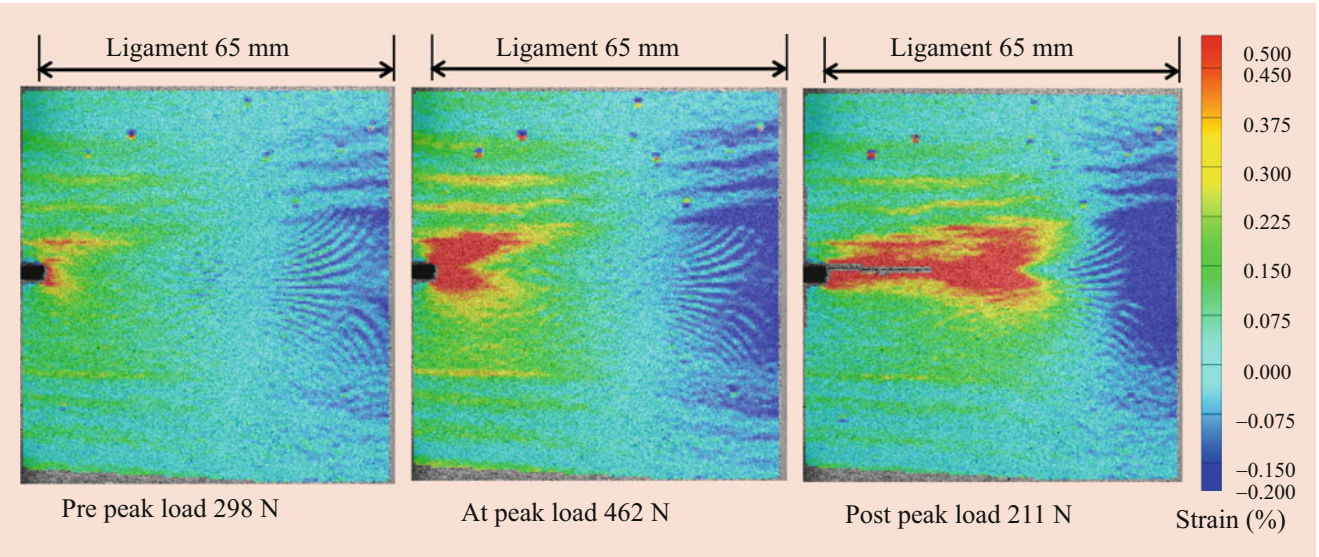

Fig. 9.27 Strain field on the surface of the ligament of a CT specimen before, at, and after peak load reported by Kristenson [68]. The strain was determined by full-field deformation measurement equipment. The specimen size was 120 × 120 × 20 mm and the notch width and depth were 2.5 and 55 mm respectively

Table 9.9 Rational type of fracture calculation models for wood engineering strength analysis

Material properties	Deterministic	Stochastic
Ideal brittle, no fracture toughness/energy	Conventional stress-based criteria	Weibull weakest link model
With fracture toughness/energy	Linear elastic fracture mechanics Generalized linear elastic fracture mechanics Nonlinear fracture mechanics	Probabilistic fracture mechanics models

strength analysis, assuming deterministic material properties and the fracture to be completely brittle corresponding to zero fracture toughness of the material and structural element failure as soon as the stress criterion is fulfilled. A major limitation of this framework is that it cannot be used if there is a sharp crack or notch in the element giving a stress singularity in which the stress theoretically is infinitely large.

In case of a sharp crack, *linear elastic fracture mechanics, LEFM,* can be used, assuming the stress capacity of the material to be infinite and instead basing a fracture criterion on a nonzero finite value of the fracture toughness or the fracture energy of the material. Elements without a pre-existing sharp crack or notch cannot be analyzed. The FPZ is assumed to have the size of a point, the point with singular stress.

Generalized linear elastic fracture mechanics models comprise various more or less approximate modifications and combinations of the two above basic models, taking into account both nonzero finite stress capacity and fracture toughness, and/or nonzero finite size of the FPZ.

By means of *nonlinear fracture mechanics* modeling it is commonly possible to simulate by numerical calculations the initiation and gradual growth of the FPZ that subsequently gives fracture, crack propagation, and failure. Most of the generalized linear and nonlinear models enable analysis of both pre-existing cracks and structural elements without any cracks.

Stochastic variation of the material properties in a structural element can, for the assumptions and limitations corresponding to the conventional linear elastic stress analysis, be considered by the *Weibull weakest link model*. Stochastic variation of material properties can also be considered for the other above-mentioned deterministic models, turning them into various *probabilistic fracture mechanics models*.

9.4.6 Conventional Stress-Based Criteria

Stress criteria can be used for the prediction of structural failure at the assumption of brittle material performance. A stress criterion does not by itself provide information about the failure mechanism: fracture or large strain compressive failure of the material structure. Stress criteria for wood are relatively comprehensive owing to orthotropy and different strength in tension and compression: all six stress components and also the sign of normal stresses may need to be considered. Several stress criteria applicable to orthotropic materials have been proposed [76] and some of those applied to wood are shown below.

A widely used failure criterion for anisotropic materials with different strength in tension and compression is the *Tsai–Wu criterion* [77]:

$$\overline{P}\overline{\sigma}^{T} + \overline{\sigma}\overline{\overline{Q}}\overline{\sigma}^{T} = 1 \tag{9.6}$$

Here, the Voigt vector notation for stress is used: $\overline{\sigma} = \left(\sigma_x \sigma_y \sigma_z \tau_{xy} \tau_{xz} \tau_{yz}\right)$. The vector $\overline{P}$ contains six material parameters, and the matrix $\overline{\overline{Q}}$ contains 36 material parameters. The $\overline{\overline{Q}}$ matrix can always be defined as being symmetrical as the quadratic stress terms are not affected by the order of multiplication. For an orthotropic material it is convenient to orient the coordinate axes according to the three principal axes of the material. With this orientation the sign of the shear stress components cannot affect the strength of an orthotropic material, meaning that all 27 linear shear stress terms must be zero. Thus, $\overline{P}$ and $\overline{\overline{Q}}$ have $3 + 9 = 12$ independent material parameters:

$$\overline{P} = \left(P_x \;\; P_y \;\; P_z \;\; 0 \;\; 0 \;\; 0\right),$$
$$\overline{\overline{Q}} = \begin{bmatrix} Q_{x\cdot x} & Q_{x\cdot y} & Q_{x\cdot z} & 0 & 0 & 0 \\ Q_{x\cdot y} & Q_{y\cdot y} & Q_{y\cdot z} & 0 & 0 & 0 \\ Q_{x\cdot z} & Q_{y\cdot z} & Q_{z\cdot z} & 0 & 0 & 0 \\ 0 & 0 & 0 & Q_{xy\cdot xy} & 0 & 0 \\ 0 & 0 & 0 & 0 & Q_{xz\cdot xz} & 0 \\ 0 & 0 & 0 & 0 & 0 & Q_{yz\cdot yz} \end{bmatrix} \tag{9.7}$$

Nine of these parameters can be determined from the uni-axial tensile, compressive, and shear tests in principal directions and the remaining three parameters by off-axis uni-axial loading tests or bi-axial loading test. This Tsai–Wu criterion is not able to consider possible shear stress interaction. Such consideration can be made possible by extending the criterion with a term representing the cubic stress component products.

For plane stress in the x–y plane, i.e., for $\sigma_z = \tau_{xz} = \tau_{yz} = 0$, the Tsai–Wu criterion becomes:

$$\begin{aligned} &P_x\sigma_x + P_y\sigma_y + Q_{x\cdot x}\sigma_x^2 + Q_{y\cdot y}\sigma_y^2 \\ &\quad + Q_{xy\cdot xy}\tau_{xy}^2 + 2Q_{x\cdot y}\sigma_x\sigma_y = 1 \end{aligned} \tag{9.8}$$

For transversely isotropic properties with isotropy in the y–z plane and plane stress in the y–z plane, the number of parameters is reduced to four and the criterion is:

$$2P_y(\sigma_y+\sigma_z)+2Q_{y\cdot y}\left(\sigma_y^2+\sigma_z^2\right)+Q_{yz\cdot yz}\tau_{yz}^2+2Q_{y\cdot z}\sigma_y\sigma_z=1 \tag{9.9}$$

The *maximum stress component criterion for orthotropic materials* can be written as:

$$\max\left[\frac{|\sigma_x|}{f_x},\frac{|\sigma_y|}{f_y},\frac{|\sigma_z|}{f_z},\frac{|\tau_{xy}|}{f_{xy}},\frac{|\tau_{xz}|}{f_{xz}},\frac{|\tau_{yz}|}{f_{yz}}\right]=1 \tag{9.10}$$

f_x, f_y, and f_z are the uni-axial strengths of the wood in compression or tension depending on the sign of the stress, and f_{xy}, f_{xz}, and f_{yz} are the shear strengths. The maximum stress criterion is frequently used in timber engineering strength design as one of the stress components in practice is often of dominant importance.

The *Norris–McKinnon stress criterion* proposed in 1956 [78] relates to plane stress:

$$\left(\frac{\sigma_x}{f_x}\right)^2+\left(\frac{\sigma_y}{f_y}\right)^2+\left(\frac{\tau_{xy}}{f_{xy}}\right)^2=1 \tag{9.11}$$

In this criterion, the uniaxial strengths f_x and f_y are also assigned different values depending on the sign of the stress.

The *Norris stress criterion* proposed in 1962 [79] relates to the general 3D state of stress:

$$\begin{cases}\left(\frac{\sigma_x}{f_x}\right)^2+\left(\frac{\sigma_y}{f_y}\right)^2-\left(\frac{\sigma_x\sigma_y}{f_xf_y}\right)+\left(\frac{\tau_{xy}}{f_{xy}}\right)^2=1\\ \left(\frac{\sigma_x}{f_x}\right)^2+\left(\frac{\sigma_z}{f_z}\right)^2-\left(\frac{\sigma_x\sigma_z}{f_xf_z}\right)+\left(\frac{\tau_{xz}}{f_{xz}}\right)^2=1\\ \left(\frac{\sigma_y}{f_y}\right)^2+\left(\frac{\sigma_z}{f_z}\right)^2-\left(\frac{\sigma_y\sigma_z}{f_yf_z}\right)+\left(\frac{\tau_{yz}}{f_{yz}}\right)^2=1\end{cases} \tag{9.12}$$

Here, the states of stress are considered separately for the three principal planes of the material and the uni-axial strengths can be assigned different values for tension and compression.

The *Hankinson stress criterion* [34] is widely used for strength analysis in the special case of uni-axially loaded wood elements in which the orientation, x', of the load $\sigma_{x'}$ forms the angle α to the orientation of fibers, x:

$$\sigma_{x'}\left(\frac{\cos^n\alpha}{f_x}+\frac{\sin^n\alpha}{f_y}\right)=1 \tag{9.13}$$

f_x is the tensile or compressive strength in the direction x of the fibers and f_y is the tensile or compressive strength in the y direction. The x'-axis is here assumed to be located in the x–y plane, but there is also a so-called 3D version of the criterion allowing for arbitrary orientation of the uni-axial load [80]. Hankinson [34] studied compressive failure and proposed parameter $n = 2$, but later comparisons with experimental data have shown that somewhat lower values of n, from 1.5 to 2.0, may provide a better experimental match.

The material parameter values needed for application of the above criteria are determined by tests at different load directions and material orientations. The strength values obtained are affected by the intrinsic material properties and also by testing conditions and method of test result evaluation. The intrinsic properties are often characterized by tree species, density, moisture content, temperature, and some quantification of knots and other defects, e.g., by rules for sorting. Influencing testing conditions include size and shaping of the test specimen, possible eigenstress, and rate of loading. The method and assumptions used to determine parameter values from recorded failure loads link the parameters to one or more failure criteria and in the common case of nonhomogeneous stress also to the constitutive model used to calculate the stress.

Table 9.10 shows the nine basic strength values for small clear wood specimens at 12% moisture content, as reported in the literature for short-term ramp loading. For comparison, corresponding strength values are also indicated according to code EN338 for a medium strength class, C24, of structural timber. These values are very different and lower for three reasons: timber has knots, the specimens are the size of structural elements, and the code values are the characteristic lower 5% fractile values. Moreover, the code values are affected by the choice of strength design calculation methods prescribed in the actual code.

9.4.7 Linear Elastic Fracture Mechanics

Linear elastic fracture mechanics, LEFM, deals with the conditions for growth of a pre-existing crack in an ideal linear elastic material with unlimited strength in terms of stress. Here, the presentation of LEFM will be limited to quasi-static plane stress and anti-plane shear conditions. Crack growth criteria can be formulated either in terms of *stress intensity factors*, K, or in terms of *energy release rate*, G. There are three stress intensity factors corresponding to the three modes of loading. They are defined by:

$$\begin{aligned}K_{\mathrm{I}}&=\lim_{x\to0}\sigma_y(x,0)\sqrt{2\pi x},\\ K_{\mathrm{II}}&=\lim_{x\to0}\tau_{xy}(x,0)\sqrt{2\pi x},\\ K_{\mathrm{III}}&=\lim_{x\to0}\tau_{yz}(x,0)\sqrt{2\pi x}\end{aligned} \tag{9.14}$$

where the x, y, z coordinates are shown in Fig. 9.28 and where $\sigma_y(x,0)$ denotes σ_y in point $(x,y) = (x,0)$, etc. The

Table 9.10 Stength (MPa) data for small clear soft- and hardwood specimens and characteristic strength code values for a medium-strength class of softwood timber

Species	Density (kg m^{-3})	Tension L	Compression L	Tension R	Tension T	Compression R	Compression T	Shear LR	Shear LT	Shear RT	Ref.
Spruce	398	63	29	4.9	2.8	3.6	3.8	6.1	4.4	1.6	[81]
Spruce	277–631	75	50	4.9	–	7.0	–	8.6	–	–	[82]
Spruce	390–480	88	40	4		7		9.5		–	[83]
Fir	480–530	104	46	4	–	7.5	–	10	–	–	[83]
Birch	630–670	137	57	7		10		12		–	[83]
Beech	670–720	135	54	7		9.5		8		–	[83]
Oak	680–750	90	59	4		11		12		–	[83]
Teak	600–690	119	64	4		7.5		8		–	[83]
Timber C24	350	14	21	0.4		2.5		4		–	[84]

T, L and R denote the tangential, longitudinal and radial directions, respectively

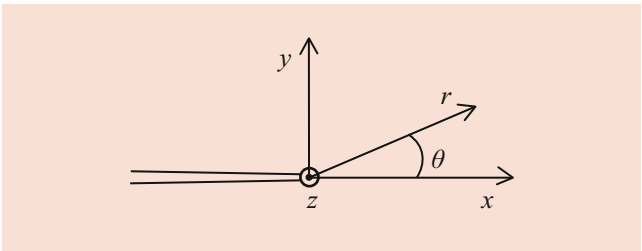

Fig. 9.28 Coordinates at the tip of a crack

three stress intensities provide a finite value quantification of the state of stress in the close vicinity of the crack tip, where $x \to 0$ and $y = 0$, as the stress components that approach an infinite value are proportional to $x^{-1/2}$ in the limit $x \to 0$. Equations for the state of stress in an orthotropic material in the vicinity of the tip of a sharp crack or a sharp notch with an arbitrary open angle are given in the literature [85–87].

The energy release rate, G, is the release (decrease) of potential energy, U, when the crack length, a, is increased by an infinitely small increment in the direction $\theta = 0$, divided by the corresponding increase in the crack area:

$$G = -\frac{1}{t}\frac{\partial U}{\partial a} \tag{9.15}$$

where t is the plate thickness, i.e., the length of the crack front. The direction of the crack increment is tacitly taken to be in the tangential direction of the crack if nothing else is stated. G is the total energy release rate, i.e., the sum for three modes of loading. Separate values for three modes can be found from the state of stress at the crack tip or by the separate opening of the three displacement components when the crack length is increased. U is the sum of the potential energy of the loads and the elastic strain energy. For a system with a single load P and specimen compliance $C(a) = \delta/P$ is

$$G = \frac{P^2}{2t}\frac{\partial C}{\partial a} \tag{9.16}$$

In simple cases, $C(a)$ can be calculated analytically and in other cases numerically. The examples of timber engineering applications of Eqs. (9.15) and (9.16) can be found in Smith et al., and Gustafsson [50, 66, 88].

As an alternative to Eq. (9.15), G can also be obtained from the crack-closing work given by the stress and crack-opening displacement in the close vicinity of the crack tip [85–87]. This also gives a relation between energy release rate and stress intensity. For an orthotropic plate in plane stress and anti-plane shear with a crack and a principal material orientation in the x-direction according to Fig. 9.28 is:

$$G = G_\mathrm{I} + G_\mathrm{II} + G_\mathrm{III} = K_\mathrm{I}^2/E_\mathrm{I}^* + K_\mathrm{II}^2/E_\mathrm{II}^* + K_\mathrm{III}^2/E_\mathrm{III}^* \tag{9.17}$$

where

$$E_\mathrm{I}^* = \sqrt{2E_xE_y/\left(\sqrt{E_x/E_y} - \nu_{xy} + E_x/(2G_{xy})\right)},$$
$$E_\mathrm{II}^* = \sqrt{2E_x^2/\left(\sqrt{E_x/E_y} - \nu_{xy} + E_x/(2G_{xy})\right)}$$
$$\text{and } E_\mathrm{III}^* = \sqrt{4G_{xz}G_{yz}} \tag{9.18}$$

where E_y, G_{xy}, G_{yz}, and G_{xz} are the elastic normal and shear stiffnesses of the material, and ν_{xy} is the strain ratio $-\varepsilon_y/\varepsilon_x$ for uni-axial stress in the x direction.

Values of K and thereby G can for *isotropic* materials be found in handbooks for a large number of geometries and loading conditions. For *orthotropic* materials calculations are in general needed for the specific structural element or specimen under consideration. Such calculations can be carried out by some numerical method such as the finite element method or in simple cases analytically. Knowing the stress and displacement fields, K and G can be obtained by substitution into known expressions for the stresses or

displacements close to the tip of the crack [85–87], by calculation of a path integral of stress and displacement quantities [89], by calculation of crack closure work, or by calculation of the energy release as the crack length is increased. The path integral calculation result is often denoted J instead of G, although $J = G$.

A general expression for the stress intensity factor for a crack in a plate is:

$$K = (P/(td))\sqrt{d}f \quad \text{(geometrical shape, elastic parameter ratios)} \tag{9.19}$$

where d is a measure of the in-plane size of the plate and where the function f includes influence of the relative crack length a/d. Note that function f is not only affected by specimen geometry shape but also by elastic parameter ratios. K is proportional to the load P and for constant nominal loading stress $P/(td)$ is K proportional to $\sqrt{d}$. G is, in turn, proportional to K^2 and in addition affected by elastic parameters according to Eq. (9.17).

When increasing the load, the crack will start to grow when a critical value of the stress intensity is reached. There are three such basic critical values for isotropic materials, one for each mode of loading. For orthotropic materials the values are different for different crack orientation. Taking mode 1 as an example, the criterion for crack growth is:

$$K_I = K_{IC} \tag{9.20}$$

where the critical value K_{Ic} is a material property parameter called the mode 1 critical stress intensity factor or fracture toughness of the material for the crack orientation considered. The crack growth will be unstable and may lead to immediate structural failure if K_I–K_{Ic} increases with crack length. The crack growth may take place in the direction of the initial crack or in some other direction, as governed by properties of the material, mode of loading, and orientation of the initial crack. The shape of the final crack may then be straight, knee-shaped, or smoothly curved. A 90° knee shape is typical for crack orientations LR and LT (Fig. 9.25) and an approximate 45° knee shape may develop at mode 2 loading of orientations TR and RT. A somewhat curved shape may develop at mode 2 loading of orientations TL and RL.

Several different crack growth criteria have been proposed for the case of mixed mode loading. A criterion often referred to for mixed mode 1 and 2 is:

$$(K_I/K_{IC})^m + (K_{II}/K_{IIC})^n = 1 \tag{9.21}$$

where the exponents m and n are determined by fitting to test results. For wood it is often assumed that $m = 1$ and $n = 2$ as proposed by Wu and Mall et al. [90, 91].

If using energy release rate G or path integral J instead of stress intensity K as a measure of the magnitude of loading of a crack, analogous material parameters and crack growth criteria can be defined. Application of LEFM can as a general rule be expected to be successful for large elements where the size of the FPZ is very small compared with the length of the crack and other relevant dimensions of the element.

Table 9.11 shows values for K_{Ic}, K_{IIc}, and G_{Ic} for different tree species and crack orientations as reported in the

Table 9.11 Fracture toughness and critical energy release rate of wood from various tree species

	K_{Ic} (kN m$^{-3/2}$) at crack orientation						
Species	TL	RL	LR	TR	RT	LT	Ref.
Balsa	–	112	–	–	–	–	[92]
Scots pine	33	360	–	290	210	–	[93]
Spruce	240	340		230	200		[93]
Douglas fir	309	410	2692	355	355	2417	[94]
Cedar	180	233					[92]
Oak, red	407	–	–	–	–	–	[92]
Maple, hard	492	–	–	–	–	–	[92]
	K_{IIc} (kN m$^{-3/2}$) at crack orientation						
Species	TL	RL	LR	TR	RT	LT	Ref.
Balsa	–	280	–	–	–	–	[92]
Scots pine	2050		–	–	–	–	[95]
Douglas fir	1162	1832	–	–	–	–	[80]
Douglas fir	1370–1560	1412–1902					[63]
	G_{Ic} (=J_{Ic}) (nm m^{-2}) at crack orientation						
Species	TL	RL	LR	TR	RT	LT	Ref.
Scots pine	184	156	–	735	364	–	[96]
Spruce	133	156	–	538	297	–	[96]

T, L and R denote the tangential, longitudinal and radial directions, respectively

literature. Test results for mode 3 referred to in Sect. 9.4.3 suggest that G_{IIIc} for larch and beech is more than twice G_{Ic}.

9.4.8 Generalized Linear Elastic Fracture Mechanics

Several *generalized linear elastic fracture mechanics models* have been proposed to overcome the limitations of conventional stress criteria calculations and LEFM, still keeping to linear elastic stress and displacement analysis. Such methods include the following.

Crack growth resistance curve (R-curve) analysis, which is an extension of LEFM that takes into account the apparent gradual increase in fracture toughness of the material as the FRZ develops during the first apparent growth of the crack [61]. The apparent location and movement of the crack tip can be determined from observations of the change in elastic stiffness of the specimen, e.g., by repeated loading and unloading. The *R*-curve is assumed to be characteristic of the material and should thus not be affected by specimen geometry.

The *initial crack analysis methods* generalize the applicability of LEFM. A virtual extension of the pre-existing crack or, if there is no pre-existing crack, a virtual additional crack is introduced before analysis by LEFM. The crack extension takes into account the effect of the finite size of the FPZ and enables LEFM analysis of structural elements without any pre-existing crack. The length, a, of the crack extension for the actual material, mode of loading, and orientation of the fracture plane can be determined by fitting to test results or can be obtained by some theoretical derivation. Such a derivation, see, for example, Gustafsson [97], gives:

$$a = \frac{1}{\pi}\left(\frac{K_{Ic}}{f_t}\right)^2 \text{ and } a = \frac{1}{\pi}\left(\frac{K_{IIc}}{f_v}\right)^2 \qquad (9.22)$$

for mode 1 and mode 2 loading respectively, f_t and f_v being the tensile and shear strengths perpendicular to the plane of fracture. Length a, for fracture growth along the grain, can typically be in the order of 1–4 mm and 5–15 mm for modes 1 and 2 respectively. A theoretical result for length a for a mixed mode 1 + 2 loaded orthotropic material can be found in Gustafsson [97].

In *mean stress analysis methods* some conventional stress criteria are used, but instead of using the stress in the point studied, some mean stress along a short line, a small surface, or a small volume surrounding the point is used. This takes in an approximate manner the finite size of the FPZ into account and also enables the use of a stress criterion for the analysis of a sharp crack. The size of the mean stress part can be roughly related to the size of the heterogeneities of the material structure [98] or in the case of mean stress along a line by a theoretical derivation, it can be found be to $2a$, where a is in accordance with Eq. (9.22) [97].

9.4.9 Nonlinear Fracture Mechanics

The nonlinear stress vs strain or stress vs deformation performance of the material in regions 3, 4, and/or 6 shown in Fig. 9.26 is taken explicitly into account in nonlinear fracture mechanics (NLFM) analysis. For ductile plastic hardening materials such as mild steel, such analysis commonly relates to the performance in region 4 whereas region 3, the FPZ, may still be modelled as a point with singular stress and/or strain. For the so-called quasi-brittle nonyielding materials such as wood, modeling of nonlinear performance commonly relates to region 3, the FPZ [64, 74, 75, 99–102].

Modeling of the material performance within the FPZ cannot be carried out by conventional "simple" continuum mechanics stress–strain characterization of the material because of the strain instability and the self-similar strain localization during fracture. The absolute size of the FPZ is governed by intrinsic material properties rather than being proportional to the absolute size of the structure. This can be modeled by nonlocal or stress gradient continuum mechanics, or more simply by stress vs strain characterization of the material for some certain pre-defined absolute width of the FPZ, the strain being forced to be homogeneously smeared over the pre-defined width. The width can also be made equal to zero and then the fracture deformations are projected to the plane of a discrete crack and the fracture properties of the material are defined by stress vs opening and/or sliding between the fracture surfaces.

The gradual damage and fracture of wood in terms of stress vs normal and shear deformation performance across an FPZ can be determined experimentally by tests designed to avoid sudden brittle failure. This entails the use of a stiff testing machine and small specimens so that the stored elastic energy in the system is low at the instant of peak load. Figure 9.29 shows fracture test recordings for perpendicular to grain tension and shear of wood from Scots pine. The complete curves show total deformation, δ, and the marked lines show the estimated deformation during unloading from peak stress. w is the additional local fracture softening and damage deformation due to the development of the FPZ, determined as the total deformation minus the distributed elastic, plastic, and damage deformations in the material according to the current load and the state of the material structure at peak load. Stress vs deformation across the FPZ is used in NLFM for material characterization and test results are available in the literature for uni-axial tension at various rates of

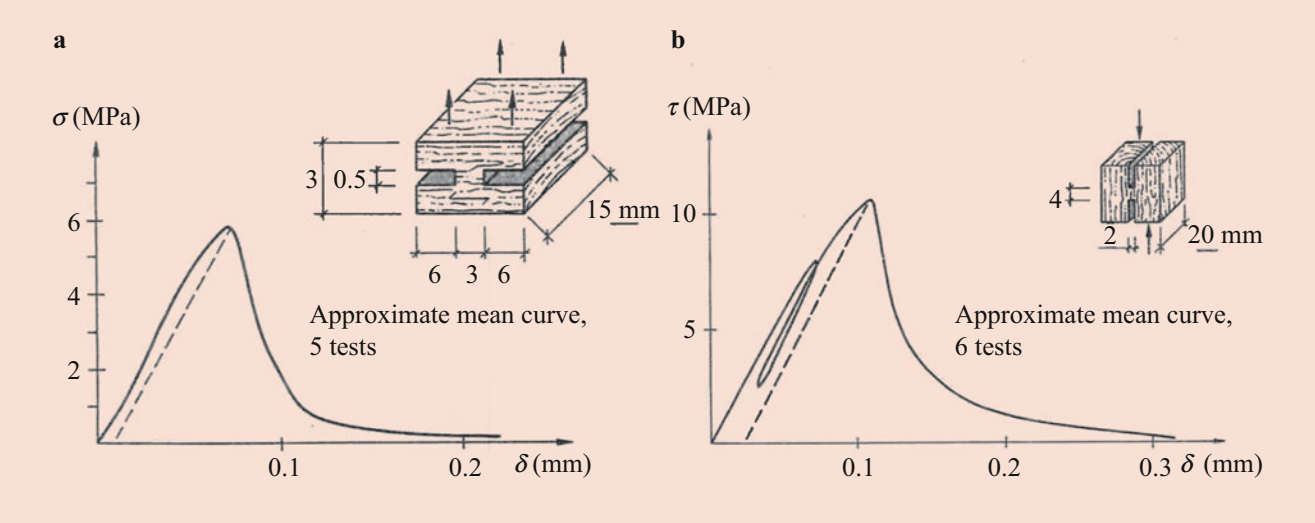

Fig. 9.29 Specimen and test recordings for (**a**) tension and (**b**) shear [103]

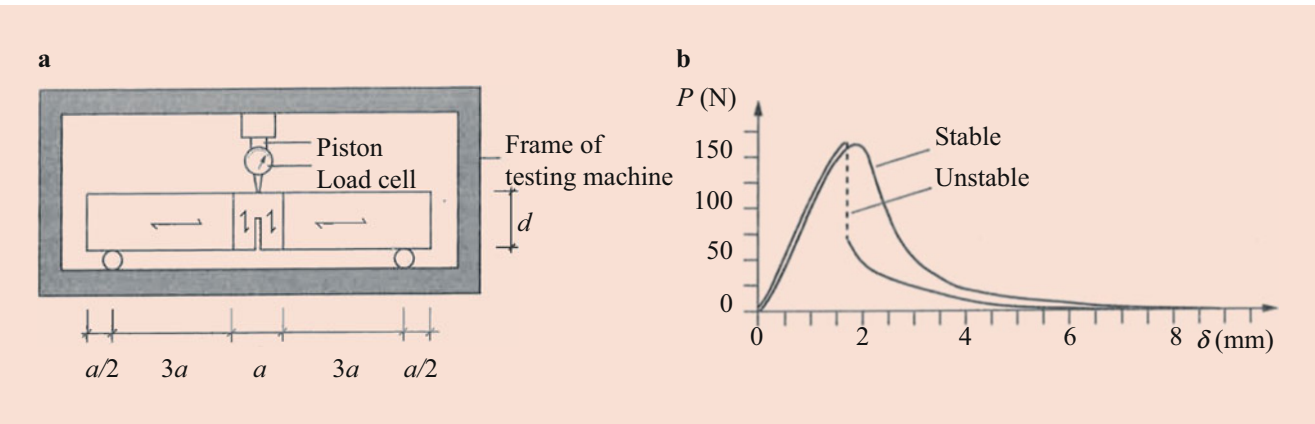

Fig. 9.30 Test set-up (**a**) for fracture energy of wood and (**b**) examples of test recordings [66]

loading and also for shear and for mixed mode loading, determined by direct testing [70, 71, 75, 102, 103] or inverse analysis [68].

The energy per fracture area dissipated in the FPZ is commonly called the fracture energy and denoted G_f. In LEFM there are 18 basic combinations of modes of loading and orientations of the crack, as shown in Figs. 9.24 and 9.25, but in NLFM there are only nine corresponding basic combinations: three basic orientations of the normal to the plane of fracture (R, T, and L) and three basic orientations of the force acting between the two fracture surfaces. The corresponding fracture energies can then be denoted G_{ijf}, where i = R, T, L is the orientation of normal to the plane and j = R, T, L is the direction of the load. The fracture energy can by its definition be determined as:

$$G_f = \int_0^\infty \sigma \, dw \tag{9.23}$$

where the orientation of the stress and the relative displacement is according to the case considered. One may expect LEFM and NLFM to predict equal load capacity of structural elements in plane stress for $G_c = G_f$ if the material performance outside the FPZ is linear elastic and the size of the FPZ is small compared with the crack length and other relevant dimensions.

The fracture energy can also be determined for tensile fracture perpendicular to grain by three point bending tests as shown in Fig. 9.30. A test standard [104] specifies $a = d = 60$ mm, notch depth $0.6d$ and specimen width b,

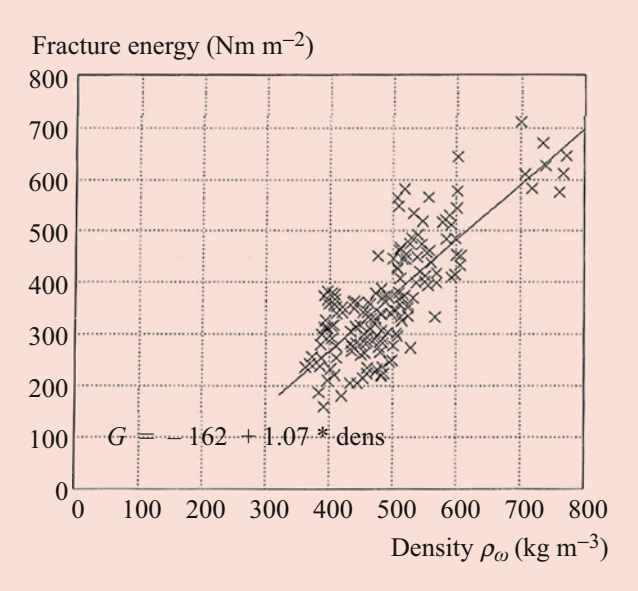

Fig. 9.31 Tensile fracture energy of Scots pine versus density [105, 106]

e.g., 45 mm. In this case G_f is evaluated from recorded load, P, vs deflection, δ, according to:

$$G_f = \frac{1}{A}\left(\int_0^\infty P\,\mathrm{d}\delta + mg\delta_o\right) \tag{9.24}$$

where $A = 0.6bd$ is the ligament area, mg is specimen weight, and δ_o the deflection when the specimens falls down because of its own weight. This method of evaluation may overestimate G_f, as defined by Eq. (9.23), as possible energy dissipation due to plastic strain outside the FPZ is included ([73, 105] annex A2, A9). Several fracture energy test results for tension in random perpendicular to grain orientation can be found in the literature [105–107]. Figure 9.31 shows a compilation of such results vs density for Scots pine with moisture content about 12%, tested at different laboratories. The perpendicular to grain tensile fracture energy for softwoods spruce (*Picea abies*) and Scots pine (*Pinus sylvestris*) of common density and moisture content is typically in the order of 300 Nm m^{-2} at room temperature, whereas the fracture energy for shear along grain is typically in the order of 2–4 times greater. Tests on wood (*Picea abies*) saturated with water [108] using small specimens ($b = d = 10$ mm) gave (G_{TTf}, G_{RRf}) = (220, 145) Nm/m^2 at a temperature of 25 °C and (140, 90) Nm m^{-2} at 95 °C.

According to contemporary NLFM models, given the orientation of the fracture plane, the direction of propagation of the FPZ should not affect the fracture energy. This is consistent with a small experimental study (Table 9.12; [106] annex A13), not showing any significant influence of direction. The study comprised a total of 16 tests of Scots pine with a mean density of 650 kg m^{-3} and 12% moisture content (MC). This study also suggests that the fracture energy is greater for tension in the T direction, mean G_{TTf} = 680 Nm m^{-2}, than in the R direction, mean G_{RRf} = 470 Nm m^{-2}. This is consistent with the study of wet wood [108], but another study ([105] annex A6) suggests an insignificant influence of the orientation (Fig. 9.32).

Table 9.12 Fracture energy for tension in tangential and radial direction, for fracture propagation along and perpendicular to grain

G_{TTf} (Nm m^{-2})		G_{RRf} (Nm m^{-2})	
L direction	R direction	L direction	T direction
656	704	445	495

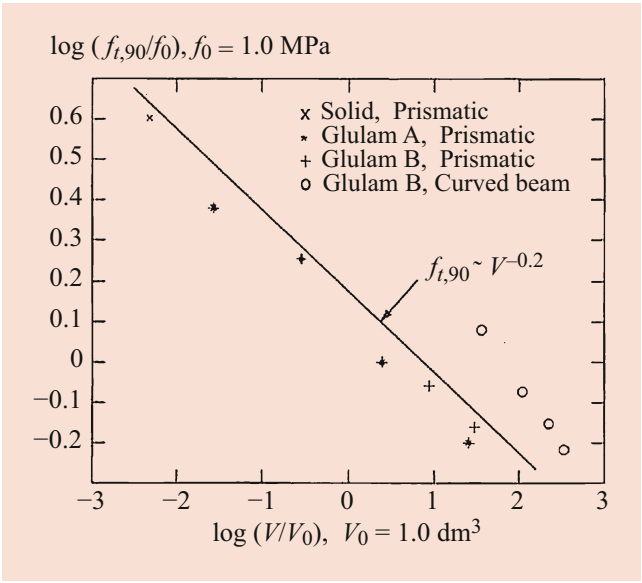

Fig. 9.32 Perpendicular to grain tensile strength versus volume of test specimen [66]

9.4.10 Weibull Weakest Link Model

Structural element strength analysis using the Weibull model has several basic assumptions in common with conventional strength analysis: the material is assumed to be linear elastic, the failure criterion is based on stress, and the material is assumed to be brittle so that the element is assumed to fail when the stress criterion is fulfilled at some point. The difference is that the strength of the material is not assumed to be deterministic but instead stochastic with random strength at different points according to the two- or three-parameter version of the Weibull distribution function [109–111]. The cumulative distribution function for the strength of a point or infinitesimal volume dV is according to the two-parameter model:

$$S(\sigma_e) = 1 - e^{-(\sigma_e/\sigma_{ef})^m} \quad (9.25)$$

where S is the probability that the point of material will fail before the effective stress σ_e is reached. The effective stress is calculated according to some choice of a stress-based failure criterion using stress components obtained by linear elastic stress analysis. σ_{ef} and m are material parameters representing magnitude and scatter in material strength. The strength distribution for a specimen or structural element with volume V made up of volumes dV is an extreme value distribution for the weakest volume dV in the element. A special and convenient feature of the two-parameter Weibull distribution is that the extreme value distribution for element strength has the same shape and coefficient of variation as the basic distribution for material strength.

Using notation $\overline{\sigma_{ef,0}}$ for the mean strength of specimens with volume V_0 in homogeneous stress it is found that the mean value for the effective stress at a point p at the instant of failure, $\overline{\sigma_{ef,p}}$, of an arbitrarily shaped and loaded specimen or element with volume V is:

$$\overline{\sigma_{ef,p}} = \overline{\sigma_{ef,0}} \ (V/V_0)^{-1/m} \left(\int_V \left(\sigma_e(x)/\sigma_{e,p}\right) (dV/V) \right)^{-1/m} \quad (9.26)$$

where $\sigma_e(x)$ is the effective stress field in V when the magnitude of load is such that the effective stress at point p is $\sigma_{e,\,p}$. The scatter in the element strength $\sigma_{ef,\,p}$ is given by m, each m corresponding to a certain coefficient of variation, e.g., (m, COV) = (5, 22.9%), (10, 12.1%), and (20, 6.3%). The last multiplier in Eq. (9.26) shows how the distribution of stress affects the strength of the element and the second last multiplier shows that the increased size of the element gives decreased strength in terms of stress at failure. The last multiplier equals 1.0 for elements under homogeneous stress. Both multipliers are equal to 1.0 in the limit $m \to \infty$, i.e., for zero scatter in material strength. The Weibull theory is not applicable to elements with a sharp crack because of the stress singularity at the tip of the crack [111]. For wood, the theory is better suited to analysis of tensile and shear failures than for bending and compressive failures because of the assumption of brittle failure. For timber, bending failure is also often brittle.

Values of m relevant for wood and timber can be determined from experimental observations about the scatter in strength or the influence of element size, shape or load distribution. Figure 9.32 shows a compilation of perpendicular to grain tensile strength results obtained for one size of solid wood and several sizes of glulam specimens [66]. In this case, a reasonable fit with the Weibull theory is found for $m = 5$, corresponding to strength $\sim V^{-0.2}$ and COV = 23%. The curved beam specimens show higher strength than the prismatic specimens. This is consistent with the Weibull theory predicting greater strength for the curved beams because of nonhomogeneous stress. In spite of this, the basic Weibull model's assumptions must be regarded as a significant simplification of the real fracture mechanisms of wood, as evidenced for instance by the empirical damage failure model for perpendicular to grain tensile failure of glulam presented in Dill-Langer [112].

9.4.11 Probabilistic Fracture Mechanics Models

Probabilistic fracture mechanics models comprise linear, generalized linear, and nonlinear fracture mechanics models in which the stochastic nature of material properties, geometry, or load is included in the model. There are at present no well-established such models for wood. An application of probabilistic linear elastic fracture mechanics to timber beams is, however, included in a comprehensive proposal for reliability-based design of timber structures [113]. This application relates to the shear force capacity of beams. The capacity was assumed to be governed by the growth of end-cracks in the beam. The length of the cracks and the mode 2 fracture toughness of timber were defined by probability density functions based on tests and observations. Beam shear strength and its variability could be calculated by linear elastic fracture mechanics. In another study [114] the stochastic variability of the fracture toughness along a crack propagation path was considered in order to find the strongest part, which was assumed to be decisive for element strength. A probabilistic model based on a combination of Weibull modelling and the above-mentioned mean stress analysis was applied to strength analysis of glulam beams with holes using finite element calculations [115]. In this case the mean stress over an area instead of the stress at a point was used in Weibull analysis, the size of the area being determined by the fracture toughness and strength properties of the material and also making it possible to apply Weibull analysis to elements with a sharp crack.

9.5 Strength of Wood and Wood-Based Materials

9.5.1 Overview

The strength (also named ultimate stress) is the stress at which the material fails (Figs. 9.33a, b and 9.35a). Up to the proportional limit σ_P there is a linear relationship between stress and strain. The ultimate strain at break at tensile load in and perpendicular to the fiber direction is about 0.7–1%, depending on the moisture content of the wood. The strain

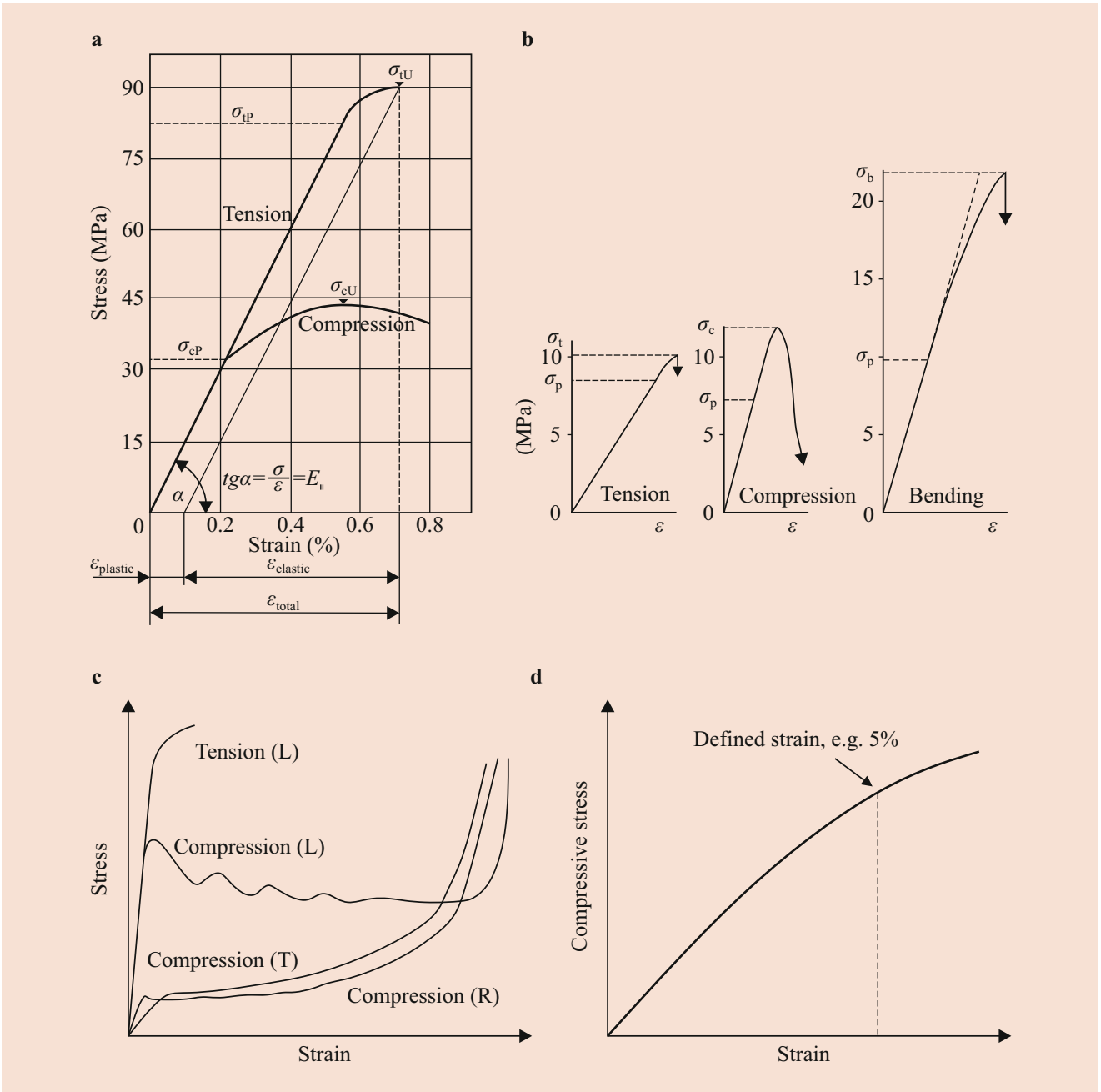

Fig. 9.33 Stress–strain diagrams of solid wood and wood-based materials. (**a**) Wood in fiber direction. (**b**) Particleboard parallel to the plane. (**c**) Comparison of solid wood parallel and perpendicular to the fiber. (**d**) Determination of maximum strain at compressive stress perpendicular to the fiber. L – longitudinal, R – radial, and T – tangential

at break increases slightly with increasing moisture content. Wood is brittle when subjected to tensile stress. Steaming makes it possible to increase the strain at break. Densified wood has a higher strain at break (ultimate strain) than uncompacted wood, as the compaction can be reversed to a certain extent [116].

Tensile strength in the fiber direction of solid wood is about twice as high as compression strength (Fig. 9.33a). In the case of wood particle-based materials, on the other hand, compression strength is equal to or higher than tensile strength (Fig. 9.33b) [117, 118].

Perpendicular to the fiber (Fig. 9.33c, d), solid wood collapses in the cell structure under compression stress, so a maximum strain is defined as the ultimate limit (e.g., 2% or 5%). Initially, the less dense earlywood collapses, later also the latewood (Fig. 9.34). With increasing compression it

results in a solidification. The stress then increases proportionally with the density. Thus, for example, spruce can be densified very well, especially in the radial direction, to 1000 kg m^{-3} and above. The technique of densification is described in, for example, Navi and Sandberg [116].

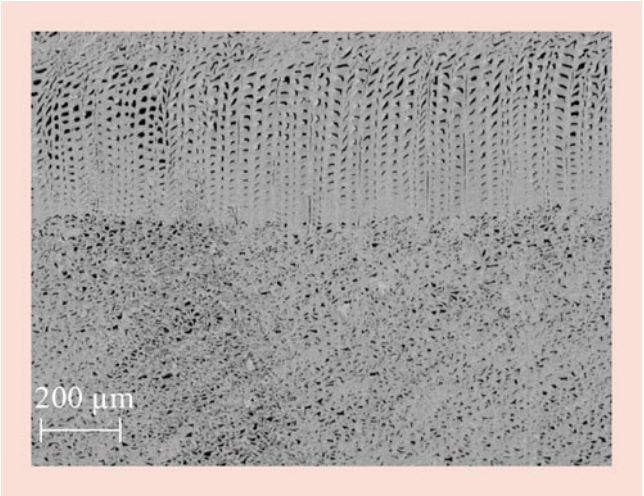

Fig. 9.34 Spruce wood densified in a radial direction. (Photo: Peschke, ETH Zürich)

In the case of particle-based materials, the particles are strongly compressed perpendicular to the plane (e.g., perpendicular to the wood grain) during hot-pressing. The compaction compared with the uncompressed solid wood is about 50% (particle boards) and up to 80% and more for MDF/high-density fiberboard.

The yield stress in the stress–strain diagram is also partly indicated. This is the stress that occurs at, for example, 0.2% plastic deformation (parallel to Hooke's straight line; Figs. 9.33a and 9.35a, b)). The surface area (integral) under the stress–strain curve (deformation energy in N·mm) is often used additionally, as this parameter contains a good prediction about ductility. Tables 9.13 and 9.14 show the strength of different woods and wood-based materials in the three main axes (reference values).

9.5.2 Plastic Properties

Ramberg–Osgood Approach

Wood has a ductile failure behavior perpendicular to the fiber direction (radial and tangential) under compression load, but more brittle in tensile load. Under uni-axial loading, the linear elastic fracture behavior of wood (Fig. 9.35a, b) can

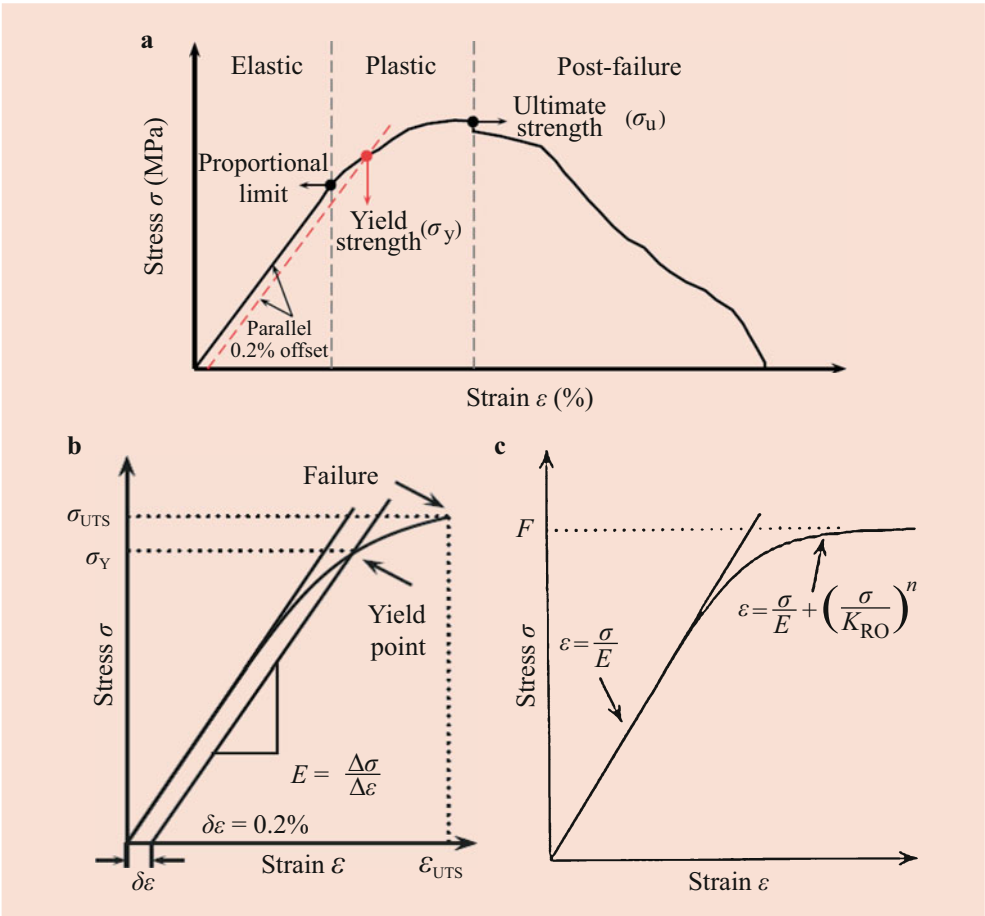

Fig. 9.35 Stress–strain diagrams. (**a**) Schematic diagram adopted from metallic materials according to ASTM-E8/E8M (2011). (**b**) Yield stress (represents 0.2% offset yield stress at the specific yield point). (**c**) Schematic stress–strain diagram in compression with modified Ramberg–Osgood material function [124]

Table 9.13 Strengths of selected wood species in the three main directions in a normal climate

Species	Strength (MPa)	Load direction			Relation
		Longitudinal (L)	Radial (R)	Tangential (T)	T: R: L
Norway spruce	Tension	87.2	3.96	3.07	1: 1.3: 28.4
	Compression	40.2	4.1	4.2	1: 0.98: 9.6
Beech	Tension	96.7	14.7	8.9	1: 1.7: 10.9
	Compression	45	11	6	1: 1.8: 7.5
Oak	Tension	73	6	7.8	1: 0.8: 9.4
	Compression	47.9	10.6	9	1: 1.2: 5.3
Maple	Tension	112	16.2	8.9	1: 1.8: 12.6
	Compression	61.5	15.4	10.3	1: 1.5: 6.0
Common ash	Tension	130	12.5	10.1	1: 1.2: 12.9
	Compression	43.4	10.5	10	1: 1.05: 4.3
Walnut	Tension	89.1	10.8	8.9	1: 1.2: 10.0
	Compression	60.4	13.4	11.9	1: 1.13: 5.1
Cherry	Tension	109	17.3	10.8	1: 1.6: 10.1
	Compression	53.5	14.4	9.5	1: 1.5: 5.6

Measurements ETH Zurich, IfB

Table 9.14 Strengths of wood particle-based materials in the three main axes

Material		Strength in the board plane (MPa)		Internal bond	Relation
		in the direction of the production line (x)	perpendicular to the production line (y)	(MPa) (z)	z: y: x
Particleboard (660 kg m^{-3})	Tension	6.3	5.7	0.45	1: 12.7: 14
	Compression	10.7	10.6		
MDF (742 kg m^{-3})	Tension	20.6	20.3	0.6	1: 33.8: 34.3
	Compression	20.3	20.4		

MDF medium-density fiberboard
ETH Zurich

Table 9.15 Moisture-dependent material parameters of the Ramberg–Osgood equation for beech wood determined in the compression test [120]

Radial				Tangential			
Moisture content (%)	E (MPa)	K_{RO} (MPa)	n (−)	Moisture content (%)	E (MPa)	K_{RO} (MPa)	n (−)
8.7	1990	20.4	17.1	8.3	669	11.9	8.3
12.9	1900	16.6	20.7	9.6	606	9.6	9.7
16.4	1570	12.8	26.6	11.2	505	7.5	11.2
18.6	1430	12.0	23.1	11.6	475	6.6	11.6

be described in a radial and tangential direction (Fig. 9.35c) as follows [7, 119, 120]:

$$\epsilon = \frac{\sigma}{E} + \left(\frac{\sigma}{K_{RO}}\right)^{n} \quad \text{mit} \quad 0 \leq \sigma \leq F \tag{9.27}$$

K_{RO} and n are material parameters that can be determined experimentally by regression. The two terms represent the elastic and the inelastic strain fraction. Similarly, with the Ramberg–Osgood equation, a simple determination of the yield strength σ_Y is possible. Table 9.15 shows the determined parameters for E, K_{RO}, and n for European beech at variable moisture content. Further explanations are given in Bodig and Jayne, Hering, Schmidt, and Reichel [7, 120–122].

Multi-Surface Plasticity Model

Multi-axial loading requires multi-dimensional approaches. The material model consists of an elastic and a ductile portion. Figure 9.36 shows the plastic deformation of European beech under pressure perpendicular to the grain. The time-dependent (rheological) behavior is not taken into account. Figure 9.37 shows the yield surface of the multi-surface plasticity model for beech; the dark gray areas indicate areas with one failure mode. For further information see, for example, Resch and Kaliske [123].

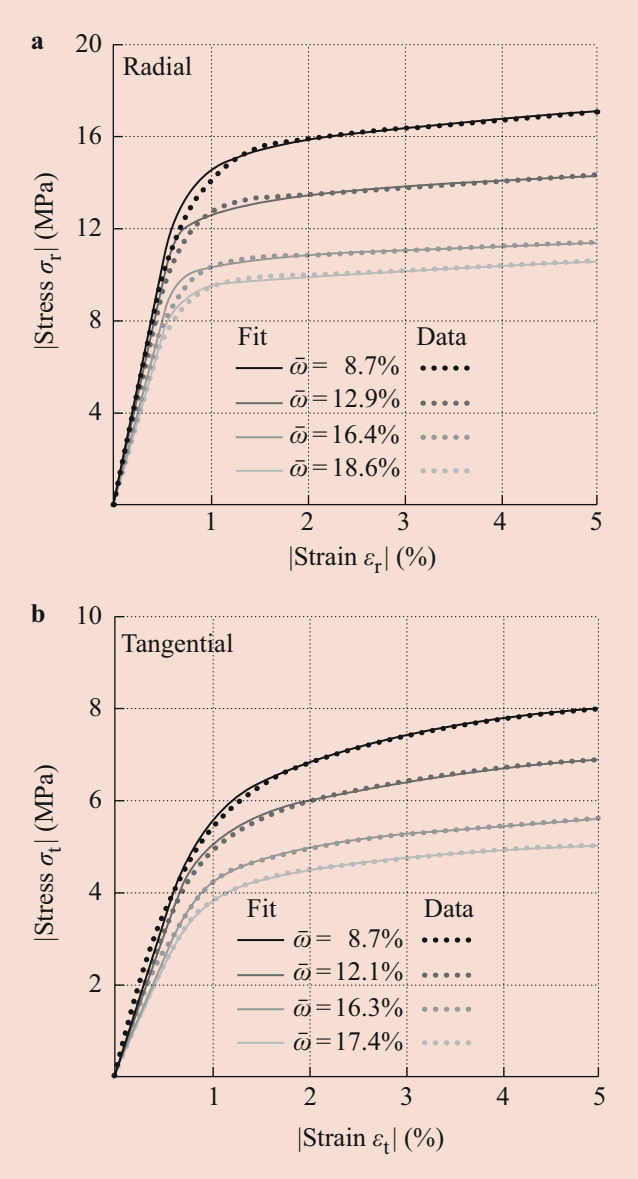

Fig. 9.36 Resulting regression and measurement data of the moisture-dependent compression test of European beech wood using the modified Ramberg–Osgood equation for radial and tangential direction [124]

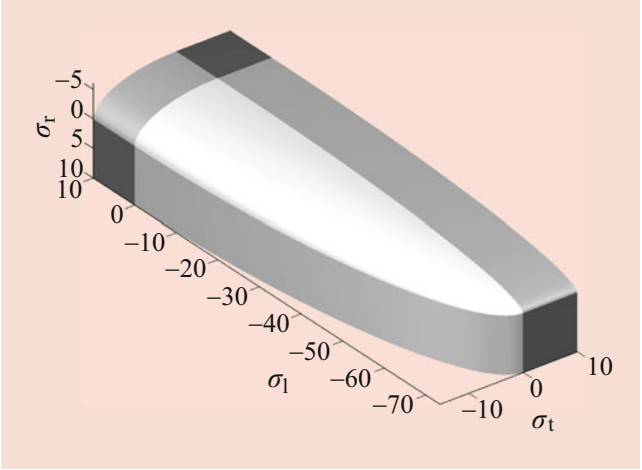

Fig. 9.37 Yield surface of the multi-surface plasticity model for beech, moisture content 8.7% [124]

9.5.3 Tensile Strength

Influence of Scaling on the Measurement Result

Wood has an extremely high strength in fiber direction owing to the parallel cellulose molecules. Thus, a tensile strength of 200–1300 MPa is found on wood fibers (calculated on the cell-wall surface, without lumen) [13]. Keunecke [54] found similarly high values for spruce and yew. Whereas a tensile strength of about 80–90 MPa is achieved for clear spruce wood and about 100 MPa for yew, the strength of the individual fibers (related to the cell-wall surface) are about 1000 MPa (spruce) and 800 MPa (yew). Under load, a significant influence of the microfibril angle as well as an interaction between the structural elements can be seen (e.g., fiber bridging in TR or RT direction (Fig. 9.19), influence of rays). The different microfibril angle has a significant effect on ultimate strength, modulus of elasticity, and elongation at break (Fig. 9.38, Table 9.16). The elongation at break is considerably higher for single fibers than for wood.

According to Kollmann and Côté [13], Meyer and Mark [125] already calculated a theoretical tensile strength of 8000 MPa for cellulose molecules that are considered endless. This strength is higher by a factor of about 100 than that of wood and shows the clear influence of the hierarchical level. The elastic properties of cellulose (modulus of elasticity) are by a factor of 10 higher than those of wood (Table 9.17). In Table 9.18, Persson [126] specifies the parameters of the basic components cellulose, hemicellulose, and lignin from spruce wood.

Testing is carried out today on the following size scales (large to small):

- Full-size members (components)
- Small defect-free samples
- Tissue structures
- Cell structures (fibers)
- Cell-wall structure
- Biochemical level

There has been little research on the interaction of the structural elements in the wood tissue ; in general, the laws of fiber composites can be applied. In situ measurements in the synchrotron offer first insights [52, 53]. Influencing factors such as water, or the effect of the extractives or of the wood cell rays are still under-studied. Burgert [56] indicates

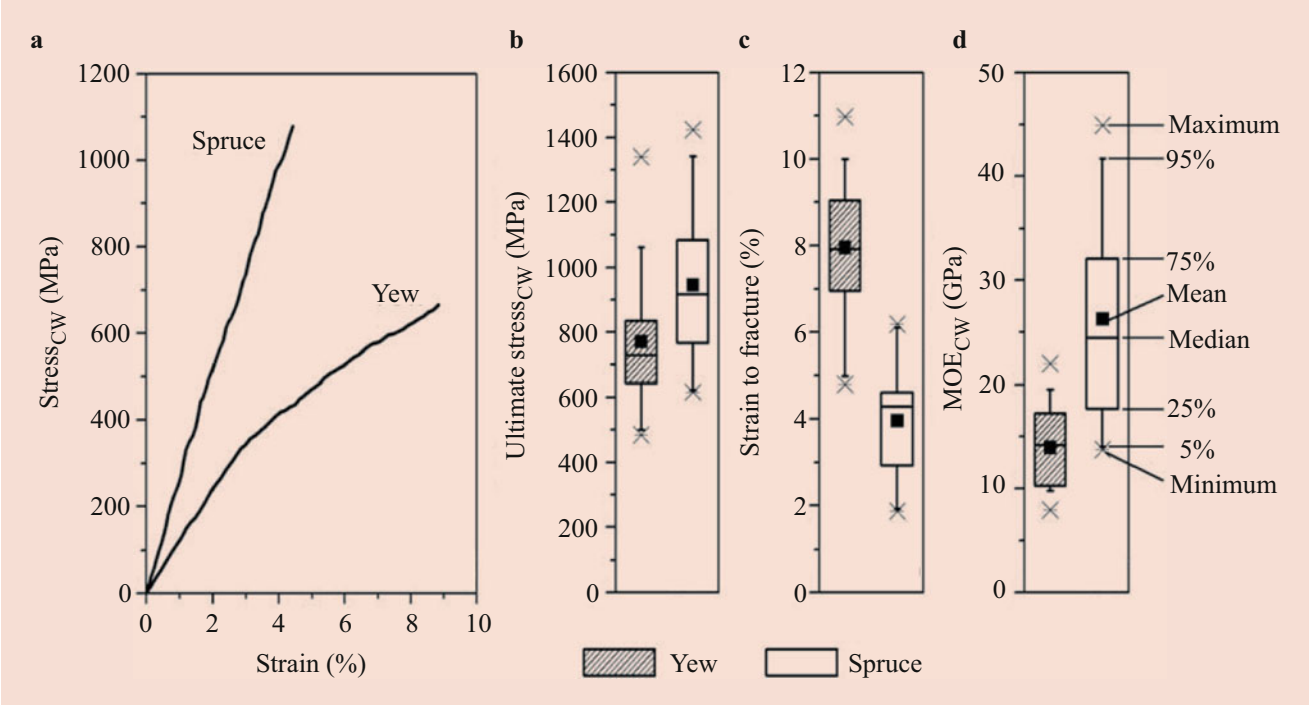

Fig. 9.38 Longitudinal tension of yew and spruce fibers calculated on the cell-wall cross-sectional area (cw), without lumen. (**a**) Stress–strain diagram. (**b**) Ultimate stress. (**c**) Elongation at break. (**d**) Modulus of elasticity. Microfibril angle: spruce 0–5°, yew 15–20° [54]

Table 9.16 Mechanical properties (mean values) of the modulus of elasticity (MPa) of yew and spruce at different structural levels [54]

	Fibers		Tissues		Small clear samples	
Species	Calculated based on cell-wall area	Calculated on total cross-section	Calculated based on cell-wall area	Calculated on total cross-section	Calculated based on cell-wall area	Calculated on total cross-section
Yew	13,900	n.t.	15,600	7000	14,300	9700
Spruce	26,200	n.t.	29,400	9900	28,100	12,100

n.t., not tested

Table 9.17 Modulus of elasticity and strength of wood

Sample	MOE (MPa)	Strength (MPa)
Full-size members, board, beam	11,000	25
Small, clear specimens	11,000	90
Mechanically separated single fiber (based on external volume)	40,000	400
Fibril aggregates	70,000	700
Crystalline areas	130,000–250,000	8000–10,000

According to Mitchell, cited in Zimmermann [127]

that the radial modulus of elasticity of the wood rays is 10 times greater than the radial modulus of elasticity of the axial tissue (fibers, vessels, axial parenchyma). The wood rays thus influence the mechanical properties and the swelling considerably. However, the influence of wood rays has so far been largely neglected in the numerous studies on modeling of wood properties [126, 128, 129]. In addition to the

Table 9.18 Stiffness coefficients of the chemical constituents cellulose, hemicellulose, and lignin of spruce wood used for modeling [126]

Parameter	Mean value (MPa)
Cellulose	
E_{11}	150,000
E_{22}	17,500
G_{12}	4500
μ_{21}	0.01
μ_{32}	0.50
Hemicellulose	
E_{11}	16,000
E_{22}	3500
G_{12}	1500
μ_{21}	0.10
μ_{32}	0.40
Lignin	
E	2750
μ	0.33

Indices: 1: in the longitudinal direction; 2: in a transverse direction; 3: in a transverse direction, perpendicular to 2; for Poisson's ratio: 2nd index in the direction of a transverse contraction

wood rays, the honeycomb structure of the cells has a significant influence [130].

Additionally tested are boards and beams (stress grading, see ▶ Chaps. 19 and ▶ 20). This test is of practical importance, above all in timber construction, in the dimensioning of glued-laminated timber. The test result is strongly influenced by wood defects such as knots and cracks, grain deviation, as well as the growth rings. The test is specified in EN 408.

In wood-based materials, the transverse tensile strength is an important quality factor for the bond quality. On particle board and fiberboard, the tensile strength perpendicular (internal bond) to the board plane is determined according to EN 319 in order to control the quality of the gluing. The determination of the tensile strength of particle boards used in humid conditions according to EN 312 is of similar significance. The tensile strength perpendicular to the plane after boiling for 2 h in water is an indicator of the weather resistance of the boards (former V 100).

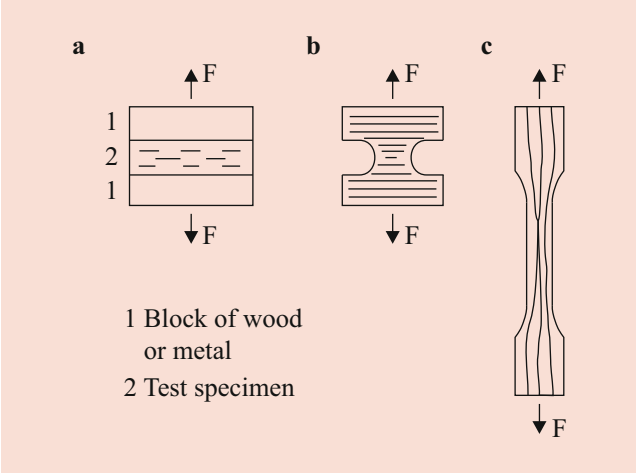

Fig. 9.39 Testing of the tensile strength of wood and wood-based materials (**a**, **b**) perpendicular to the fiber or to the plane and (**c**) parallel to the fiber or to the plane

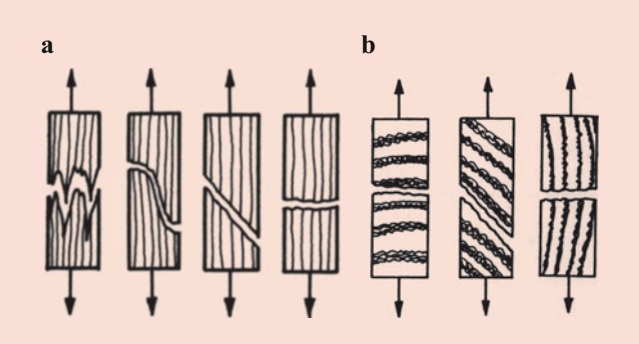

Fig. 9.40 Typical failure of small clear wood in tension (**a**) in fiber direction and (**b**) perpendicular to the grain according to Bodig and Jayne [7]

Strength Parallel and Perpendicular to the Fiber

Parameters

The tensile strength is the resistance of wood or wood-based materials to breakage under tensile stress.

By definition:

$$\sigma_{tU} = \frac{F}{A} \tag{9.28}$$

σ_{tU} – Tensile strength (Pa)
F – Ultimate load at fracture (N)
A – Fracture area (cross-sectional area; m^2)

Testing Methods

The tensile strength can be determined:

- Parallel to the grain (in fiber direction) or parallel to the board plane or
- Perpendicular to the grain/fiber (e.g., in radial or tangential direction) or perpendicular to the plane (Fig. 9.39)

The determination of the tensile strength of wood parallel to the fiber (Fig. 9.39c) is carried out on small, clear (defect-free) specimens, e.g., according to ISO 13061-6 or DIN 52188. Perpendicular to the fiber, either the specimen is shaped according to Fig. 9.39a or in a constricted way as in the tensile test in fiber direction (Fig. 9.39b). For tensile specimens often the so-called dog bone sample is also used (constriction in the middle area) [18, 131]. Figure 9.40 shows typical failures parallel and perpendicular to the fiber at tension.

Influencing Factors and Material Parameters

Important factors influencing the tensile strength are:

- The density: as the density increases, the tensile strength increases
- The grain angle: as the grain angle increases, the tensile strength decreases. The tensile strength perpendicular to the fiber direction is only 3–4% of the longitudinal tensile strength [34]:

$$\sigma_{tU\varphi} = \frac{\sigma_{tU\parallel} \cdot \sigma_{tU\perp}}{\sigma_{tU\parallel} \cdot \sin^n \varphi + \sigma_{tU\perp} \cdot \cos^n \varphi} \tag{9.29}$$

φ – Grain angle
n – 1.5 . . . 2.0

Table 9.19 Strength (MPa) parameters of wood and wood-based materials

Material	Bending strength	Tensile strength in grain/plane direction	Tensile strength perpendicular to the grain/plane	Compression strength in grain/plane direction	Compression strength perpendicular to the grain/plane
Particleboard	15 . . . 25	8 . . . 10	0.35 . . . 0.4	8 . . . 16	–
Plywood	30 . . . 60	30 . . . 60	–	20 . . . 40	–
High-density fiberboard	45 . . . 50	20 . . . 24	0.8 . . . 1.0	23 . . . 26	–
Norway spruce	78	90	2.7	43	5.8
Scots pine	87	105	3	55	7.7
Black poplar	60	67	2.3	34	–
European oak	94	90	4	60	11
Common ash	120	165	7	52	11
Bamboo [132]	84. . .270	–	–	20. . .40	–

$\sigma_{tU||}$ – Tensile strength parallel to the fiber (Pa)
$\sigma_{tU\perp}$ – Tensile strength perpendicular to the fiber (Pa)

- The cutting direction (angle in the RT plane): the tensile strength is radially larger than tangential (generally radial about twice as large as tangential), a minimum is located at about 45°
- Knots and cracks: knots and cracks cause a strong decrease in the tensile strength. Wood with knots only has a tensile strength of 15–20% of the tensile strength of wood without knots
- The moisture content: with increasing moisture content, the tensile strength initially increases from the dry state – maximum at 5–10% – and then falls until the fiber saturation point is reached; each 1% change in humidity reduces the tensile strength by about 3%
- The temperature: with increasing temperature the tensile strength decreases

For particle board, the particle geometry, the density and the solid resin content are of crucial importance for the tensile strength perpendicular to the board plane. Values of the tensile strength of wood and wood-based materials are given in Table 9.19.

Breaking Length

The breaking length (usually in km) is the length of a test specimen, in which it would rupture by its own weight. It is used in particular in paper and textile technology.

$$L_R = \frac{\sigma_{tU}}{\rho \cdot g} \tag{9.30}$$

L_R – Breaking length (m)
ρ – Density (kg m^{-3})
g – Acceleration of gravity (m s^{-2})

For oak a density of 690 kg m^{-3} and a tensile strength in grain direction of 90 MPa result in a breaking length of 13.3 km in fiber direction, for balsa a density of 140 kg m^{-3} and a tensile strength of 73 MPa result in a breaking length of 53.2 km.

9.5.4 Compression Strength

Parameters

Compression strength is the resistance of wood or wood-based materials against breakage under compressive stress parallel or perpendicular to the fiber direction or board plane. Its results are calculated from the maximum breaking load (ultimate stress) and the cross-sectional area.

$$\sigma_{cU} = \frac{F}{A} \tag{9.31}$$

σ_{cU} – Compression strength (Pa)
F – Ultimate stress (or stress at defined strain when loaded perpendicular to the fiber or board plane) (N)
A – Cross-sectional area (m^2)

Testing Methods

The compression strength of wood is tested, e.g., according to DIN 52185 (parallel) or DIN 52192 (perpendicular to the grain). Figure 9.41 shows schematically the basic possibilities of testing the compressive strength. Thereby, the tests with local loads are used, e.g., to evaluate compression strength for a rail situation (bar pressure) [133].

A pressure load parallel to the grain or parallel to the board plane results in a clear failure of the structure of the test specimen. The fracture pattern is very strongly influenced by the structure of the test specimen, especially in wood-based materials. Figure 9.42 shows the typical fracture patterns of wood.

In the case of compressive stress perpendicular to the grain or board plane, the load can be applied over the entire sample cross-section (Fig. 9.41) without a definitive break occurring. The structure of the specimen is only compressed (densified).

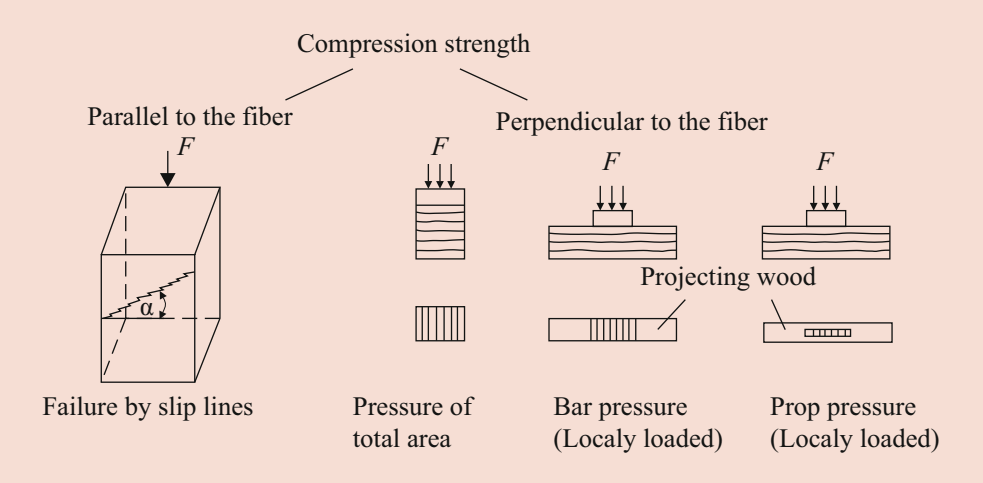

Fig. 9.41 Principle of testing the compression strength of wood and wood-based materials

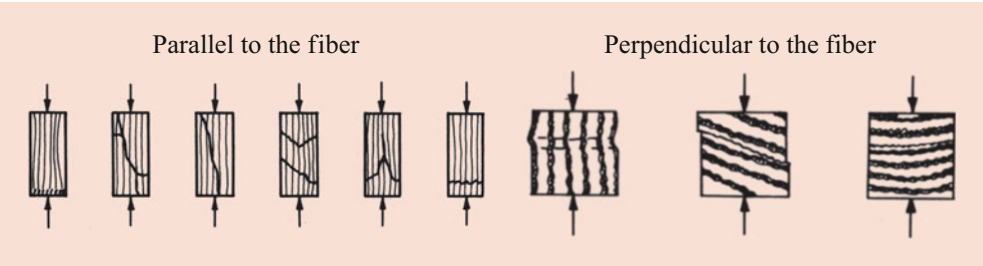

Fig. 9.42 Typical fracture patterns in testing the compressive strength of wood and wood-based materials (Bodig and Jayne [7])

As a measure of compressive strength, therefore, the yield point is used, which marks the point at which the deformation of the test specimen greatly increases on the stress–strain diagram (e.g., 1% (EN 408), 2% or 5% compaction). Perpendicular to the grain direction, plastic deformation occurs under compressive loading.

Influencing Factors and Material Parameters

Key factors influencing the compression strength are:

- The density: as the density increases, the compression strength increases (Fig. 9.43)
- The wood species: it influences the compression strength indirectly via the density as well as the structural parameters such as fiber length, lignin content, and latewood content
- The grain angle: as the grain angle increases, the compression strength decreases. According to Hankinson [34] (see also ▶ Chap. 8):

$$\sigma_{cU\varphi} = \frac{\sigma_{cU\parallel} \cdot \sigma_{cU\perp}}{\sigma_{cU\parallel} \cdot \sin^n \varphi + \sigma_{cU\perp} \cdot \cos^n \varphi} \qquad (9.32)$$

φ – Grain angle
n – 2.0. . .2.5
$\sigma_{cU\parallel}$ – Compression strength in grain direction (Pa)
$\sigma_{cU\perp}$ – Compression strength perpendicular to the grain (Pa)

- Deviations from the microstructure: uneven structure, knots, cracks, etc., strongly influence compression strength
- The moisture content: as the moisture content increases, the compression strength decreases (Fig. 9.43)
- The temperature: as the temperature increases, the compression strength decreases

Reference values of the compression strength of solid wood and wood-based materials are shown in Table 9.19. In solid wood, the tensile strength is about twice as high as the compressive strength; for particle materials, the compression strength is equal to or greater than the tensile strength.

9.5.5 Bending Strength (Modulus of Rupture)

Parameters

The bending strength is the resistance of wood and wood-based materials against failure under bending stress. It is a frequently used material characteristic for wood and wood-based materials, which is defined as follows:

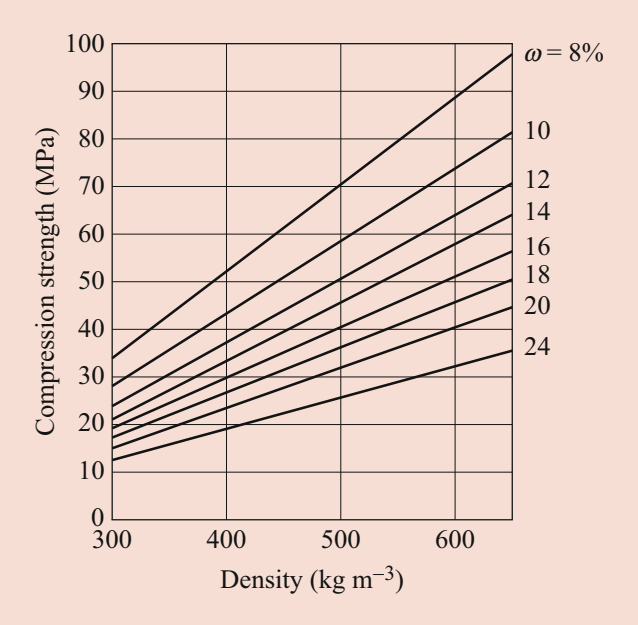

Fig. 9.43 Influence of density and moisture content on compression strength of white pine (*Pinus sabiniana* Dougl.) in grain direction [134]

$$\sigma_{bU} = \frac{M_b}{W_b} \qquad (9.33)$$

σ_{bU} – Bending strength (Pa)
M_b – Bending moment (N m)
W_b – Section modulus (m^3)

Testing Methods

Bending strength is determined for solid wood according to DIN 52186 and for particle board according to EN 310. Figure 9.44 shows schematically the test arrangement for three- and four-point bending, and Fig. 9.45 shows typical fracture patterns of wood. The stress distribution over the sample cross-section in wood is illustrated in Fig. 9.46.

A linear stress distribution occurs only as long as the proportional limit is not exceeded. At higher loads, there is a non-uniform distribution of the stress across the sample cross-section. This is due to the differences in stress–strain behavior and the large difference in tensile and compressive strength.

In the pressure-loaded area of the bending beam, the stress increases up to the ultimate compression strength; on the tension-loaded side the stress increases further and approaches the ultimate tensile strength. The neutral axis is therefore shifted toward the tensile zone as the load increases. If the wood is without defects (e.g., knots), the bending strength will be between tensile and compression strength. Knots often provoke premature breakage in the tension zone.

For particle board and MDF, there is no displacement of the neutral axis (Fig. 9.47a). This can also be proven by metrology [135], than tensile and compression strength

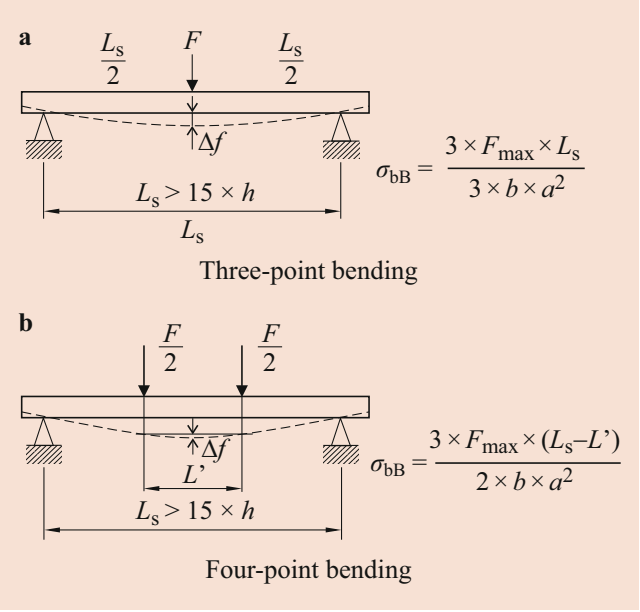

Fig. 9.44 Setup for bending strength testing

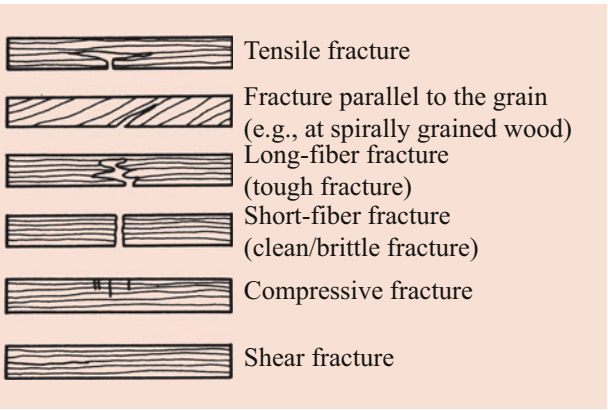

Fig. 9.45 Typical fracture patterns when testing bending strength of solid wood

have similar values; sometimes compression strength is slightly higher.

The bending strength of particle board and MDF is generally greater than their tensile and compression strength (Table 9.19). The reason for the greater bending strength is mainly attributed to plastic deformation during failure [136]. If the tensile strength perpendicular to the plane of the board (internal bond) is low, shear fracture occurs during bending stress (shearing of the middle layer).

In the case of plywood, assuming a constant elongation in the bonded veneer layers, low tension occurs owing to the bearing of the veneer layers in the layers perpendicular to the load direction (Fig. 9.47b). The outer fiber strain in the bending test can be calculated according to Eq. 9.34 (DIN 53452).

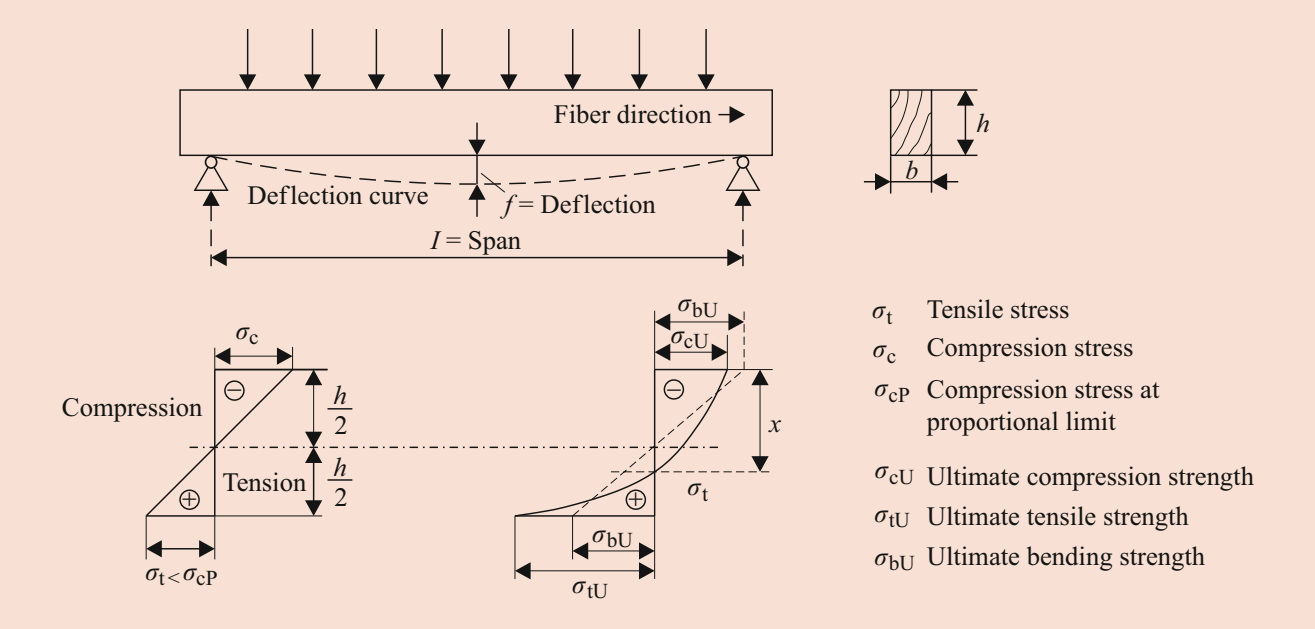

Fig. 9.46 Stress distribution over the wood cross-section when bending wood as a function of the load (left: low load below the proportional limit, right: high load well above the proportional limit)

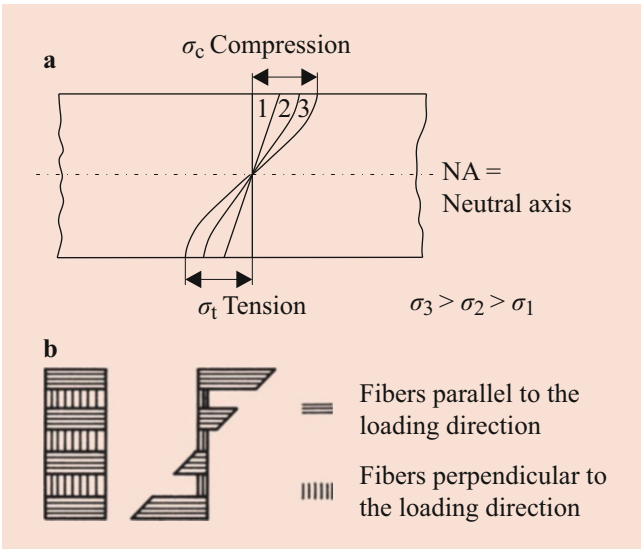

Fig. 9.47 Stress distribution across the cross-section of plate-shaped wooden materials when bent as a function of the load (1–3: load increasing with increasing numbers). (**a**) particle board/medium-density fiber board. (**b**) Plywood/cross-laminated timber

$$\epsilon = \left[\frac{(600 \cdot h)}{l_s^{\,2}}\right] \cdot f \qquad (9.34)$$

f – Deflection in the center of the sample (m)
h – Sample thickness/sample height (m)
l_s – Span (m)

Influencing Factors and Material Parameters

Essential influencing factors of bending strength of wood are:

- The density: as the density increases, the flexural strength increases
- The grain angle: an increase in the grain angle causes a decrease in bending strength. Even an angle of 15° causes a drop in strength to around 60%. In this case, according to Hankinson [34]:

$$\sigma_{bU\varphi} = \frac{\sigma_{bU\parallel} \cdot \sigma_{bU\perp}}{\sigma_{bU\parallel} \cdot \sin^n\varphi + \sigma_{bU\perp} \cdot \cos^n\varphi} \qquad (9.35)$$

φ – Grain angle
n – 1.5. . .2.0
$\sigma_{bU\parallel}$ – Bending strength in grain direction ($\varphi = 0°$; Pa)
$\sigma_{bU\perp}$ – Bending strength perpendicular to the grain ($\varphi = 90°$; Pa)

- Knots/cracks: knots cause a strong decrease in bending strength
- The moisture content: an increase in moisture content causes a significant reduction in bending strength. When the moisture content increases by 1%, bending strength is reduced by approximately 4%
- The temperature: the bending strength decreases with increasing temperature

For particle board, the particle geometry, the density, and the density profile are decisive for the bending strength. Similar to solid wood, changes in the climate affect bending

strength. Reference values for the bending strength of wood and wood-based materials are given in Table 9.19.

9.5.6 Shear Strength

Parameters

Shear strength parallel to the grain is related to torsional properties. Shear is complicated, mostly superposed by bending or compression [13]. Keylwerth (1945), cited in Kollmann and Côté [13] specifies 18 possible load cases. In the cross-cut plane (plane of shearing) shear is very difficult to test owing to a strong wood densification perpendicular to the grain.

Shear strength is the resistance that a body opposes to the displacement of two adjacent surfaces where:

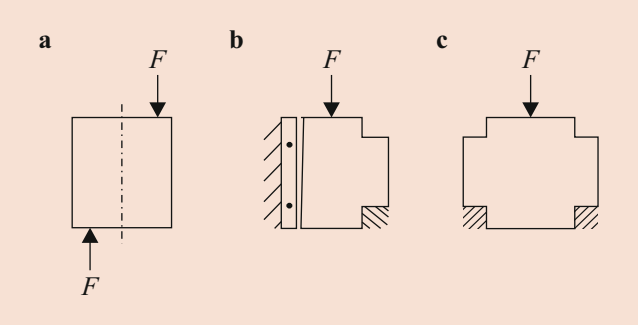

Fig. 9.48 Testing the shear strength of wood and wood-based materials

$$\tau = \frac{F}{A} \tag{9.36}$$

τ – Shear strength (Pa)
F – Ultimate load (N)
A – Shear area (m^2)

Testing Methods

On solid wood, shear strength is determined according to DIN 52187, on particle board (and analogous on OSB and MDF) according to DIN 52367 (see also Dunky and Niemz and Schulte [39, 137]). Figure 9.48 shows possible test specimen shapes for solid wood and Fig. 9.49 the different test orientations.

Based on the shape of the test specimen, more or less strong secondary stresses (bending, tensile, compression) occur apart from shear stresses, so that the measurement result is not always clear. Shear stresses also occur in glued joints and in wood joints such as finger joints.

Main Influencing Factors of the Shear Strength

The cutting plane and grain direction (important planes of shearing are shown in Fig. 9.49, a complete overview is included in Kollmann and Côté [13]) are the main influencing factors of shear strength. The shear strength parallel to the grain of the wood is greater than that perpendicular to it (Fig. 9.50). Vorreiter [134] gives the ratio $\tau_{\parallel}/\tau_{\perp}$ of 1.2 to 1.6. For shear stress parallel to the grain, a distinction must be made between a tangential and a radial course. In practice,

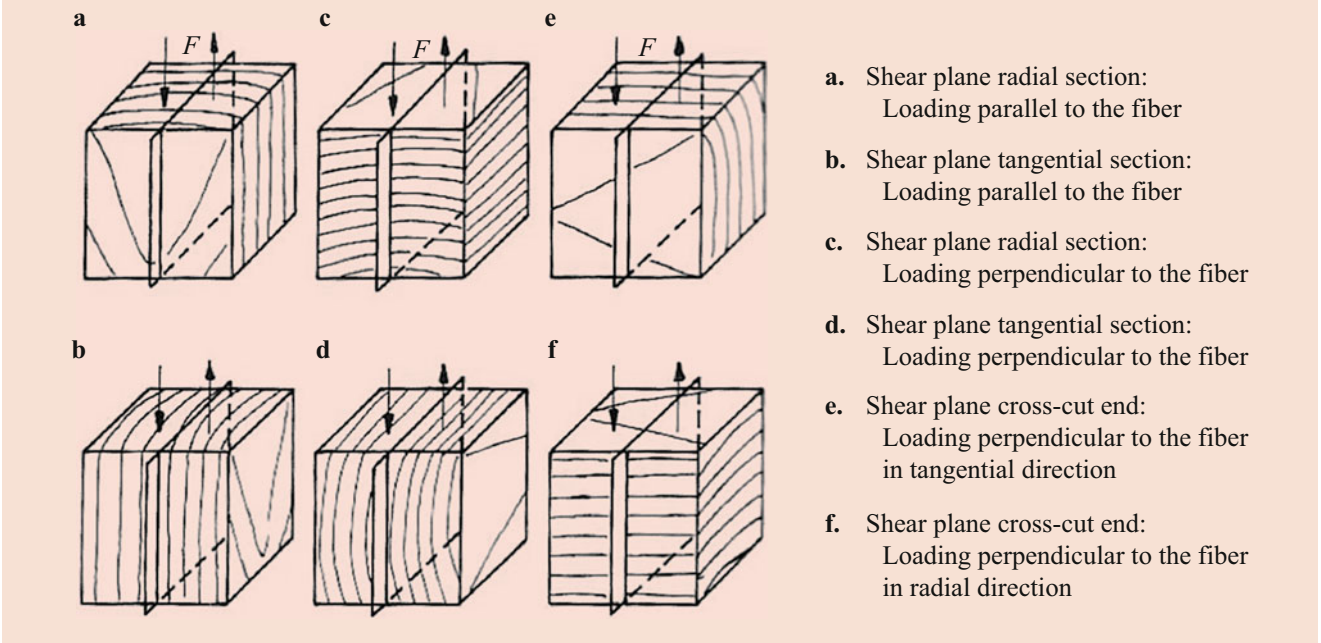

a. Shear plane radial section:
Loading parallel to the fiber

b. Shear plane tangential section:
Loading parallel to the fiber

c. Shear plane radial section:
Loading perpendicular to the fiber

d. Shear plane tangential section:
Loading perpendicular to the fiber

e. Shear plane cross-cut end:
Loading perpendicular to the fiber
in tangential direction

f. Shear plane cross-cut end:
Loading perpendicular to the fiber
in radial direction

Fig. 9.49 Selected load directions when testing the shear strength of solid wood

the mean value from both directions is usually tested and used. The shear strength in the tangential plane of shearing in the majority of cases is greater than that in the radial plane of shearing owing to the influence of the rays (shearing applies in a radial plane parallel to the rays (weakening) and in tangential plane perpendicular to the rays (strengthening)). For the influence of the grain angle the following applies:

$$\tau_\varphi = \frac{\tau_\parallel \cdot \tau_\perp}{\tau_\parallel \cdot \sin^n \varphi + \tau_\perp \cdot \cos^n \varphi} \qquad (9.37)$$

φ – Grain angle
n – 2.5. . .3.0

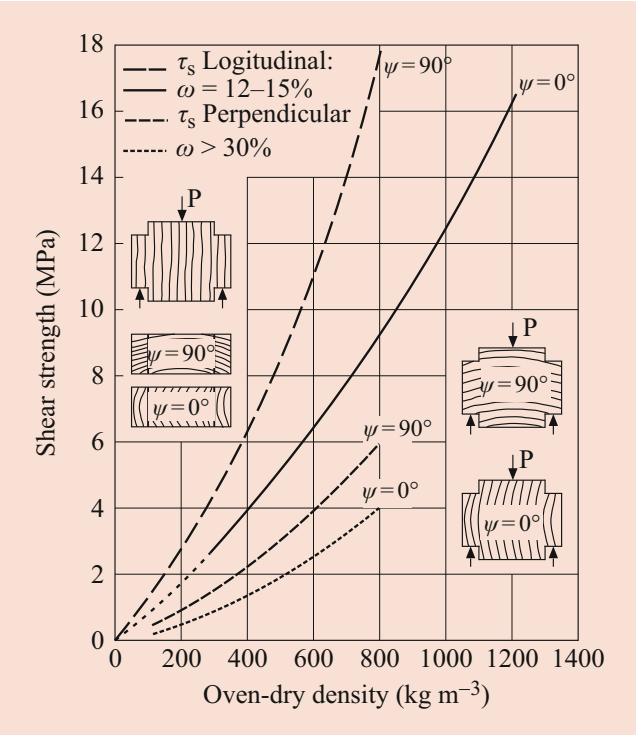

Fig. 9.50 Influence of density on the shear strength of solid wood [134]

$\tau_\parallel$ – Shear strength parallel to the grain (Pa)
$\tau_\perp$ – Shear strength perpendicular to the grain (Pa)

- The density: as the density of the wood increases, the shear strength increases
- The moisture content: a moisture content of up to about 5% increases the shear strength of the wood and then it falls until it reaches the fiber saturation point

The shearing properties of particle boards are significantly influenced by particle geometry, density, and solid resin content [138]. Extensive investigations into particle boards were carried out by Kruse [139]. Shear strength values of selected wood species are shown in Table 9.20.

9.5.7 Torsional Strength

Parameters/Testing Methods

The torsional strength is the resistance that a rod (beam) opposes to breakage by twisting. Figure 9.51 shows schematically the test carried out on a cantilever rod. The rod can be stressed to torsion parallel or perpendicular to the fiber direction. The stress parallel to the fiber leads to a splitting of the rod in the longitudinal direction.

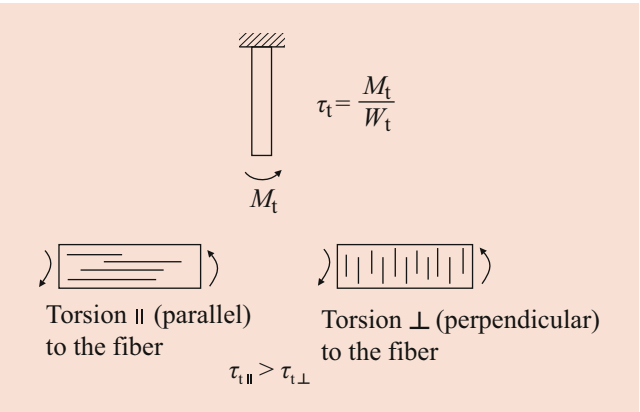

Fig. 9.51 Testing the torsional strength of wood

Table 9.20 Shear strength, torsional strength, and cleavage strength of wood[a, b]

Species	Shear strength (MPa)				Torsional strength (MPa)	Cleavage strength (MPa)	
	$\tau_{\parallel}$ (LT)	$\tau_{\parallel}$ (LR)	$\tau_{\perp}$ (RL)	$\tau_{\perp}$ (TL)	$\tau_{t\parallel}$	σ_s (T)	σ_s (R)
Norway spruce	9.1. . .9.3	9.5. . .10.5	1.8	2.0	9	0.34	0.25
Scots pine	10.0		–	–	16	0.37	0.36
Beech	15.7. . .19.7	12.7. . .14.8	5.7. . .7.6	5.5. . .6.6	15	0.35	0.45
European oak	13.5	12.4	4.9	4.1	20	0.53	0.48
Maple	17.9	14.3	7.3	6.6	26	1.60	1.00
Black poplar	5.0		–	–	–	0.74	0.51

[a]Indices: ∥ parallel to the grain, ⊥ perpendicular to the grain, *L* in fiber direction (longitudinal), *R* radial, *T* tangential; the planes of shearing are indicated in parenthesis (1st index = loading direction)
[b][9, 120, 140–143]

The torsional strength is calculated as follows:

$$\tau_t = \frac{M_t}{W_t} \tag{9.38}$$

τ_t – Torsional strength (Pa)
M_t – Torsional moment (N m)
W_t – Torsion resistance moment (m^3)

Extensive work was carried out, e.g., by Höring, cited in Kollmann and Côté [13] and Chen [144, 145]. If the torsional stress is within Hooke's range, the torsion modulus can also be determined during the test [146]. The following applies:

$$G = \frac{M_t \cdot l}{\varphi \cdot I_t} \tag{9.39}$$

G – Torsion modulus/torsional shear modulus (Pa)
l – Sample length (m)
φ – Angle of twist/torsion angle (–)
I_t – Polar moment of inertia (m^4)

Influencing Factors and Material Parameters

The main influencing factors of the torsional strength are:

- The density: as the density of the wood increases, the torsional modulus increases
- The wood species: hardwood has a higher torsional strength than softwood
- The moisture content: as the moisture content of the wood increases, the torsional strength decreases
- The grain direction
- The cutting direction

Numerical values of the torsional strength of wood are given in Table 9.20.

9.5.8 Cleavage Strength (Splitting Resistance)

Parameters/Testing Methods

Cleavage strength is the resistance of wood against splitting into two parts by wedge-shaped tools or two forces acting perpendicular to the longitudinal axis. Figure 9.52 shows schematically the test arrangement. First works were published by Nördlinger in 1860 (including the test-body shape shown in Fig. 9.52) [147].

Cleavage strength or splitting resistance is determined according to the following relationship:

$$\sigma_{sp} = \frac{F}{b} \tag{9.40}$$

or

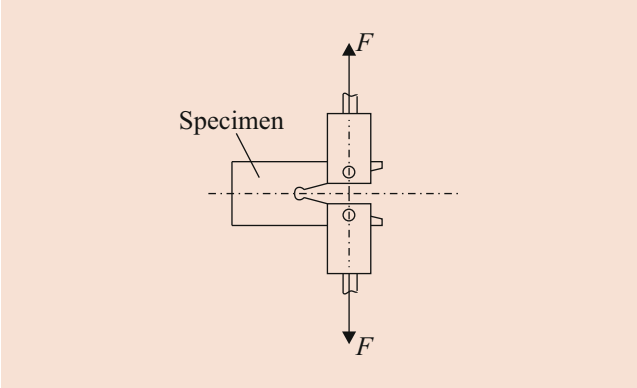

Fig. 9.52 Specimen for the cleavage test

$$\sigma'_{sp} = \frac{F}{l \cdot b} \tag{9.41}$$

σ_{sp} – Cleavage strength (N m^{-1})
σ'_{sp} – Cleavage strength (Pa)
F – Ultimate load (N)
l – Sample length (m)
b – Sample width (m)

Partially, the reciprocal of the cleavage strength – also referred to as cleavability – is used. Wood with a high cleavage strength is therefore difficult to split.

Influencing Factors and Material Parameters

The cleavage strength is significantly influenced by the angle at which the splitting plane runs to the grain or ring angle (Fig. 9.53).

The lowest cleavage strength is in the radial direction, where the cleavage plane runs in the direction of the wood rays. Wood with broad rays usually has a lower cleavage strength than wood with small rays. As the density increases, the cleavage strength in hardwoods increases to a greater extent than in softwoods. From oven-dry to a moisture content of 12–17%, the cleavage strength increases; above this moisture content it decreases. Deviations such as branches or a disturbed fiber profile can significantly increase cleavage strength. Values and categories of cleavage strength of wood are given in Tables 9.20 and 9.21.

9.5.9 Nail and Screw Withdrawal Resistance

Parameters and Testing

The withdrawal resistance of nails and screws is an important feature for the processing of wood and wood-based materials. The screw withdrawal resistance is the ultimate load required to pull out a screw in relation to the screw-in depth (N m^{-1}).

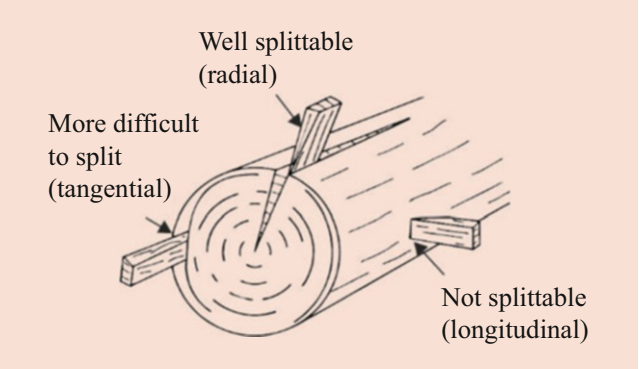

Fig. 9.53 Cleavage of wood in the main cutting directions

Table 9.21 Classification of wood and bamboo to cleavage

Degree of cleavage	Species
Completely splittable	Bamboo
Very easy to split	Spruce, poplar, Douglas fir
Splittable	Beech, willow, chestnut, pine, larch, red oak
Difficult to split	Oak, ash, maple, fruit trees
Very difficult to split	Elm, hornbeam, birch
Almost unsplittable	Mountain ash, Queen ebony
Unsplittable	Lignum vitae

Changed according to Mette [148]

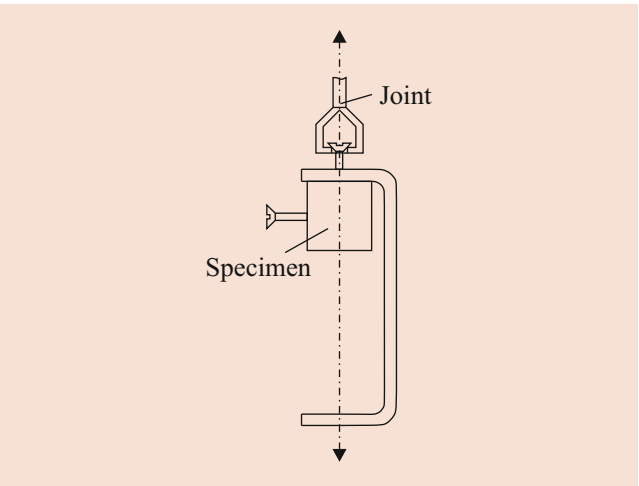

Fig. 9.54 Schematic representation of the test for nail and screw withdrawal

The measurement result obtained depends on the test method (for particle board and fiberboard, for example EN 320:2011, for wood according to EN 1382:2016).

Analogous, the nail pull-out resistance is the force required to extract a nail, based on the cross-sectional area of the nail (Pa) or the impact depth (N m^{-1}). Figure 9.54 shows schematically the test arrangement of screw withdrawal resistance.

Influencing Factors and Material Parameters

The nail and screw withdrawal resistance of wood depends on the density and the cutting direction; in the case of particle materials, it is additionally influenced by the density profile perpendicular to the plane, the type of particles (geometry and size), the solid resin content, and the transverse tensile strength [149]. The impact or screwing direction (parallel or perpendicular to the plane or fiber direction) is also a significant influence on the nail or screw pull-out resistance. In the case of wood, the structure is a decisive influencing factor (for example, the nail or screw withdrawal resistance increases with increasing density. But the shape of the screw and nail also clearly affects the measurement result. Nail and screw withdrawal resistance values of wood and wood-based materials are given in Table 9.22.

9.5.10 Hardness and Abrasion Resistance

Hardness

The hardness is the resistance that wood or wood-based materials oppose to the penetration of a harder body. According to the speed of the build-up of strength, a distinction can be made:

- Static test methods (slow build-up of strength)
- Dynamic test methods (sudden impact)

Static Hardness Test

The hardness test according to Brinell (for wood and wood-based materials according to EN 1534) is the most commonly used static test method. A polished steel ball (diameter 2.5, 5, or 10 mm) is pressed into the sample within a

Table 9.22 Nail and screw withdrawal resistance of wood and wood-based materials

Material (density kg m^{-3})	Nail withdrawal resistance[a] (MPa)		Screw withdrawal resistance[a] (N mm^{-1})	
	Perpendicular	Parallel	Perpendicular	Parallel
Softwood (500)	2.5...4.0	1.5...2.2	80...110	60...80
Hardwood (650...750)	–	–	170...200	100...150
Particleboard (600)	1.2...2.0	0.8...1.5	–	–
Particleboard[b] (650...700)	–	–	50...80	35...60
MDF[b] (730...780)	–	–	55...85	40...70

[a]Perpendicular or parallel to the fiber or to the plane
[b]Tested by means of wood screw, form B (chipboard screw), 4 × 40 mm; pre-drilled: 0.8 × screw diameter [22]

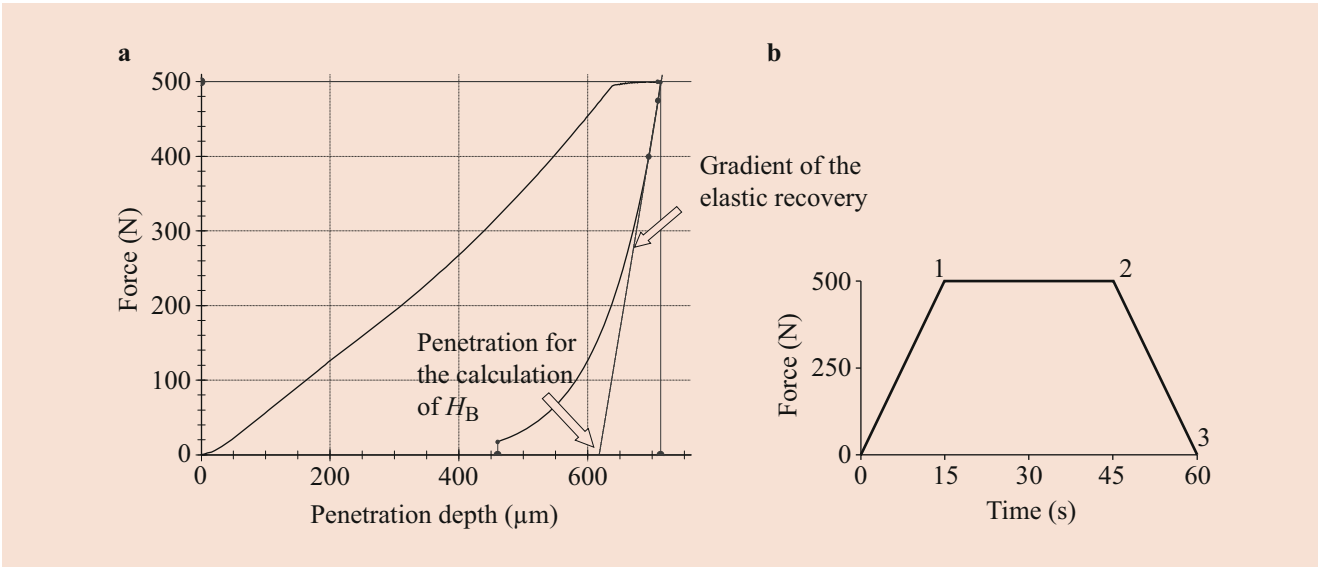

Fig. 9.55 (**a**) Force-penetration depth diagram and (**b**) force-time diagram of Brinell hardness in the instrumented hardness test [151]

certain time with a defined force F (100–1000 N) and the diameter of the indented spherical cap is measured (Fig. 9.55b). From the diameter of the sphere D (mm), the force F, and the diameter of the spherical cup d (mm), the Brinell hardness H_B is then calculated as follows:

$$H_B = \frac{2 \cdot F}{\pi \cdot D \cdot \left(D - \sqrt{D^2 - d^2}\right)} \text{ (MPa)} \qquad (9.42)$$

Often, the hardness is also calculated from the penetration depth h (mm):

$$H_B = \frac{F}{D \cdot \pi \cdot h} \qquad (9.43)$$

Thus, force-deflection diagrams can be evaluated in a similar manner to the micro hardness measurement (nano-indentation) (Fig. 9.55a), see, for example, Wimmer et al. [150]. Detailed explanations are given in Sonderegger and Niemz [151]. A good overview of the hardness of different wood species for parquet is compiled by Schwab [152].

A further method for determining the hardness of wood and wood-based materials is Janka hardness. In this hardness test, a polished steel ball with a diameter of 11.284 mm is pressed continuously up to half-way into the sample. The required penetration force directly indicates the hardness. This method is often used in the USA and South America.

Dynamic Hardness Test

Either a cylindrical steel needle (e.g., in the hardness test according to the Pilodyn method [Proceq, Zurich/Switzerland] or the Mayer–Wegelin method) or a prismatic steel rod of a certain dimension (e.g., 3 × 20 mm in the testing of particle board according to the former factory standard FHIS 255 of today's IHD Dresden) is driven into the sample with a defined energy. Both methods are based on the principle of the rebound test (Schmidt–Hammer), which is used to estimate the quality (and strength) of concrete (EN 12504-2:2012, ASTM C805, ASTM D5873).

When kinetic energy acts on a material, some of that energy is converted (e.g., into heat during deformation). The harder the material is, the less energy is absorbed and transformed into deformation. It should be noted that, depending on the modulus of elasticity of the material, the compressive strength may vary within the same hardness.

Penetration depth and the correlation with the density (and also the tensile strength perpendicular (internal bond) to the plane of particleboard) were investigated, for example, by Walter and Knitsch [153]. The penetration depth correlates with the density and the density with the tensile strength perpendicular to the plane.

The Pilodyn method is used to measure the density of wood [154] or even of standing trees, but also to detect rotting infestation in piles (even under water) [155, 156]. Figures 9.56 and 9.57 show schematically selected test devices. Llana et al. [157] investigated the suitability of the Pilodyn method for evaluating the quality of commercial timber. Also, the screw withdrawal resistance was used for quality assessment of wood.

Influencing Factors and Material Parameters

Essential factors that influence the hardness of wood (Fig. 9.58) are:

Fig. 9.56 Testing devices for the hardness of materials with dynamic methods ((**a**) Pilodyn and (**b**) Schmidt–Hammer, Proceq, Zurich, Switzerland). (Photo P. Niemz)

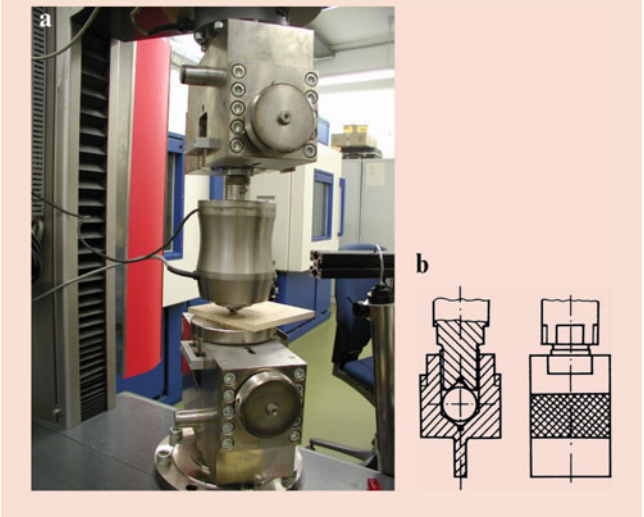

Fig. 9.57 Testing device for measuring the hardness of wood and wood-based materials. (**a**) Determination of Brinell hardness. (**b**) Determination of the surface hardness of wood particle materials (former factory standard FHIS 255, IHD Dresden). (Photo: P. Niemz, ETH Zurich)

- Wood species, in particular their density: as the density increases, the hardness increases and the penetration depth under constant load decreases. See also Niemz and Sonderegger [8]
- Cutting direction: end hardness (hardness of end-grain wood, i.e., load parallel to the fiber) is up to 2.5 times greater than side hardness (load in a radial or a tangential direction)
- Moisture content: the hardness increases with decreasing moisture content, the maximum value is reached at the oven-dry state
- Lignin and resin content
- Test load: the wood is compacted during the test and the hardness increases with compaction

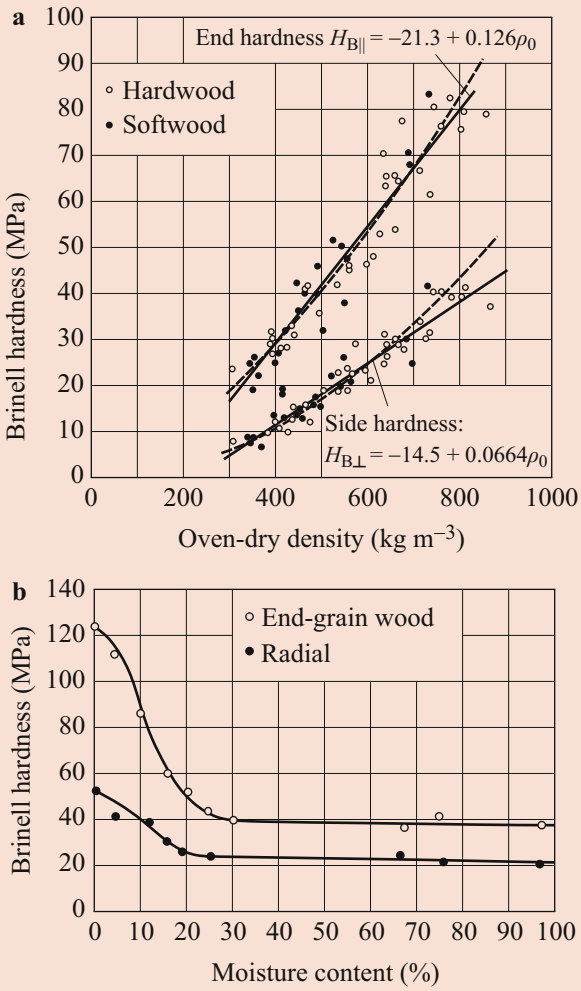

Fig. 9.58 Influence of (**a**) oven-dry density and (**b**) moisture content on Brinell hardness of wood [11]

Table 9.23 gives information on the moisture dependence of Brinell hardness on selected wood species and wood-based materials, and Table 9.24 shows a classification of the wood species according to the hardness. According to Koch et al. [132], bamboo with a density between 500 and 900 kg m^{-3} has a Brinell hardness of 60–80 MPa and a Janka hardness of 17–25 kN.

Abrasion Resistance

Sandblast

In this method, sand of a certain particle size is applied to a defined sample surface by means of a sandblast blower and the loss of mass (in g cm^{-2}) or volume loss (in cm^3) resulting from removal is measured. Owing to the differences in hardness between early- and latewood, there is an uneven removal over the sample surface (greater removal of the less dense

Table 9.23 Brinell hardness H_B perpendicular to the fiber/board plane of selected wood species and wood-based materials depending on moisture according to Sonderegger and Niemz [151, 158]

Species/material	Density (kg m^{-3})	$H_{B,35}$ (MPa)	$H_{B,65}$ (MPa)	$H_{B,80}$ (MPa)
European larch	620...650	36	31	25
Scots pine	510...570	21	20	17
European beech	690...750	41	32	26
European oak	670...690	35	30	24
Red iron wood (Bongossi)	1030...1110	99	73	62
Makassar ebony	1150...1180	109	94	72
Plywood (beech)	730...780	27...32	26...30	24...26
Particleboard 6 mm	760	21	19	14
Particleboard 10–19 mm	630...700	21...25	18...22	15...17
Particleboard 25–40 mm	610...620	28...30	26...28	18...19
OSB	620...650	29...35	28...32	19...25
MDF, 3–6 mm	830...840	35...41	31...39	25...27
MDF, 10–25 mm	730...800	28...62	26...56	19...39
MDF, 40 mm	760	87	81	50
Low-density fiberboard	530	19	17	13

Index: 35, 65, 80 = Brinell hardness at different moisture content, e.g., after conditioning at 20 °C and relative humidities of 35%, 65%, and 80%
OSB, oriented strand board; MDF, medium-density fiberboard

Table 9.24 Classification of wood by hardness according to Kollmann [11], classification based on Nördlinger [147]

Oven-dry density (kg m^{-3})	Hardness classes after Brinell–Mörath	Janka Hardness $H_{J\parallel}$ (MPa)	Brinell hardness $H_{B\parallel}$ (MPa)	Brinell hardness $H_{B\perp}$ (MPa)	Species
200...550	Very soft	< 35	10...40	5...20	Yellow pine, willow, lime, aspen, poplar
350...650	Soft	35...50	20...60	10...30	Norway spruce, silver fir, larch, Scots pine, Douglas fir, common birch, alder
500...700	Medium hard	50...65	40...65	20...40	Elm, chestnut, European oak, European plane, walnut, pitch pine
600...920	Hard	65...100	60...100	30...60	Yew, beech, ash, robinia, hornbeam, fruit trees
900...1050	Very hard	100...150	100...130	50...80	Boxwood, privet, lilac
1000...1400	As hard as bone	> 150	120...200	70...140	Tropical wood species such as lignum vitae, ebony

$\parallel$ loaded parallel to the fiber (end hardness), $\perp$ loaded perpendicular to the fiber (side hardness)

early wood); there are also differences among the three main cutting directions of the wood. According to studies by Schulz [159] hardwood and softwood show characteristic hardness profiles during sandblasting, which can complement the usual structuring in tree rings, earlywood and latewood, or growth ring zones.

Thus, after sandblasting in cross-section, wooden parts become visible that probably contribute to the strength formation of the wood (mechanical systems in the radial direction, Fig. 9.59). It is assumed that the particular wood species build up different mechanical systems and that these vary in wood formation depending on the requirements.

Sanding Resistance Method

The sanding method allows a more practical testing of the abrasion resistance than sandblasting. In this case, as shown in Fig. 9.60, the abrasion of a specimen is determined after a defined number of sanding movements over the specimen.

This test method is used for both wood and wood-based materials. Parameters are:

(a) *The abrasion coefficient related to the dimension of the test specimen* t_a

$$t_a = a \cdot \frac{m_1 - m_2}{m_1} \tag{9.44}$$

or

(b) *The mass-related coefficient of abrasion* t_m

$$t_m = \frac{m_1 - m_2}{m_1} \tag{9.45}$$

a – Thickness of the test sample (mm)
m_1 – Mass of the test sample before the test (g)
m_2 – Mass of the test sample after the test (g)

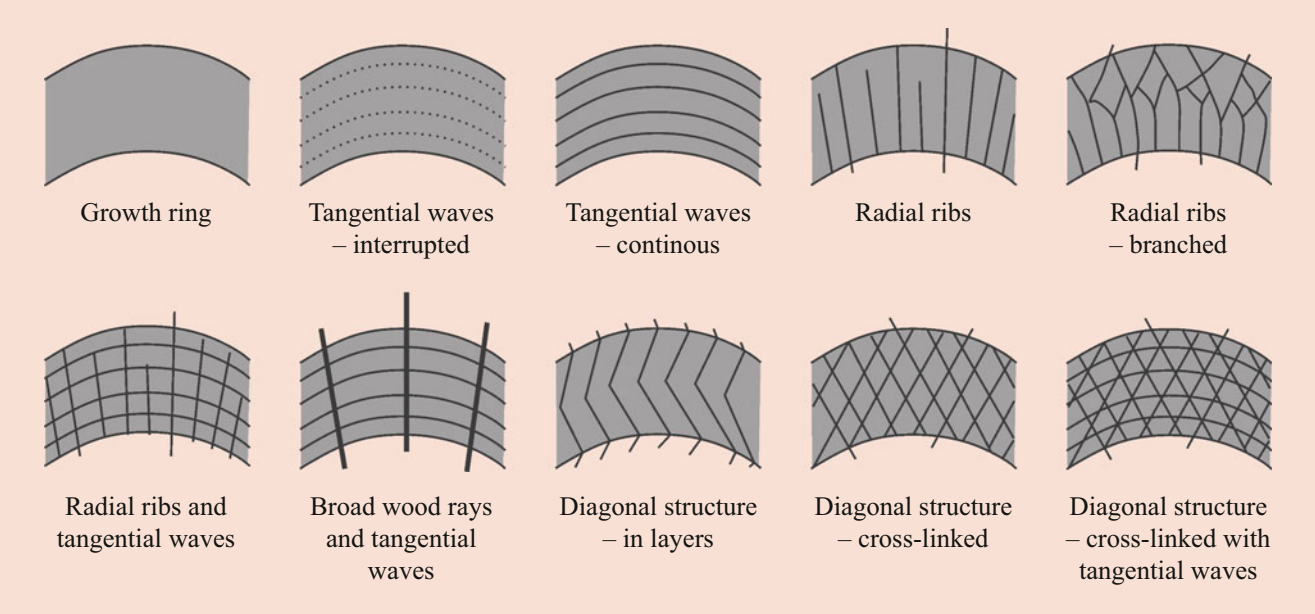

Fig. 9.59 Hardness patterns in cross-sections of hardwoods and conifers in a simplified provisional representation [159]

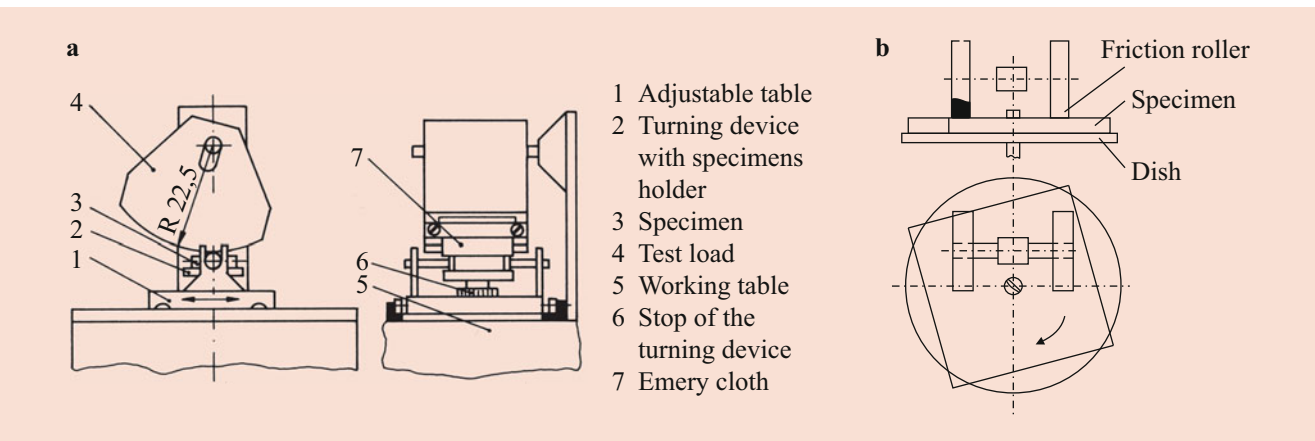

Fig. 9.60 Determination of the abrasion index of (**a**) wood and (**b**) coated surfaces

The abrasion resistance can also be determined by a roll of two abrasives covered with abrasive paper on the specimen surface. For example, the "Taber Abraser" (measuring coated materials) is used for this test. The characteristic used is, for example, the abrasion index in *g*/100 revolutions. Thus, laminate flooring is, for example, tested to EN 13329, HPL to EN 438 T 2.

Influencing Factors and Material Parameters

The abrasion resistance of wood is significantly influenced by the following parameters:

- The density (abrasion resistance increases with increasing density)
- The moisture content
- The cutting direction (abrasion resistance is significantly greater in the radial and tangential directions than on the cross-section [in the fiber direction])

Also, the relation of the abrasion resistance of different wood species to a specified species is used. For example, Mette [148] relates the values to beech (Table 9.25).

9.5.11 Impact Bending Strength

Impact bending strength is related to the dynamic wood properties. It describes the behavior of wood and wood-based materials against impact stress, which is used in practice, for example, for testing the material of tool handles.

Table 9.25 Abrasion resistance of wood [148] related to European beech = 1

Species	Abrasion resistance
Robinia	0.37
Ash	1.53
European oak	1.56
Alder	3.34
Scots pine	1.73
Larch	1.83
Norway spruce	2.00

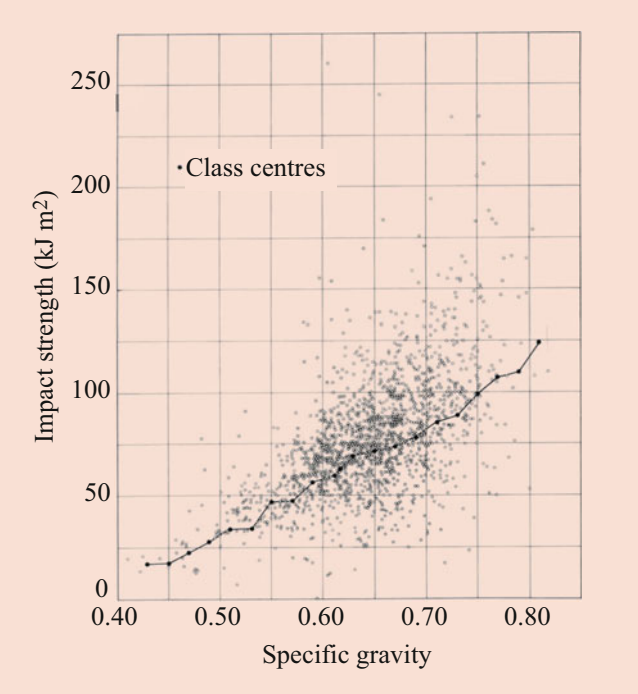

Fig. 9.61 Effect of specific gravity on the impact for air-dry ash [160]. (Cited in Kollmann and Côté [13], changed)

According to ISO 13061-10:2017, impact bending strength is calculated as follows:

$$A_W = \frac{1000 \cdot Q}{b \cdot h}$$

A_W – Impact bending strength (kJ m^{-2})
Q – Energy required for fracture of the test piece (J)
b, h – Dimensions of the test piece in the radial and tangential directions (mm)

Influencing factors of impact bending strength are wood species, density (Fig. 9.61), moisture content (Fig. 9.62), fiber angle (Fig. 9.63), but also fungal attack (Fig. 9.64). For further information see Sect. 9.6, which gives an in-depth description of impact wood testing (testing apparatus, evaluation and comparability of test results).

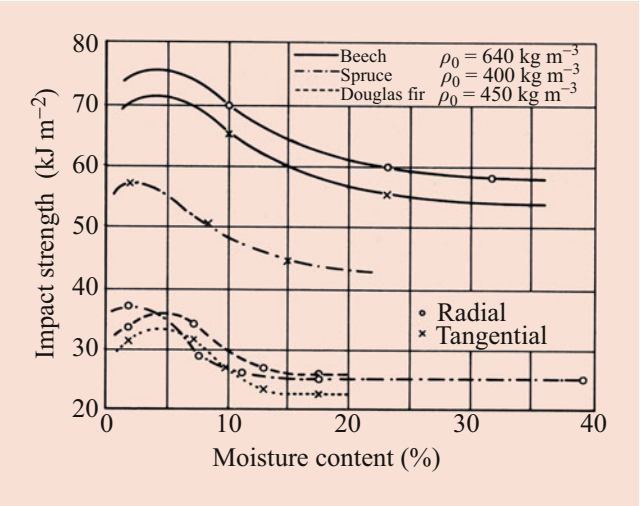

Fig. 9.62 Influence of moisture content on the impact resistance of wood [67]

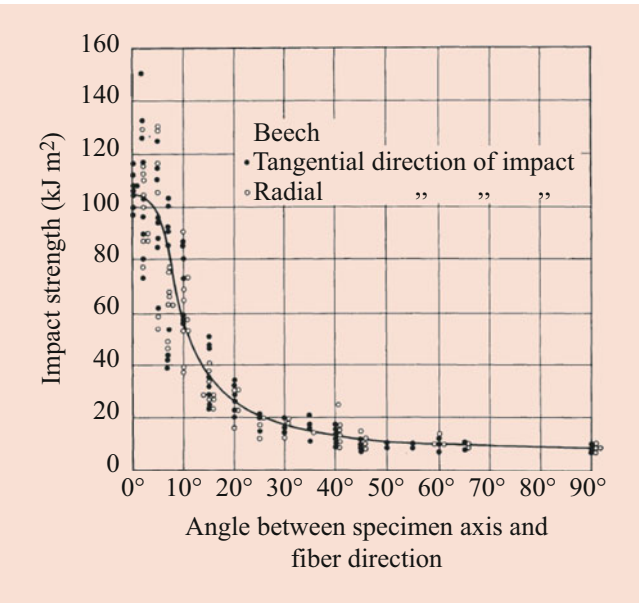

Fig. 9.63 Decrease in toughness with an increase in the angle between the specimen axis and the fiber direction according to Ghelmeziu. (Cited in Kollmann and Côté [13], changed)

9.5.12 Fatigue

Parameters and Testing

Repeated loading and unloading of wood and wooden materials leads to fatigue. The fatigue strength is significantly lower than that determined in the static test (Fig. 9.65). Under dynamic load, the component is exposed to load changes (e.g., cyclic loading under bending), whereas the allowable stress in a material decreases. A failure can occur, even if the strength determined in the short-term test has not yet been reached. A limit of fatigue strength is controversially

discussed in materials science. Often, fatigue strength is defined after a certain number of cycles (e.g., 1×10^6).

"Time under intermittent loading has a cumulative effect. In tests where a constant load was periodically placed on a beam and then removed, the cumulative time the load was actually applied to the beam before failure was essentially equal to the time to failure for a similar beam under the same load applied continuously" [17].

Partially, it is also referred as fatigue in static loading (duration of load [DOL] test, time to failure; see ▶ Chap. 8 [50]). The fracture begins with micro cracks that are cumulated. They divide into static (= DOL) and dynamic (cyclic loading) fatigue. Windmill blades must resist for millions of cycles. Seismic damage has by contrast a short duration (a few cycles) and a high load. In the literature, high cycle fatigue (HCF) and low cycle fatigue (LCF) are also distinguished. HCF is defined as the failure, which is caused by more than 10,000 cycles [50].

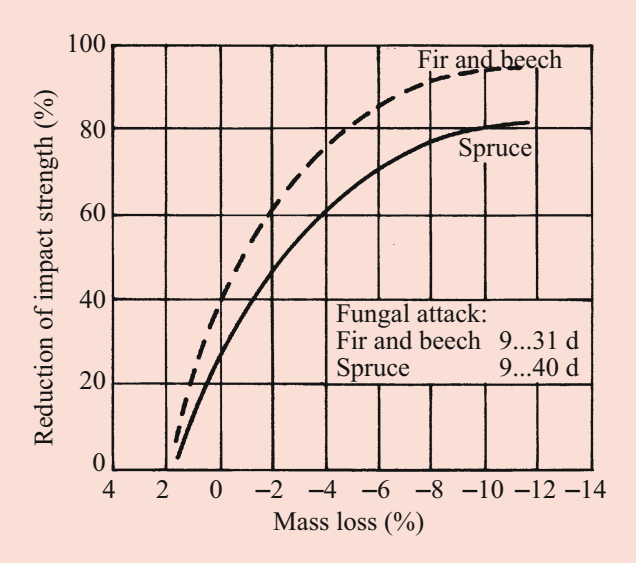

Fig. 9.64 Influence of mass loss due to fungal attack on the impact bending strength of wood [134]

Figure 9.65 shows schematically possible load cases with repeated loading and unloading cycles. As a result, a distinction is made between two limit states in terms of strength:

(a) Pulsating load (the stress changes between a value 0 and a value >0)
(b) Alternating load (the stress changes between two equal limits with values >0 and <0, e.g., tension and compression)

Both load cases lead to an increasing number of load cycles until fatigue and breakage of the material. Also important is the height of the load compared with the strength in the static short-term test.

The fatigue strength is determined in the Wöhler test (August Wöhler, 1819–1914). Several test bodies are loaded cyclically, often under a sinusoidal load–time–function, depending on the experiment carried out by tensile/compressive loading, bending, torsion, or shear (fracture mechanical tests on adhesive joints).

In practice, such stresses occur on structures that are exposed to constantly changing wind loads (bridges, electricity pylons, towers, multi-story wooden buildings, or wooden airplanes, especially those used in World War II, and wind mill blades).

Material Parameters and Influencing Factors

The fatigue strength in wood is 25–40% of the flexural strength determined in the static short-term test; in wood-based materials it is 20–30%. There are very few, often old statements from World War II about these tests. All the above-mentioned structural and climatic factors have an effect on the alternating bending strength. The slightly lower alternating bending strength of particle board and

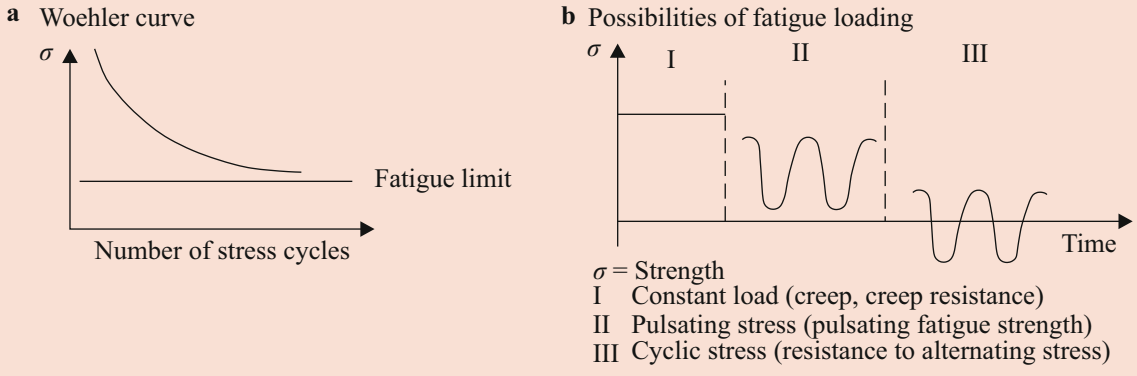

Fig. 9.65 Possible load cases when testing the fatigue of wood (for comparison static load, creep, and duration of load test (time to failure))

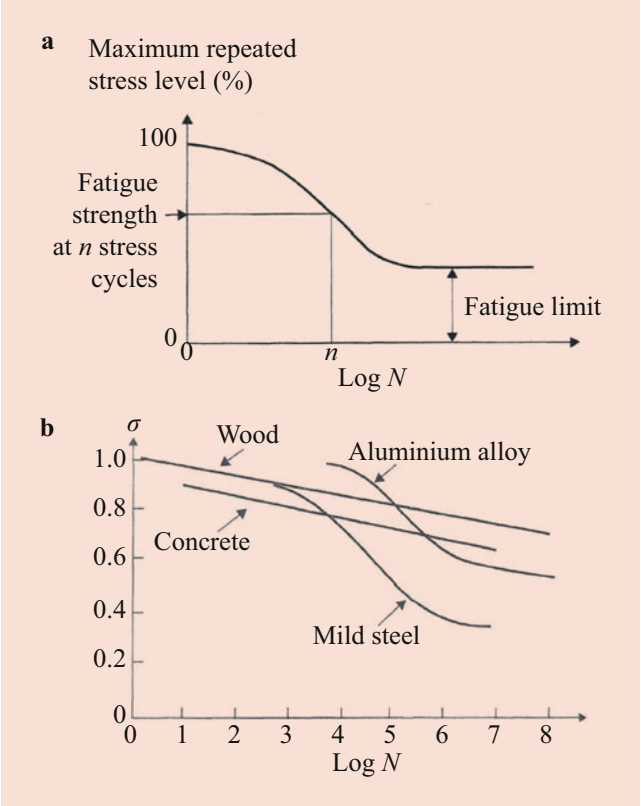

Fig. 9.66 Stress levels versus fatigue life. (**a**) Stress levels versus number of cycles to failure (*S*–*N*) curve. (**b**) Stress levels versus fatigue life (*σ*–*N*) diagrams (schematic) for mild steel, aluminum, concrete, and wood [50]

fiberboard is attributed to the relatively brittle urea-formaldehyde resin (see also Fig. 9.67) [161]. The tensile threshold strength for particle boards is 35–45% of the static tensile strength. A review of the state of knowledge is available in Mohr [162]. The influence of wood species and application in construction practice are described.

Nielsen [31] found that for long-term exposure to variable levels of stress, the frequency of stress also has an effect. Thus, according to an overview by Reichel [122] the number of load cycles until fracture can decrease up to 100 times, if the frequency of the load is reduced from 0.1 Hz to 1/2 h.

During the test, the specimens are exposed to different levels of stress until failure, the number of load cycles to failure is determined, and the strength is plotted against the number of load cycles or their logarithms (Figs. 9.66 and 9.67). Such loads are also common for tensile shear specimens used to control the bond quality (EN 302-1, see Fig. 9.68). A typical example of a wood specimen broken by a dynamic load is a smooth, short-fiber fracture (Fig. 9.69).

This also applies to wood that breaks long-fibrous during static bending tests. Owing to the constant stress, the structure loosens up both in the middle lamella and in the cell wall itself [165]. Ultimately, this loosening leads to breakage. The result of long-term stress occurs because of the friction processes. A warming of the wood occurs, which leads to a reduction of wood moisture.

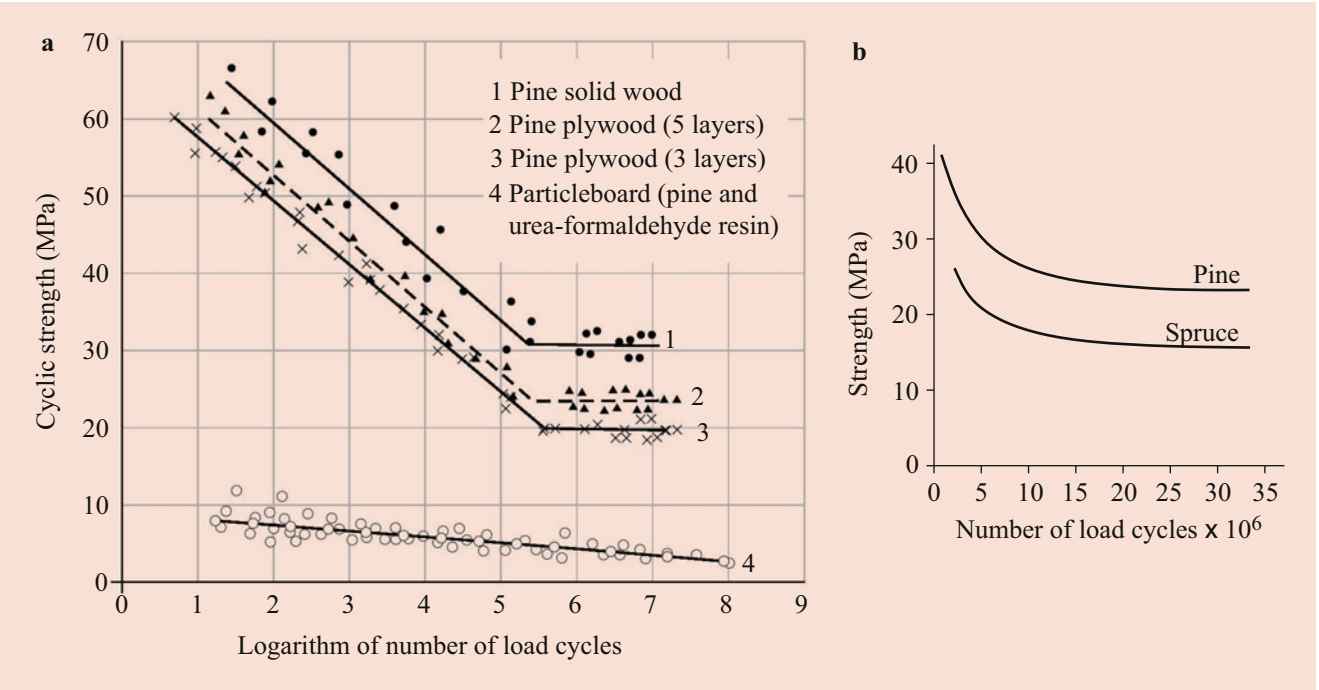

Fig. 9.67 Fatigue of wood and wood-based materials. (**a**) Pine and wood-based materials according to Gillwald [163]. (**b**) Spruce and pine according to Kollmann [25]

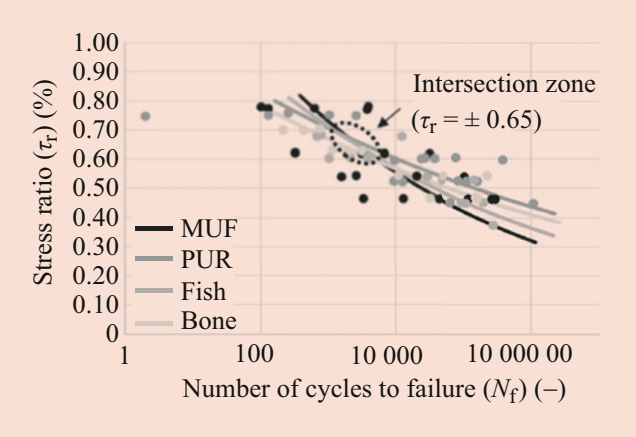

Fig. 9.68 S–N curves for glued wood (shear specimens according to EN 302-1) [164]

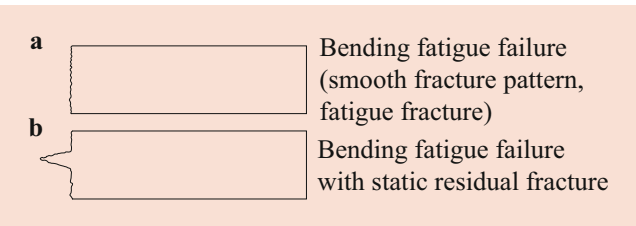

Fig. 9.69 Fracture of wood under cyclic loading (fatigue)

According to investigations by Rose [165] on non-broken samples as well, the continuous stress leads to property changes. Rose noticed both a disruption and a solidification of the specimens. Climate change causes long-wave fluctuations in humidity and tensions.

According to the Swiss standard SIA 265/1:2003, the following reduction coefficients for fatigue strength (alternating strength) in timber construction are proposed (Table 9.26). For the fatigue bending strength of several species Bodig and Jayne [7] list endurance ratios (ratio of endurance limit to ultimate static stress) between 0.22 and 0.38; this means a reduction to about one-quarter to one-third of the ultimate static stress. Table 9.27 shows results of several studies on the approximate fatigue life depending on wood sample, cyclic frequency, and maximum stress per cycle [17].

9.5.13 Properties Calculated at Molecular Level

In recent years, work has been increasingly carried out on the interaction between structure and properties at the micro level, nano level, and also at the molecular level. This is promoted by the ever faster development of measuring

Table 9.26 Reduction coefficients for dynamic fatigue life according to SIA 265/1: 2003

Loading	$k_{fat\infty}$
Compression	1.0
Tension	0.5
Bending	0.5
Cyclic tension–compression	0.5
Shear	0.3

technology (in particular the combination of mechanical and chemical test methods, see also Sect. ▶ 9 in ▶ Chap. 6) and the increased use of simulation methods (see ▶ Chap. 10). Initial estimates of the properties of cellulose molecules were obtained as early as 1930 by Meyer and Mark [125, 166]. Mark [166] estimated according to Kollmann and Côté [13] "that a sample consisting of uninterrupted parallel glucosidic chains would exhibit tenacities of 100,000 to 400,000 kp cm^{-2} (about 9,800 to 39,000 MPa, author's note). In practice pure cellulose fibers do not consist of endless molecules." "Calculations which have been made lead to a value of 12,500 to 15,000 kp cm^{-2} (1230–1470 MPa, author's note)" [13]. For pure cellulose as early as 1936, a modulus of elasticity of about 110,000 MPa was determined, for flax fibers about 100,000 MPa [11]. The tensile strength of separate single conifer fibers calculated based on the cell wall surface was determined by Jayne [167, 168] in Kollmann and Côté [13] to be between 324 and 1020 MPa.

Jayne [169] presented in his book the first calculation models for the properties of natural fiber composites. In the early 1980s, the interactions of structural elements under mechanical and moisture-induced stress were investigated [47]. Figure 9.70 shows schematically the structure of hardwood (a) and softwood (b) on various structural levels.

Research on the following areas has been intensified in recent years:

(a) ***The correlation of wood properties (strength, fungal resistance, aging,* etc.*) with the chemical structure*** using, for example, near-infrared (NIR) spectroscopy and multivariate statistics, see, for example, Tsuchikawa, Tsuchikawa and Schwanninger, Hofmeyer and Pederson, Meder et al., and Thumm and Meder [170–174].

The relationship between the chemical properties and other experimentally determined standard properties such as strength is determined. Figure 9.71 shows examples for the measurement of the strength and density of wood by NIR spectroscopy. Also, fungal infestation, aging, and adhesive content are tested. When measuring the wood moisture content of particles or fibers with NIR, the method has been established for decades (see ▶ Chap. 20).

(b) ***Research on the properties of wood on the level of cell-wall properties and properties of basic chemical***

Table 9.27 Summary of reported results on cyclic fatigue, EMC 12–15%, Wood Handbook 2010 [17]

Property	Range ratio (minimum stress per cycle related to maximum stress)	Cyclic frequency (Hz)	Maximum stress per cycle (%) related to static strength	Approximate fatigue life ($\times 10^6$ cycles)
Bending, clear, straight grain				
Cantilever	0.45	30	45	30
Cantilever	0	30	40	30
Cantilever	−1	30	30	30
Center-point	−1	40	30	4
Rotational	−1	–	28	30
Third-point	0.1	8.33	60	2
Bending, third-point				
Small knots	0.1	8.33	50	2
Clear, 1:12 slope of grain	0.1	8.33	50	2
Small knots, 1:12 slope of grain	0.1	8.33	40	2
Tension parallel to grain				
Clear, straight grain	0.1	15	50	30
Clear, straight grain	0	40	60	3.5
Scarf joint	0.1	15	50	30
Finger joint	0.1	15	40	30
Compression parallel to grain				
Clear, straight grain	0.1	40	75	3.5
Shear parallel to grain				
Glued-laminated	0.1	15	45	30

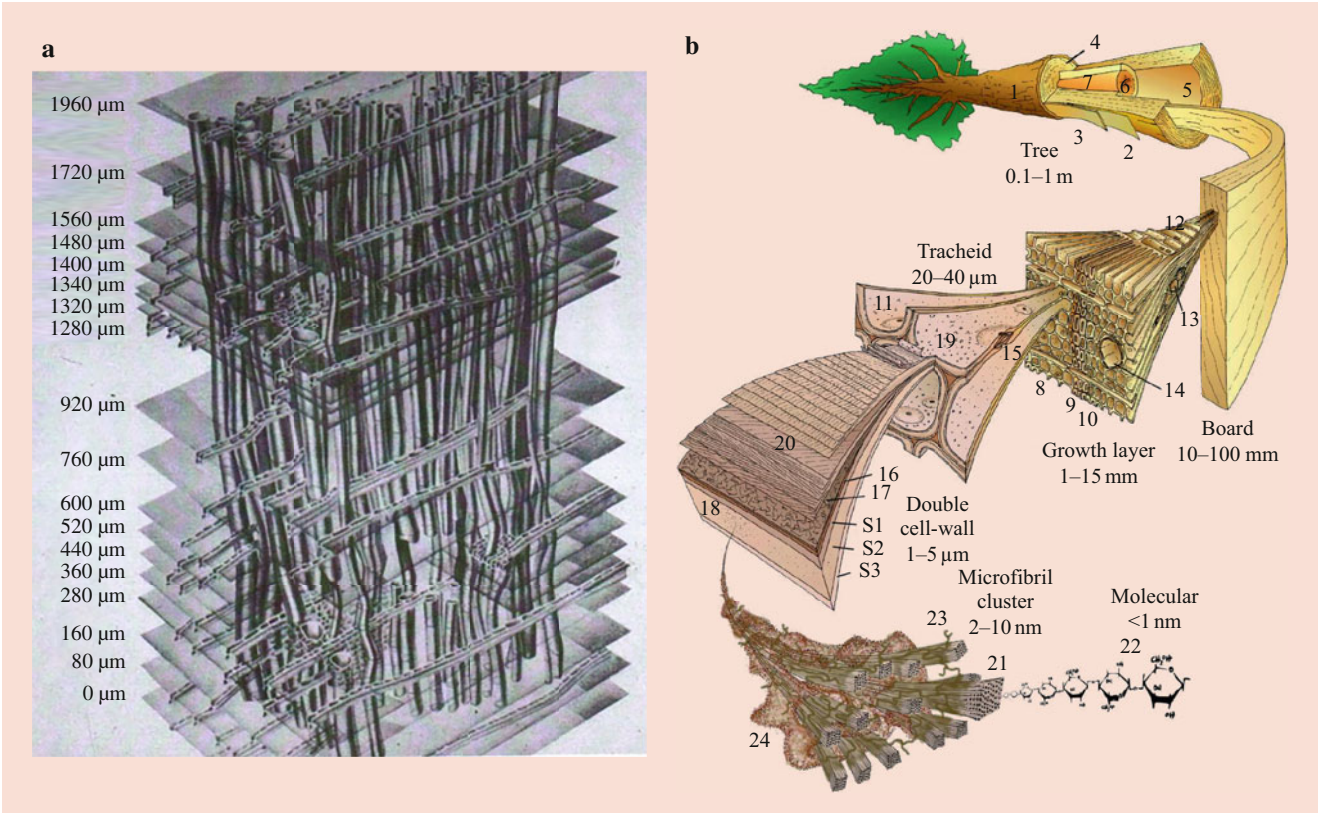

Fig. 9.70 Wood structure at different levels. (**a**) Reconstruction of vessel alignments in a hardwood. (Photo: ETH Zurich). (**b**) Softwood structure at different levels [128]

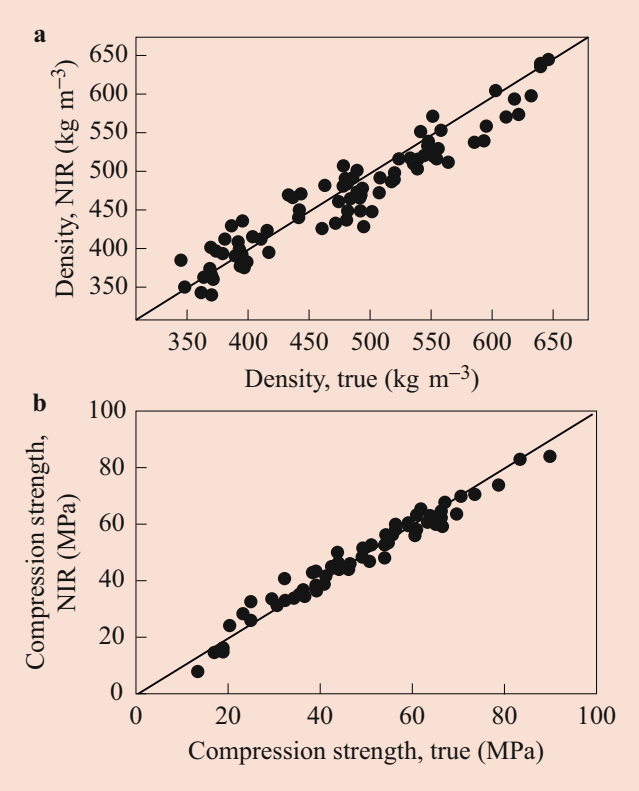

Fig. 9.71 Relationship of near-infrared-determined (**a**) density and (**b**) compression strength with conventionally tested properties (true properties) of Norway spruce. (Adapted from [172])

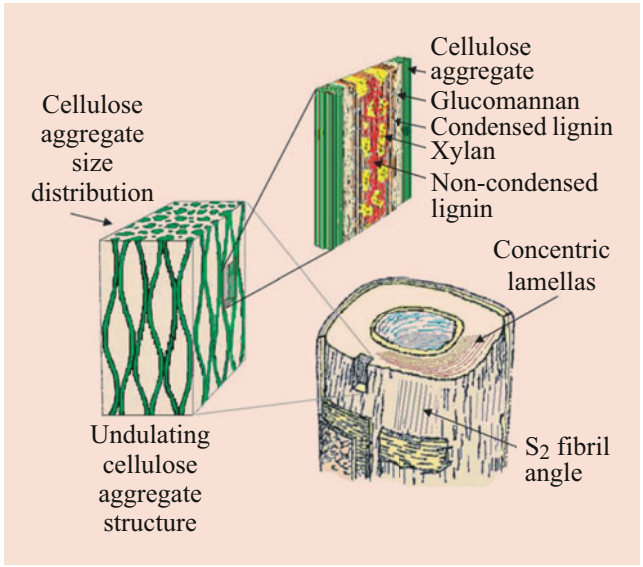

Fig. 9.72 Orientation of cell-wall polymers and micro-fibril angle in S2 [179]

constituents (cellulose, hemicellulose, lignin, extractives, interactions) with Raman/atomic force microscope, see, for example, Lichtenegger et al., Keplinger, Gierlinger and Schwanninger, Kulasinski et al., and Salmén and Burgert [175–179] (Fig. 9.72).

Persson [126] modeled the properties of spruce wood from the chemical components, Sjölund [130] calculated the influence of the honeycomb structure, and Harrington [128] modeled hygro-elastic properties of softwood.

The first work on the analysis of the wood structure in the synchrotron was carried out by Trtik et al. [180]. Subsequently, Zauner [52] and Baensch [53] investigated the failure of wood and of glued joints in situ in the synchrotron. The method also allows the interactions of the structural elements (e.g., detecting the influence of the wood rays) to be quantified.

(c) ***Molecular level studies (e.g., moisture uptake, strength, swelling, etc.)***

Rowell [181] gives a brief overview of molecular-level interactions under load. The distance of the molecules (hydrogen bonds) under load is changed within the elastic range. Also, the degree of polymerization of cellulose is affected. Figure 9.73 shows schematically the influence of strain on the hydrogen bonds according to Rowell in the elastic region of the stress–strain diagram [181]. Figure 9.74 shows the processes above the elastic limit in the area of plastic deformation. More recent work has been carried out by Kulasinski, Derome et al., and Geitmann and Gril [182–184]. A very good overview is available in the book by Geitmann and Gril [184]. Derome et al. [183] show examples to simulate the sorption and swelling behavior of the wood at a molecular level (Fig. 9.75).

The results of Kulasinski [182] can be summarized as follows (quoted):

> It is demonstrated that the initial stage of adsorption differs qualitatively from the behavior at higher moisture contents. At the early stage of adsorption, the water molecules are in diluted state, filling the existing voids between polymer chains and forming strong hydrogen bond(s) with adsorption sites. The polymeric material experiences a little swelling and an increase in porosity whereas free volume available per water molecule decreases. The pore structure is characterized mainly by pores of the size <1 nm and the distribution of moisture within the material is more or less uniform. The mechanical properties change by a relatively small amount and the diffusion coefficient is small as long as a molecule does not experience the presence of other water molecules. Concurrently, the heat of adsorption is high due to strong hydrogen bonds. At higher moisture content porosity and total volume increase linearly with moisture content. In microfibril and S2, the moisture starts to adsorb substantially at the interfaces. The number of hydrogen bonds decreases with moisture content which is directly related to weakening observed as a substantial decrease, by 1–2 orders of magnitude, of bulk, Young's and shear moduli, and accompanied by an increase of Poisson's ratio to nearly 0.5.

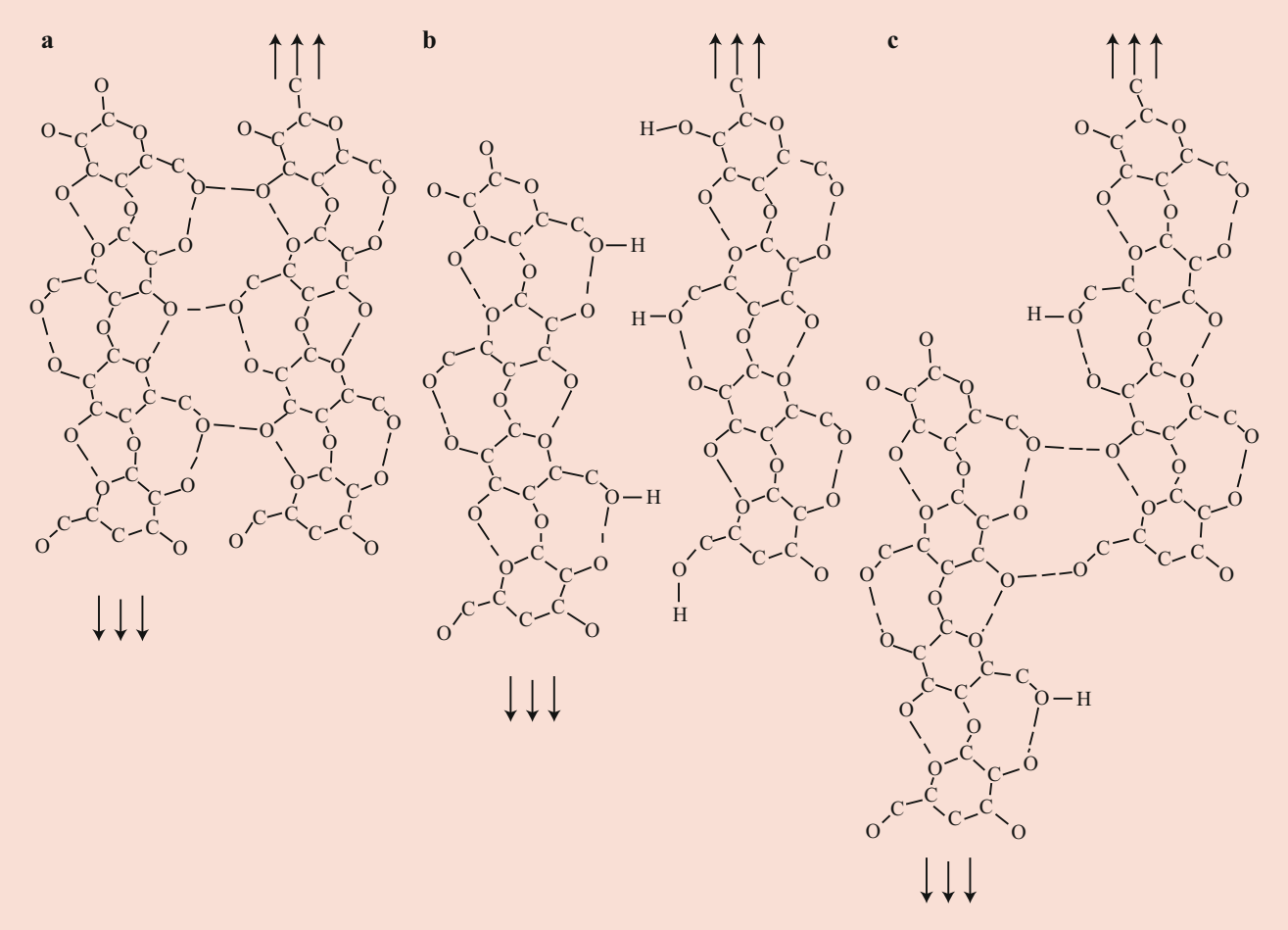

Fig. 9.73 Influence from shear stress at molecular level between polysaccharide chains below the proportional limit (elastic strength). (**a**) Hydrogen bonding (bonded). (**b**) Hydrogen bonding (sliding, unbounded). (**c**) Hydrogen bonding (rebounded) [181]

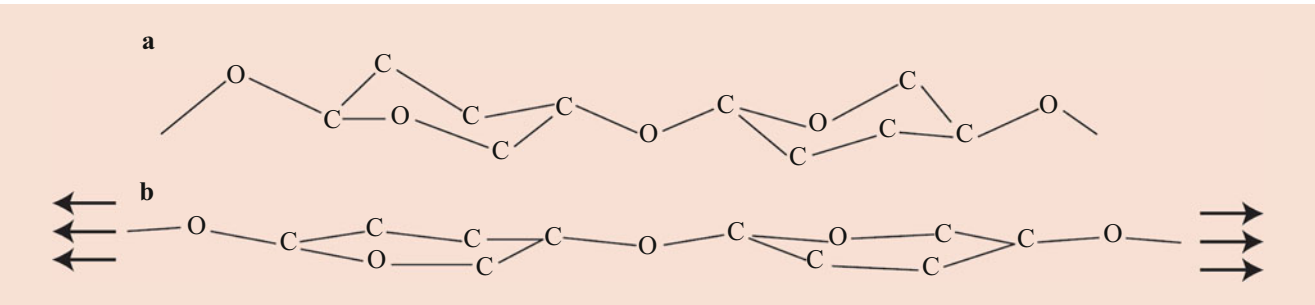

Fig. 9.74 Flexing and elongation of polysaccharide molecules under tensile force. (**a**) No tensile force. (**b**) Tensile force (elongation) [181]

9.6 Basics of Impact-Bending Testing

9.6.1 Overview

Measurement of wood constitutive properties from impact-bending testing requires fundamental knowledge of elastic mechanical vibrations of infinite continuum beams. It is necessary to understand the limitations and assumptions made regarding the physics of the impact problem. Saint-Venant, Boussinesq, Rayleigh, Timoshenko, Lee, Hoppmann, Barnhart and Goldsmith, Goldsmith, Crafton, Kolsky, Johnson, Graff, Ewins, Weaver et al., Clough and Penzien, Meyers, Abrate, Jones, and Stronge [185–203] provide a thorough background reading for the necessary (material-independent) principles applied to impact-bending strength predictions and

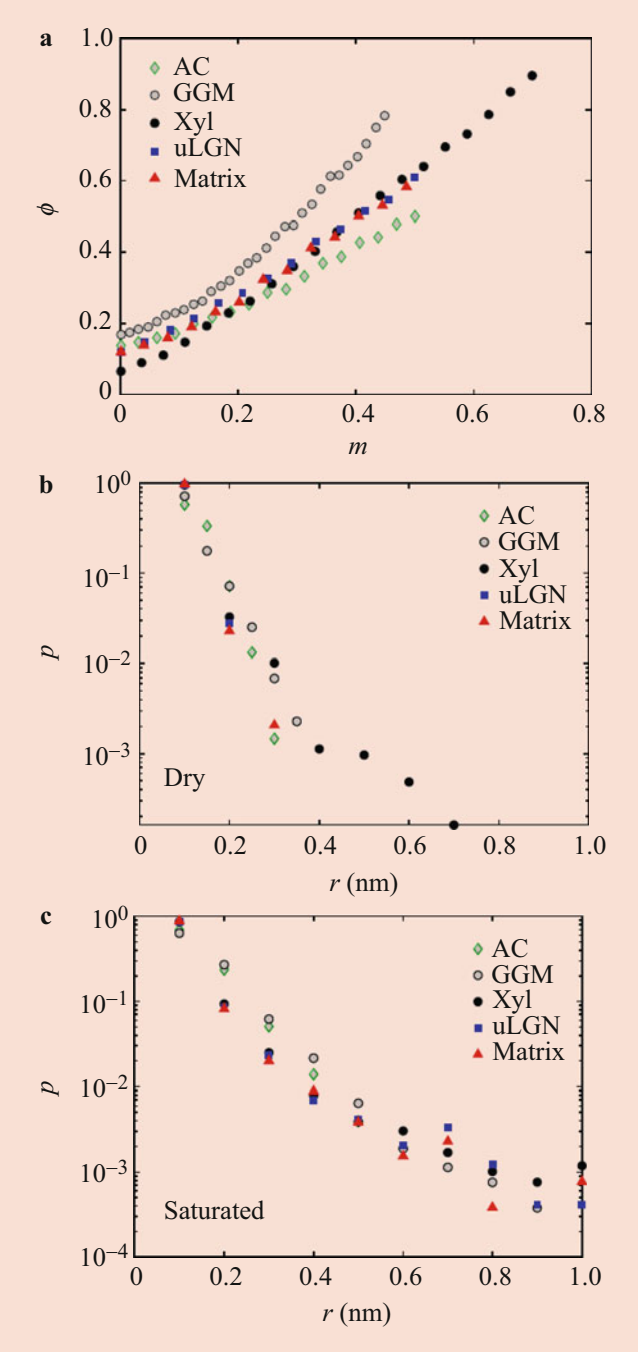

Fig. 9.75 (**a**) Porosity (Φ) of homogenous components and the amorphous composite as a function of moisture content (m). Pore size distribution (ρ) of (**b**) dry and (**c**) saturated systems, corresponding to moisture content for amorphous cellulose (AC) of 50%, galactoglucomannan (GGM) 44.8%, arabinoglucoronoxylan (Xyl) 70%, uncondensed lignin (uLGN) 48.5%, and matrix 49%, in a function of equivalent pore radius (r) [183]

evaluations. Section 9.6.2 provides more context on the means and methods of obtaining impact-bending strength, stiffness, toughness, and DOL measurements for wood.

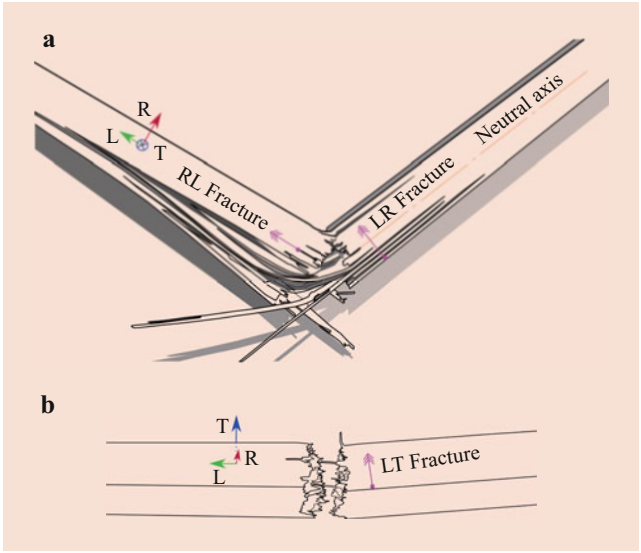

Fig. 9.76 Low-velocity impact testing of pine (*Pinus sylvestris*) beams. Growth rings and beam specimen oriented in (**a**) the *LR* and (**b**) *LT* impact direction. The figure shows (**a**) the tough and (**b**) brash failure modes. Close examination of (**a**) shows a distinct change in failure mode above and below the neutral axis, easily identifying the tension and compression failures. Fracture plane nomenclature is defined with two letters: the first letter represents the normal axis to the fracture plane and the second the axis direction of fracture propagation

Bending strength, in wood science, generally refers to the modulus of rupture (MOR). As noted in the FPL Wood Handbook [17], the MOR calculation is valid only up to the elastic limit, which, when applied to impact-bending means that there is an assumption that the wood beam remains linearly elastic up to the point of failure. This assumption is a necessary step to understanding the force–deflection, force–time, and strain–time plots that result from instrumented impact testing.

There is an important distinguishing element between the discussion presented here and the impact-bending that is presented in the FPL Wood Handbook [17]: the tabulated impact-bending *deflection* results in the FPL Wood Handbook are the results of incremental drop tests made by a falling hammer, whereas presented here are the general principles of impact-bending and the *MOR* resulting from single-blow testing.

When conducting incremental drop tests (i.e., starting from a small drop height and slowly increasing the drop height until either failure occurs or the beam has deflected more than 152 mm) there are small (*subcritical cracks*), progressive failures that accumulate in the specimen and result in failure modes that no longer represent the dynamic stress-rate- or strain-rate-dependent failure modes. Incremental failure is not an appropriate measurement of dynamic material properties. Moreover, the neutral axis likely attains a new, unknown location with the development of cracks. Figure 9.76 presents resulting failure modes of pine specimens subjected to low-velocity, single-blow impact-bending tests.

The failure modes presented in Fig. 9.76 are phenomenologically different than those typically seen in quasi-static testing because of the time-dependent fracture properties of wood [204–206]. Failure from quasi-static bending tests is generally initiated with a fracture in the extreme tension fiber, and then subcritical crack growth allows for gradual extension (often parallel to the beam neutral axis). This delayed failure mode causes less of a difference between strong and weak wood beams (i.e., lower COV). Impact-bending testing has higher stress-rates (strain-rates), and "...at very high loading rates, there is not enough time for subcritical crack growth to occur..." [206]; viz., Fig. 9.76b does not show *TL* fractures. At the higher strain rates of impact-bending tests there is a higher COV because the wood beams with inherently fewer initial subcritical cracks (internal defects) do not allow for these delayed failures to occur, and therefore have a strength increase (strength defined as the stress at failure, not the stress at the end of the proportional limit). However, Fig. 9.77 shows that initially weaker specimens do not have a strength increase. The experimental results of Fig. 9.77 are consistent with those of other researchers [30, 207–213]; however, there is further evidence that wood does not have a strongly strain-rate-dependent bending strength [214].

The impact-bending MOR has frequently been calculated using simplified dynamical models [215–227]. The result of using a simplified dynamical model for the impact-bending test has been detrimental to the understanding of strain-rate material behavior of wood, often leading to controversial empirical relationships that cannot be verified through physical principles. Section 9.6.2 presents clarifications for the experimental design, how to obtain impact-bending material properties, and the results of some validations of the impact dynamics theory in comparison with the experimental measurements.

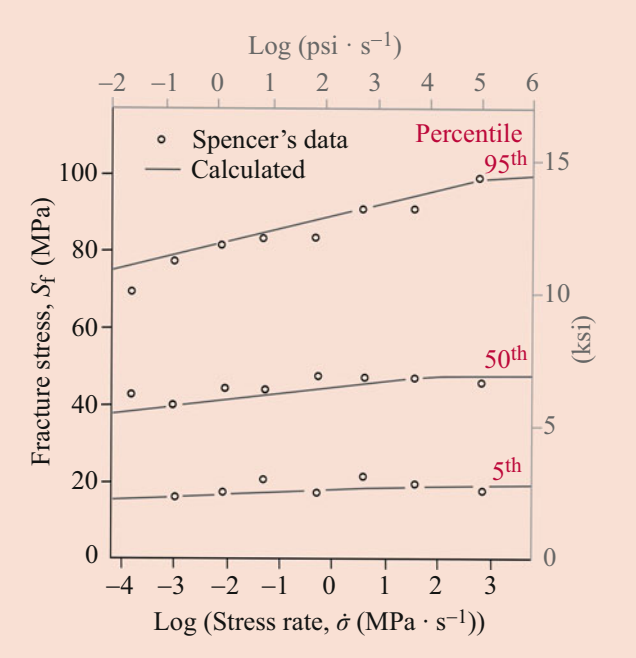

Fig. 9.77 Spencer's [213] data points for the 95th, 50th, and 5th percentiles of strength of dimension lumber. The lines are calculated from the fracture mechanics model by the method described in the article by Nadeau et al. [206]. The image shows a good correlation between the fracture mechanics explanation for the impact testing data collected by Spencer [213]. (Image by Nadeau et al. [206], permission to reuse granted)

9.6.2 Influencing Factors on Impact-Bending

The measured quantities during the impact experiment are both dependent on testing apparatus and specimens. Because the testing apparatus response is equally as important as the beam specimen response, the following sections discuss different influences of the apparatus on testing, as well as the material behavior of wood.

Transverse impact testing of beam specimens can be done with a variety of loading types (patterns or rates) as well as boundary conditions: free-free, pinned-pinned, spring-spring with and without overhangs included [214], fixed-free end conditions (cantilever beams) [228, 229], and sometimes fixed-fixed [230]. Boundary conditions influence the beam compliance, and therefore the modal shapes and frequencies. Interpretation of the impact load-time history to obtain material properties requires knowledge of the vibration characteristics of the entire system. (Applicable to impulse loading testing (e.g., pressure waves from blast, tsunami, etc.) such as research by Jacques et al. and Lacroix et al. [226, 227]. A discontinuous pressure wave front reflects and interacts with an elastic structure. So long as the structure remains linearly elastic the same principles of mechanical vibrations remain accurate.)

Unlike quasi-static testing, intermediate and higher strain-rate testing is difficult to make load controlled or deflection controlled because there is insufficient time for feedback. Whether the impact is considerably small, "tap-testing" (i.e., no observable indentation) – or – single-blow testing to cause failure, the physics of the mechanical vibrations are one and the same for shock and vibration loads [193].

Testing Apparatus

Unlike the quasi-static testing, it is not reasonable to synchronize two impact loading points; therefore, four-point bending loading is not an option found in the literature, nor is "standardized" impact-bending testing. There are four different testing apparatuses:

1. The Hatt–Turner test [231] (drop-tower experiment) is a test with a falling mass attached to a transverse crosshead, which centrally impacts a beam specimen that has both ends supported. If used as a single-blow impact-bending test there are two distinguishing differences in dynamics in comparison with the pendulum impact-bending test:

- Constant gravitational acceleration adds force that is not influential in pendulum impact bending
- Rayleigh's [187] assumption to ignore the vibrations of the falling mass are generally still applicable

2. The Charpy test [232] has a pendulum swinging and centrally impacting a beam specimen supported at both ends. The pendulum can be either a compound pendulum, where the mass and stiffness of the connecting elements (vibrational properties) cannot be ignored – or – a ballistic pendulum, where the mass and stiffness of the connecting element can be neglected. Quite often, the Charpy and Izod tests are carried out with notched specimens to obtain fracture mechanics properties [233, 234]
3. The Izod test is a pendulum test with a cantilever beam specimen that is transversely impacted at the free end
4. The FPL Toughness Tester [216] has the tup and the specimen starting in contact, and a sudden release of the mass pulls the beam specimen past the anvils via a chain. The steel chain that pulls the specimen is subject to longitudinal and out-of-plane mechanical vibrations. The apparatus can be used for toughness measurements and bending-strength measurements [220, 221]

Gerhards [235, 236] and Drow et al. [237] found that Charpy pendulum testing is the most reproducible test apparatus of the four listed. Wood material testing standards DIN 52189 [238] and ISO 3348 [239] specify using a single-blow Charpy test, whereas ASTM 143-09 [240] recommends the incremental Hatt–Turner test.

The pendulum elevation, Fig. 9.78a, shows a discontinued pendulum arm, which is indicative that it is exceedingly long or is of variable length. All impact-bending testing methods employ the elementary principle of changing potential energy into kinetic energy by raising a mass and releasing it. The problem that arises is designing the impact-bending to be within a certain incidence velocity (velocity at the moment of contact between the tup and the specimen). Higher incidence velocities can be easily achieved by increasing the length of the pendulum arm, but at the coat of increasing mechanical vibrations. A long flexible pendulum arm is prone to causing contact chatter. Contact chatter is where multiple sub-contacts (repeated loss of contact) occur within the duration of the impact event. Possible reasons for contact chatter are:

1. Beam specimen vibration
2. Pendulum beam vibration
3. Both vibrating together
4. Mass ratio between the impactor and the specimen

It is recommended to design the compound pendulum with the center of percussion (COP) as close as possible to the center of strike (COS) (Fig. 9.78b) to reduce contact chatter. The COP is a point along the length of the pendulum where the impact force cancels out the rotational inertia of the pendulum and no reaction is produced at the center of rotation, ensuring that as little energy as possible is lost in vibration. From Fig. 9.79, it is clearer that the COP is neither a nodal point nor an anti-nodal point.

Contact chatter should not be interpreted as noise or problems with the data acquisition system, and in fact great attention and care should be taken when filtering impact-bending signals from any of the instruments.

The most often validated and instrumented variable is the impact force; see Fig. 9.80 for force-time history data from an incrementally increasing release angle. To understand the shape of the force–time history plot, one must understand the different phases of motion the beam specimen travels through.

1. At incidence, the fastest elastic waves begin to propagate outward from the contact point. These elastic waves are the body (bulk) waves: dilatational, distortional, Rayleigh, Stonely, and Lamb, which are difficult to measure with the load cell. Because of the transfer of momentum, conservation of momentum indicates that the specimen must reach a velocity accordingly
2. The first load peak seen in Fig. 9.80 is known as the *inertial load* [233]. It is during the inertial loading that the dispersive flexural waves propagate outward from the contact point. Because the force–time history plots by Kollmann et al. [241] at the anvil mimic the same pattern, this means that the load at the supports comes with a delay but in the same shape, and then the beam ends come out of contact with the anvil. It is during these earliest stages of impact-bending that the beam may be considered as a free-free beam, until the motion of the beam encounters the anvils once more. Kollmann et al. [241] speculated that during the inertial loading there should be adiabatic material properties that are important to consider because of the noticeably short loading duration, but this has not been validated by any other research
3. Although higher modes do not contribute greatly to displacement, but are due to the small radius of curvature that is superpositioned in modal analysis, higher modes can have a greater proportional contribution to bending strain [185, 190, 191]. Owing to the elastic resistance of the beam, during the moments that the beam and tup are no longer in contact the beam begins to retract. Just because the specimen and tup are no longer in contact does not mean that the tup has been rebounded off the specimen and changed direction. If the pendulum still has momentum, it has been slowed down in its direction of travel but still catches up to the specimen beam

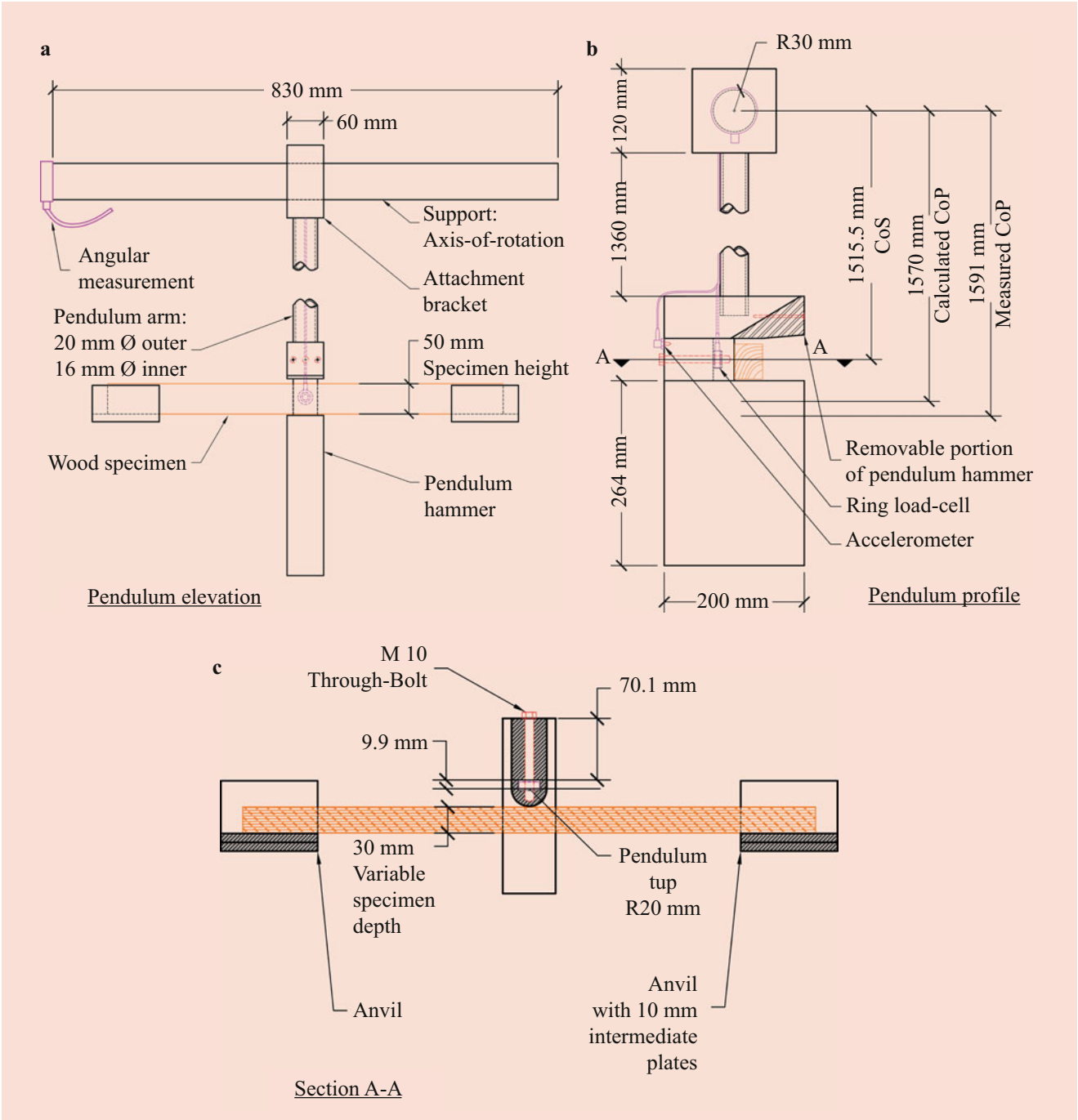

Fig. 9.78 The compound pendulum built for low-velocity impact testing. Schematic (**a**) shows the interrupted elevation of the pendulum; (**b**) the pendulum profile, possible instrumentation locations, and a geometric interpretation of where the measured and calculated center of percussion lies; (**c**) is the section cut through the impact plane. (Image by Polocoşer [214], permission to reuse granted)

4. Looking at the next phase of motion, from 1 ms to 2 ms in Fig. 9.80b, the pendulum and the beam specimen travel together, whereas both vibrate in their modal shapes causing a complex oscillatory pattern. Both the pendulum and the specimen have damping properties that continue to act. Gradually, the higher modes dampen out, the pendulum displacement is dominated by the rigid body mode, and the beam specimen displacement is in the fundamental mode. Figure 9.81 shows that impact-bending behavior is repeatable, where n is the number of test replicates. The small dip in the force–time history at approximately 20 ms is most likely the friction of the specimen as it returns into

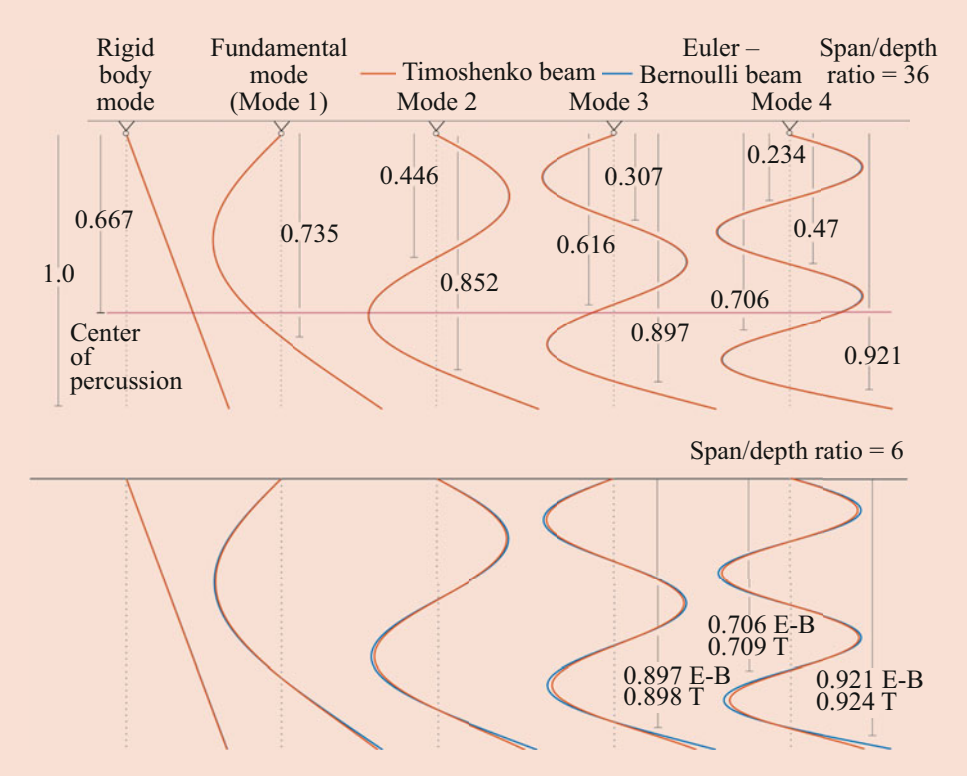

Fig. 9.79 Compound pendulum imagined as a pendulum beam. The center of percussion does not always align with a nodal point, shear deformations affect higher modes of vibration, and there is a need to include the rigid body motion in dynamic analysis. (Image by Polocoşer [214], permission to reuse granted)

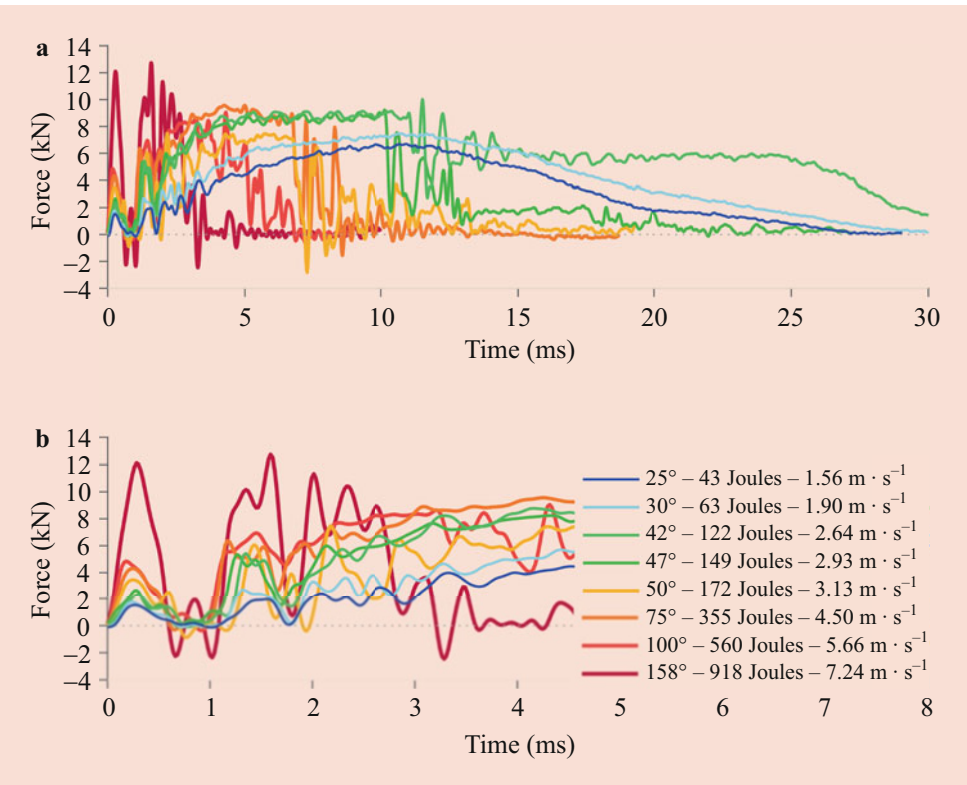

Fig. 9.80 Characteristic force–time histories of low-velocity impact, ranging over incrementally greater incidence velocity. (**a**) At the smallest release angle, the beam force returns to zero and upon examination has no failures, indicating an elastic impact. With increasing impact velocity the time to failure decreases and the impact force increases, but the force reaches a plateau. (**b**) Negative loads following the inertial load can be ameliorated by higher sampling rates. (Image by Polocoşer [214], permission to reuse granted)

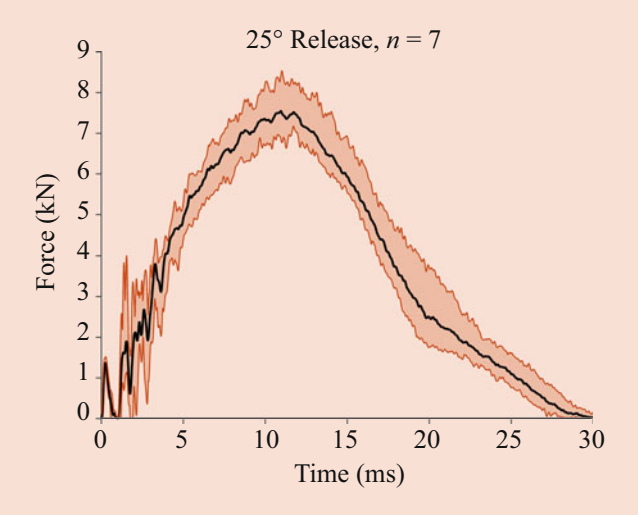

Fig. 9.81 95th percentile, mean, and 5th percentile of low-velocity impact testing of pine species from a small release angle. The inertial load has low variability given the low variability in species mass density. Complex dynamics of the testing apparatus and the specimen play a significant role in the section in the time after the inertial load (chattering possible). After 5 ms the higher modes tend to dampen out and the rest is bending load from the fundamental mode. (Image by Polocoşer [214], permission to reuse granted)

place against the anvils. The frictional properties of wood most likely cause the larger COV at this characteristic moment in the plot

One other principle that can be checked through the force measurements is to integrate the force–time history signal to obtain the impulse–time history. The impulse can be well correlated with the work, and together they can help to identify the time when indentation occurs.

Methods of reducing the inertial load are to grease the tup [233] or place a damping device between the tup and the specimen [214, 242]. The damping device prolongs the initial contact time, thereby reducing the effects of the higher modes of vibration.

Impactor: Specimen Mass Ratio

The first time the separate equations of motion of the impactor and of the beam were included in the impact prediction, Timoshenko [188] found that contact chatter occurred when there was a greater impactor-to-specimen mass ratio; and because it has been found [192, 203, 243, 244] to be the most important parameter for determining the beam response, Polocoşer [214] tabulated the mass ratios found in impact-bending testing conducted in the wood science literature. Results showed great variability in this parameter, and many times, comparisons of the wood material properties have been made between research articles without giving adequate consideration of the differences between the dynamics of the testing apparatus.

Slenderness Ratio

A large slenderness ratio (span length/bending depth) >16 is recommended for quasi-static beam testing because it reduces the cross-sectional shear effect and is within the assumptions of Euler–Bernoulli beam theory. However, for impact-bending testing a higher slenderness ratio means that higher modes become more important [203]. How many higher modes are important to include in modal analysis is discussed below for bending strain predictions.

Kollmann et al. [241] found there to be a sink relationship (a local minimum) between slenderness ratio and bending toughness. This is a possible *size effect* [30] that is often attributed to wood properties that need statistical correction.

The slenderness ratio and contact stiffness help to define whether the impact-bending response will be either local (purely penetration at contact), transitional, or global behavior (specimen bending) [245].

Contact Constitutive Relationship

Contact duration is coupled with modal analysis of higher modes [188], and concentrated localized behavior caused by knifing or penetration [246, 247] into the beam specimen may prevent bending behavior. However, a large radius tup tends to cause shear failure in the beams, so it is important to choose a tup radius with a neutral penetrating projected surface [248].

Figure 9.82 shows the quasi-static indentation testing done to obtain differing contact stiffness and recovery parameters needed for the elastic and elastic–plastic simulations. Two methods of modeling impact contact are:

1. Hertzian [249] elastic contact law
2. Hysteretic elastic–plastic contact law developed by Barnhart and Goldsmith [191]

Beams impacted from a low velocity had indentations indicating that plastic contact occurs even for beams that had no bending failure. Plastic contact may occur at any point along the force–time history but is likely at the highest peak in the curve. Figure 9.80 shows that the inertial load increases proportionately for incrementally increasing incidence velocities, but the load that follows increases up to a plateau. It is the plateau in the force–time history that indicates that plastic contact is occurring.

Toughness

Impact-bending has been primarily used for obtaining the toughness properties of wood [13, 17, 216–220, 235–239, 241, 250–256]. Toughness is a measurement of a material's capability to absorb energy; however, how this measurement

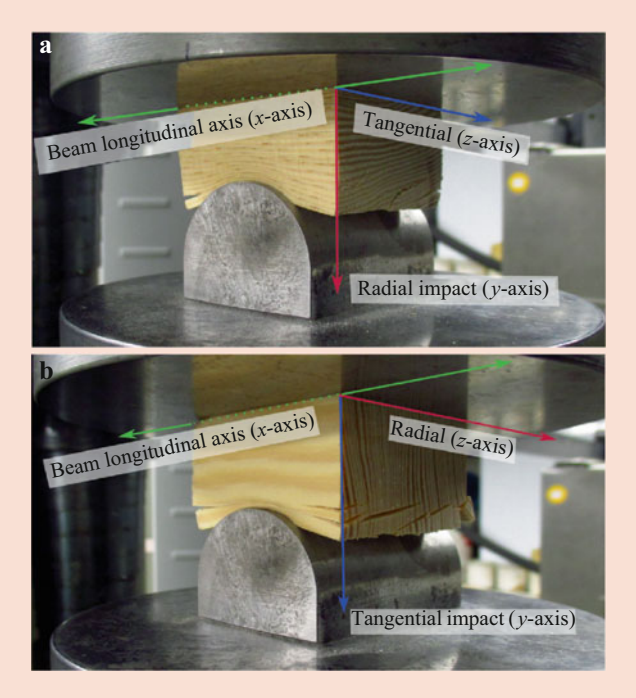

Fig. 9.82 There is little research that attempts to describe dynamic contact in wood; therefore, values were obtained from static indentation testing (**a**) and (**b**). (Image by Polocoşer [214], permission to reuse granted)

is interpreted has not been consistent and some caution is needed when looking at the values reported. The units used to express toughness have been found to vary from standard to standard and within research. One definition of toughness is the area under the stress–strain curve that has units Pa = J·m^{-3}. This could mean that the energy absorbed is normalized to the volume of the specimen [235]. Although some standards [238, 239] normalize the energy to the cross-section (J·m^{-2}), the FPL Wood Handbook [17] recommends reporting toughness as the difference in the potential energy of the impactor (J).

The failure of a specimen can be categorized as *brash* [250] to indicate little capacity for energy absorption (often observable by the short fibers), and *tough* to indicate a large energy absorption capacity (Fig. 9.76 shows an example). The categories describe failures within a species, not across species, i.e., it is incorrect to describe one species as being tougher than another. It is difficult to designate an entire wood species as being either brash or tough because of the dependence on ring orientation, moisture, slenderness ratio, specimen size, and testing apparatus.

Fracture patterns in Fig. 9.76 show that toughness is ring orientation dependent [256]. To complicate the matter more, toughness is dependent on whether the rings are oriented with the pith side or the bark side on the impact face [255]. There is a substantial difference between the toughness values for differing ring orientations for softwoods, whereas for differing ring orientation in hardwoods there is negligible difference in toughness values [17, 237]. Research into the effect of moisture content on toughness [220, 237, 252, 253] showed that toughness reaches a minimum of between 12% and 16% MC.

Koehler [250] said that visual inspection of fiber length may lead to the conclusion that a species is brash at a certain beam length (slenderness ratio) whereas it might be tough at another. Kollmann et al. [241] investigated toughness in relationship to slenderness ratio, finding that toughness reaches a minimum at a slenderness ratio of 12.

Toughness measurements cannot be compared between different apparatus [235, 237], between different specimen sizes [235, 252], or correlated with toughness measurements from quasi-static testing [252]. The toughness test is difficult to standardize for wood and the reported values serve best as comparative to judge how well one specimen absorbs energy compared with another in individual laboratories. Energy loss of the apparatus is not systemic but specimen dependent.

Stiffness

Wood is a visco-elastic material, which may cause a perceived strain-rate-dependent stiffness. *Dynamic* can be understood to represent creep, quasi-static, as well as the impact-bending properties being discussed. Wood science research for rapid and impact testing [214] has inconclusive results if there is a strain-rate-dependent bending stiffness. For quasi-static bending testing, the MOE (or E) is the initial linear portion of the bending stress–strain curve, where the stress and strain are either derived from the measured force-deflection curve – or – for greater accuracy measured from the force–strain curve [257]. By examining the force–time histories (Fig. 9.80), it is evident that measuring E is not done from a linear, initial portion because of the inertial effects.

Modulus of Elasticity/Young's Modulus, *E*

In creep and quasi-static testing there is no concern for the inertial load seen at the beginning of Fig. 9.80, but as the loading rate increases there is evidently more influence of the beam mass. It is possible for bending failure to occur in brash wood within the inertial load. Some researchers [258, 259] try to correct for the inertial load, whereas ISO-17281 [233] filters out the inertial load. The apparent paradox in impact testing is that the E is required to calculate the bending stress needed to plot the stress–strain diagram, from which E is obtained.

The most common alternative method to measuring E is vibration testing [257, 260–271]. Some of the standards

[269, 270] refer to this vibration testing as a method of obtaining the *dynamic* Young's modulus – meaning, a dynamic method of obtaining E, not to be confused with an E that is dependent on time or strain-rate. As discussed in the introduction to Sect. 9.6.2, the dynamics for tap-testing are the same as for impact-bending; therefore, the method of measuring the impact-bending stiffness is just as applicable. The method employed is known as the Timoshenko–Goens–Hearmon (TGH) method, where the frequencies of multiple modes of a free-free beam are measured. With the frequencies measured, an overdetermined system of equations is used to determine the E, which gives the best fit for all the modes. If the Maxwell, Voigt, and standard linear solid discrete element models for visco-elastic systems are examined, it is clear that any measurement of frequency or displacement will convolve the effects of the spring element, E with other elements, such as a dashpot, c.

Modulus of Rigidity/Shear Modulus, *G*

The TGH method is also applicable to determining the shear modulus; however, ASTM 1876 [91, 270] recommends torsional vibration methods. One possible purpose for determining G (in impact bending applications) is for inclusion in Timoshenko's beam theory, which may be important for flexural waves in close vicinity to the impact point or higher modes of vibration.

Strength/Modulus of Rupture

As discussed previously in Sect. 9.6.1, quasi-static bending strength is generally known in wood science as the MOR. Aside from the research by Jansson [272], most of the impact-bending testing done since Elmendorf [215] has assumed that the beam specimen is only affected by the fundamental mode of vibration [273–285]. The assumption that the beam is a single degree of freedom may be adequate for determining the displacement but is inadequate for determining the bending stress and strain. Choosing the number of modes for superposition is highly dependent on the beam compliance. Figure 9.83 shows the result of using one or seven modes for low and high velocity impacts [214]. The measured force–time histories were used as forcing functions, with the E from quasi-static testing, to calculate the bending stress and strain at each time step. Figure 9.83a, b validate the need to include higher modes than the fundamental mode in the calculation of the bending strain.

Plotting the time to failure on a logarithmic axis with impact, quasi-static, and creep bending strengths together has led to the DOL factors used to design structures [273]. These factors were empirically established based on testing that made some rudimentary assumptions for impact-bending testing and weighed the quasi-static and creep results more heavily. The initial DOL factor for impact-bending strength is approximately twice that of quasi-static testing, but there have been more research indicating it is more likely on the order of 1.07–1.15 [30, 213, 214, 272]. This information is combined with the fracture mechanics research by Nadeau et al. [206], which indicates that weak wood, wood at the lowest 5th percentile, should not be permitted by building codes to have increased bending strength properties at short duration loading.

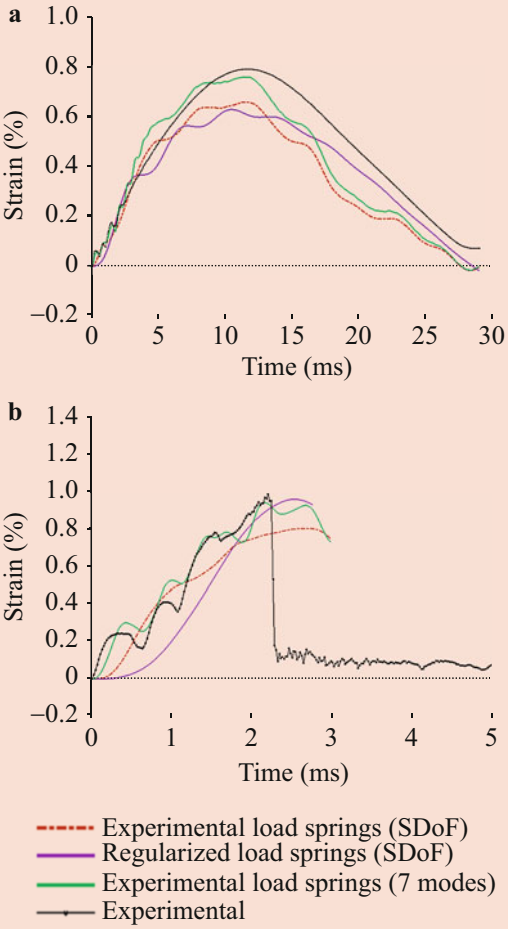

Fig. 9.83 The resulting predictions of the bending strain–time history is compared with the strain gauge measurements for (**a**) 1.25 m·s^{-1} incidence velocity and (**b**) 7.25 m·s^{-1} incidence velocity. When the measured load from the (**a**) low-incidence velocity and (**b**) high-incidence velocity is used as a forcing function, the single degree of freedom and multi-degree of freedom models are validated respectively. Included is the regularized measured force, indicating that there is no need for regularization. (Image by Polocoșer [214], permission to reuse granted)

Acknowledgments
Sections 9.1, 9.2, 9.3, and 9.5 of this chapter include several parts that have been previously published in the following book:
Peter Niemz and Walter Sonderegger: Holzphysik, Physik des Holzes und der Holzwerkstoffe (Wood physics. Physics of wood and wood-based materials). Fachbuchverlag Leipzig im Carl Hanser Verlag, Munich 2017.
The selected paragraphs from the original publication have been translated into English, and the content has been expanded and adapted to the structure of the Springer Handbook of Wood Science and Technology. The authors and Springer are grateful to Carl Hanser Verlag Munich for kind permission.

References

1. Scheffler, M.: Bruchmechanische Untersuchungen zur Trocknungsrißbildung an Laubholz. PhD Thesis, TU Dresden, Dresden (2000)
2. Steiger, R.: Mechanische Eigenschaften von Schweizer Fichten-Bauholz bei Biege-, Zug-, Druck- und kombinierter M/N Beanspruchung: Sortierung von Rund- und Schnittholz mittels Ultraschall. PhD Thesis, ETH Zurich, Zurich (1996)
3. Glos, P.: Holz-Zentralblatt. **108**, 153–155 (1982)
4. Fink, G.: Influence of Varying Material Properties on the Load-Bearing Capacity of Glued Laminated Timber. PhD Thesis, ETH Zurich, Zurich (2014)
5. Denzler, J.K.: Modellierung des Größeneffektes bei biegebeanspruchtem Fichtenschnittholz. PhD Thesis, TU of Munich, Munich (2007)
6. Neuhaus, H.: Ingenieurholzbau, 3rd edn. Vieweg +Teubner, Wiesbaden (2011)
7. Bodig, J., Jayne, B.A.: Mechanics of Wood and Wood Composites, 2nd edn. Krieger Publishing, Malabar (1993)
8. Niemz, P., Sonderegger, W.: Schweiz. Z. Forstwes. **154**, 489–493 (2003)
9. Knigge, W., Schulz, H.: Grundriss der Forstbenutzung. Parey, Hamburg (1966)
10. Görlacher, R.: Klassifizierung von Brettschichtholzlamellen durch Messung von Longitudinalschwingungen. PhD Thesis, University of Karlsruhe, Karlsruhe (1990)
11. Kollmann, F.: Technologie des Holzes und der Holzwerkstoffe, vol. 1, 2nd edn. Springer, Berlin (1951)
12. Niemz, P., Bekhta, P.: Holz-Zentralblatt. **128**, 684 (2002)
13. Kollmann, F., Côté Jr., W.A.: Principles of Wood Science and Technology Solid Wood, vol. 1. Springer, Berlin/Heidelberg (1968)
14. Trendelenburg, R.: Das Holz als Rohstoff. J. F. Lehmanns Verlag, Munich (1939)
15. Sonderegger, W., Mandallaz, D., Niemz, P.: Wood Sci. Technol. **42**, 281–298 (2008)
16. Timell, T.E.: Compression Wood in Gymnosperms. Springer, Berlin (1986)
17. Ross, R.J. (ed.): Wood Handbook. Wood as an Engineering Material, Centenial ed. Forest Products Laboratory, Madison, (2010)
18. Ozyhar, T.: Moisture and Time Dependent Orthotropic Mechanical Characterization of Beech Wood. PhD Thesis, ETH Zurich, Zurich (2013)
19. Halligan, A.F., Schniewind, A.P.: Wood Sci. Technol. **8**, 68–78 (1974)
20. Niemz, P., Hug, S., Schnider, T.: Forstarchiv. **85**, 163–168 (2014)
21. Sonderegger, W., Niemz, P.: Holz Roh Werkst. **64**, 385–391 (2006)
22. Autorenkollektiv: Lexikon der Holztechnik, 4th edn. Fachbuchverlag, Leipzig (1990)
23. Sonderegger, W., Kránitz, K., Bues, C.-T., Niemz, P.: J. Cult. Herit. **16**, 883–889 (2015)
24. Hassani, M.M., Wittel, F.K., Hering, S., Herrmann, H.J.: Comput. Method. Appl. Mech. Eng. **283**, 1032–1060 (2015)
25. Kollmann, F.: Technologie des Holzes und der Holzwerkstoffe, vol. 2, 2nd edn. Springer, Berlin (1955)
26. Arnold, M., Steiger, R.: Mater. Struct. **40**, 57–68 (2007)
27. Sonderegger, W., Niemz, P.: Holz Roh Werkst. **62**, 335–342 (2004)
28. Burmester, A.: Holz Roh Werkst. **25**, 11–25 (1967)
29. Lawniczak, M., Raczkowski, J., Wojciechowicz, B.: Holz Roh Werkst. **22**, 372–376 (1964)
30. Madsen, B.: Structural Behaviour of Timber. Timber Engineering, North Vancouver (1992)
31. Nielsen, L.F.: Holz Roh Werkst. **65**, 223–229 (2007)
32. Eisenacher, G.: Charakteristik und Modellierung von Fichtenholz unter dynamischer Druckbelastung. PhD Thesis, TU Berlin, Berlin (2014)
33. Langendorf, G., Schuster, E., Wagenführ, R.: Rohholz, 4th edn. Fachbuchverlag, Leipzig (1990)
34. Hankinson, R.L.: Investigation of Crushing Strength of Spruce at Varying Angles of Grain Air Service Information Circular 3(259). U. S. Air Service (1921)
35. Burger, N., Glos, P.: Holz Roh Werkst. **54**, 333–340 (1996)
36. Glos, P., Schulz, H.: Holz Roh Werkst. **44**, 293–298 (1986)
37. Hübner, U.: Mechanische Kenngrößen von Buchen-, Eschen- und Robinienholz für lastabtragende Bauteile. PhD Thesis, Technical University of Graz, Graz (2013)
38. Khaloian Sarnaghi, A., van de Kuilen, J.W.G.: Wood Sci. Technol. **53**, 535–557 (2019)
39. Dunky, M., Niemz, P.: Holzwerkstoffe und Leime: Technologie und Einflussfaktoren. Springer, Berlin (2002)
40. Ehlbeck, J.: Durchbiegung und Spannungen von Biegeträgern aus Holz unter Berücksichtigung der Schubverformung. PhD Thesis, Universität Karlsruhe, Karlsruhe (1967)
41. Colling, F.: Tragfähigkeit von Biegeträgern aus Brettschichtholz in Abhängigkeit von den festigkeitsrelevanten Einflussgrössen. PhD Thesis, University of Karlsruhe, Karlsruhe (1990)
42. Blass, H.J.: Tragfähigkeit von Druckstäben aus Brettschichtholz unter Berücksichtigung streuender Einflussgrössen. PhD Thesis, University of Karlsruhe, Karlsruhe (1987)
43. McNatt, J.D., Wellwood, R.W., Bach, L.: For. Prod. J. **40**, 10–16 (1990)
44. Böhme, C.: Einfluss der Prüfkörperabmessungen bei Spanplatten WKI-Kurzbericht 21, 22, 23. Braunschweig (1999)
45. Kisser, J., Steininger, A.: Holz Roh Werkst. **10**, 415–421 (1952)
46. DeBaise, G.R., Porter, A.W., Pentoney, R.E.: Mater. Res. Standard. **6**, 493–499 (1966)
47. Kucera, L.J., Bariska, M.: Wood Sci. Technol. **16**, 241–259 (1982)
48. Mindess, S., Bentur, A.: Wood Sci. Technol. **20**, 145–155 (1986)
49. Patton-Mallory, M., Cramer, S.M.: For. Prod. J. **37**, 39–47 (1987)
50. Smith, I., Landis, E., Gong, M.: Fracture and Fatigue in Wood. Wiley, Chichester (2003)
51. Forsberg, F., Sjödahl, M., Mooser, R., Hack, E., Wyss, P.: Strain. **46**, 47–60 (2010)
52. Zauner, M.: In-Situ Synchrotron Based Tomographic Microscopy of Uniaxially Loaded Wood: In-Situ Testing Device, Procedures and Experimental Investigations. PhD Thesis, ETH Zurich, Zurich (2014)
53. Baensch, F.: Damage Evolution in Wood and Layered Wood Composites Monitored in Situ by Acoustic Emission, Digital Image

Correlation and Synchrotron Based Tomographic Microscopy. PhD Thesis, ETH Zurich, Zurich (2015)
54. Keunecke, D.: Elasto-Mechanical Characterisation of Yew and Spruce Wood with Regard to Structure-Property Relationships. PhD Thesis, ETH Zurich, Zurich (2008)
55. Ammann, S.D.: Mechanical Performance of Glue Joints in Structural Hardwood Elements. PhD Thesis, ETH Zurich, Zurich (2015)
56. Burgert, I.: Die Mechanische Bedeutung der Holzstrahlen im lebenden Baum. PhD Thesis, University of Hamburg, Hamburg (2000)
57. Stanzl-Tschegg, S., Keunecke, D., Tschegg, E.: J. Mech. Behav. Biomed. **4**, 688–698 (2011)
58. Czaderski, C., Steiger, R., Howald, M., Olia, S., Gülzow, A., Niemz, P.: Holz Roh Werkst. **65**, 383–402 (2007)
59. Steiger, R., Gülzow, A., Czaderski, C., Howald, M., Niemz, P.: Eur. J. Wood Prod. **70**, 141–153 (2012)
60. Niemz, P.: Untersuchungen zum Kriechverhalten von Spanplatten unter besonderer Berücksichtigung des Einflusses der Werkstoffstruktur. PhD Thesis, TU Dresden (1982)
61. Anderson, T.L.: Fracture Mechanics: Fundamentals and Applications, 2nd edn. CRC Press, Boca Raton (1995)
62. Ewalds, H.L., Wanhill, R.J.H.: Fracture Mechanics. E. Arnold/ Delftse U. M., London/Delft (1991)
63. Valentin, G.H., Boström, L.R., Gustafsson, P.J., Ranta-Maunus, A., Gowda, S.: Application of Fracture Mechanics to Timber Structures RILEM State-of-the-Art Report, Research Notes 1262. Technical Research Centre of Finland, Espoo (1991)
64. Danielsson, H.: Perpendicular to Grain Fracture Analysis of Wooden Structural Elements – Models and Applications. PhD Thesis, Div. of Structural Mechanics, Lund University (2013)
65. Aicher, S., Gustafsson, P.J., Haller, P., Petersson, H.: Fracture Mechanics Models for Strength Analysis of Timber Beams with a Hole or a Notch A Report of RILEM TC-133, TVSM-7134. Div. of Structural Mechanics, Lund University (2002)
66. Gustafsson, P.J.: Fracture Perpendicular to Grain – Structural Applications. In: Thelandersson, S., Larsen, H.J. (eds.) Timber Engineering. Wiley, Chichester (2003)
67. Niemz, P., Sonderegger, W.: Holzphysik – Physik des Holzes und der Holzwerkstoffe, 2nd edn. Carl Hanser Verlag, München (2017)
68. Kristenson, K.B.: Crack Propagation in Wood – An Experimental and Numerical Study. Master Thesis, Dep. of Civil Engineering, Technical University of Denmark (2007)
69. Vasic, S., Smith, I.: Eng. Fract. Mech. **69**, 745–760 (2002)
70. Holmberg, S.: A Numerical and Experimental Study of Initial Defibration of Wood. PhD Thesis, Div. of Structural Mechanics, Lund University (1998)
71. Stefansson, F.: Fracture Analysis of Orthotropic Beams – Linear and Nonlinear Methods. Licentiat Thesis, Div. of Structural Mechanics, Lund University (2001)
72. Stefansson, F.: Mechanical Properties of Wood at Microstructural Level. Master Thesis, Div. of Structural Mechanics, Lund University (1995)
73. Persson, K., Gustafsson, P.J., Petersson, H.: Influence of plastic dissipation on apparent fracture energy determined by a three point bending test. In: Proceedings of COST 508 Wood Mechanics Workshop on Plasticity and Damage, University of Limerick, Ireland, pp. 123–133 (1993)
74. Gustafsson, P.J.: Chapter 4.7, Strength of wood beams jagged at support. In: Fracture Mechanics Studies of Non-Yielding Materials Like Concrete: Modelling of Tensile Fracture and Applied Strength Analyses. Div. of Building Materials, Lund University, PhD thesis (1985)
75. Boström, L.: Chapter 4, Examination of the compact tension specimen. In: Method for Determination of the Softening Behaviour of Wood and the Applicability of a Nonlinear Fracture Mechanics Model. Div. of Building Materials, Lund University (1992)
76. Sandhu, R.S.: A Survey of Failure Theories of Isotropic and Anisotropic Materials Technical Report AFFDL-TR-72-71. NTIS, Springfield (1972)
77. Tsai, S.W., Wu, E.M.: J. Compos. Mater. **5**, 58–80 (1971)
78. Norris, C.B., McKinnon, P.F.: Compression, Tension and Shear Tests on Yellow-Poplar Plywood Panels of Sizes That Do Not Buckle with Tests Made at Various Angles to the Face Grain Report No. 1328. Forest Products Laboratory, Madison (1956)
79. Norris, C.B.: Strength of Orthotropic Materials Subjected to Combined Stresses Report No. 1816. Forest Products Laboratory, Madison (1962)
80. Bodig, J., Jayne, B.A.: Mechanics of Wood and Wood Composites. Van Nostrand Reinhold, New York (1982)
81. Dahl, K.B.: Mechanical Properties of Clear Wood from Norway Spruce. PhD Thesis, Dep. of Structural Engineering, Norwegian University of Science and Technology, Norway (2009)
82. Eberhardsteiner, J.: Mechanisches Verhalten von Fichtenholz: Experimentelle Bestimmung der biaxialen Festigkeitseigenschaften. Springer, Vienna (2002)
83. Burström, P.G.: Byggnadsmaterial – Uppbyggnad, Tillverkning Och Egenskaper. Studentlitteratur, in Swedish, Lund (2007)
84. EN-338: *Structural Timber – Strength Classes* (2009)
85. Leicester, R.H.: *Some Aspects of Stress Fields at Sharp Notches in Orthotropic Materials* Division of Forest Products Technological Paper No. 57. CSIRO, Melbourne (1971)
86. Sih, G.C., Paris, P.C., Irwin, G.R.: Int. J. Fract. Mech. **1**, 189–203 (1965)
87. Lekhnitskii, S.G.: Theory of Elasticity of an Anisotropic Elastic Body. Holden-Day, San Francisco (1963)
88. Gustafsson, P.J.: A study of strength of notched beams. Paper 21-10-1. In: Proceedings of CIB W18A Meeting 21, Canada (1988)
89. Rice, J.R.: J. Appl. Mech. **35**, 379–386 (1968)
90. Wu, E.M.: J. Appl. Mech. **34**, 967–974 (1967)
91. Mall, S., Murphy, J.E., Shottafer, J.E.: J. Eng. Mech. **109**, 680–690 (1983)
92. Johnson, J.A.: Wood Sci. **6**, 151–158 (1973)
93. Wright, K., Fonselius, M.: Fracture toughness of wood – mode I. In: Proceedings of Joint Meeting CIB W18 and IUFRO S5.02, vol. 1, Italy, p. 14 (1986)
94. Schniewind, A.P., Centeno, J.C.: Wood Fiber. **5**, 152–159 (1973)
95. Pearson, R.G.: Holzforschung. **28**, 11–19 (1974)
96. Riipola, K., Fonselius, M.: Evaluation of Critical J-Integral for Wood Material Research Report 528. Technical Research Centre of Finland (1988)
97. Gustafsson, P.J.: Mean stress and initial crack approaches. In: Fracture Mechanics Models for Strength Analysis of Timber Beams with a Hole or a Notch – A Report of RILEM TC-133, TVSM-7134. Div. of Structural Mechanics, Lund University (2002)
98. Masuda, M.: Theoretical consideration on fracture criteria of wood – proposal of finite small area theory. In: Proceedings of International Conference on Timber Engineering, pp. 584–595 (1988)
99. Mackenzie-Helnwein, P., Eberhardsteiner, J., Mang, H.A.: Comput. Mech. **31**, 204–218 (2003)
100. Schmidt, J., Kaliske, M.: Eng. Struct. **31**, 571–579 (2009)
101. Danielsson, H., Gustafsson, P.J.: Eng. Fract. Mech. **98**, 137–152 (2013)
102. Olejniczak, P., Gustafsson, P.J.: Rate effect in tangential tension fracture softening performance. In: Proceedings of COST 508 Wood Mechanics Workshop on Service Life Assessment of Wooden Structures, pp. 137–148 (1994)
103. Gustafsson, P.J.: Some test methods for fracture mechanics properties of wood and wood adhesive joints. In: Proceedings of

RILEM TC 133-TF Workshop on Determination of Fracture Mechanics Properties of Wood, Bordeaux, p. 14 (1992)
104. Nordtest-1993-11: Wood: Fracture Energy in Tension Perpendicular to the Grain Nordtest Method NT BUILD 422. Nordtest, Espoo (1993)
105. Larsen, H.J., Gustafsson, P.J.: Fracture energy for wood in tension perpendicular to the grain, results from a joint testing project. Paper 23-19-2. In: Proceedings of CIB W18A Meeting 23 (1990)
106. Larsen, H.J., Gustafsson, P.J.: Fracture energy for wood in tension perpendicular to the grain. Paper 24-19-1. In: Proceedings of CIB W18A Meeting 24 (1991)
107. Rug, W., Badstube, M., Schöne, W.: Determination of the fracture energy of wood for tension perpendicular to the grain. Paper 23-19-1. In: Proceedings of CIB W18A Meeting 23 (1990)
108. Ottestam, C., Salmén, L.: Nord. Pulp Pap. Res. J. **16**, 140–142 (2001)
109. Weibull, W.: A Statistical Theory of the Strength of Materials Ingeniörsvetenskapsakademiens Handlingar No 151. Generalstabens Litografiska Anstalts Förlag, Stockholm (1939)
110. Weibull, W.: The Phenomenon of Rupture in Solids Ingenjörsvetenskapsakademiens Handlingar No 153. Generalstabens Litografiska Anstalts Förlag, Stockholm (1939)
111. Gustafsson, P.J.: Lecture Notes on Some Probabilistic Strength Calculation Models TVSM-7161. Div. of Structural Mechanics, Lund University (2014)
112. Dill-Langer, G.: Schädigung von Brettschichtholz bei Zugbeanspruchung rechtwinklig zur Faserrichtung. PhD Thesis, University of Stuttgart, Stuttgart (2004)
113. Foschi, R.O., Folz, B.R., Yao, F.Z.: Reliability-Based Design of Wood Structures Structural Research Series Report No. 34. University of British Columbia, Canada (1989)
114. Gustafsson, P.J., Jockwer, R., Serrano, E., Steiger, R.: A strongest link model applied to fracture propagating along grain. Paper 48-19-2. In: Proceedings of INTER Meeting 48, Croatia (2015)
115. Danielsson, H., Gustafsson, P.J.: Eur. J. Wood Prod. **69**, 407–419 (2011)
116. Navi, P., Sandberg, D.: Thermo-Hydro-Mechanical Processing of Wood. EPFL Press, CRC-Press, Lausanne (2012)
117. Plath, E.: Holz Roh Werkst. **29**, 377–382 (1971)
118. Schreiber, J., Niemz, P., Mannes, D.: Holztechnologie. **48**, 1–10 (2007)
119. Ramberg, W., Osgood, W.R.: Description of Stress-Strain Curves by Three Parameters Technical Report. National Advisory Committee for Aeronautics (1943)
120. Hering, S.: Charakterisierung und Modellierung der Materialeigenschaften von Rotbuchenholz zur Simulation von Holzverklebungen. PhD Thesis, ETH Zurich, Zurich (2011)
121. Schmidt, J.: Modellierung und numerische Analyse von Strukturen aus Holz. Habilitation Thesis, TU Dresden, Dresden (2009)
122. Reichel, S.: Modellierung und Simulation hygro-Mmechanisch beanspruchter Strukturen aus Holz im Kurz- und Langzeitbereich. PhD Thesis, TU Dresden, Dresden (2015)
123. Resch, E., Kaliske, M.: Comput. Struct. **88**, 165–177 (2010)
124. Hering, S., Saft, S., Resch, E., Niemz, P., Kaliske, M.: Holzforschung. **66**, 373–380 (2012)
125. Meyer, K.H., Mark, H.: Der Aufbau der hochpolymeren organischen Naturstoffe. Akademische Verlagsgesellschaft, Leipzig (1930)
126. Persson, K.: Micromechanical Modelling of Wood and Fibre Properties. PhD Thesis, Lund University, Lund (2000)
127. Zimmermann, T.: Fortschritte in der Nanocelluloseforschung. In: Proceedings of Tagungsband 3. Holzanatomisches Kolloquium. IHD Dresden (2015)
128. Harrington, J.: Hierarchical Modelling of Softwood Hygro-Elastic Properties. PhD Thesis, University of Christchurch, New Zealand, Christchurch (2002)
129. Rafsanjani, A.: Multiscale Poroelastic Model: Bridging the Gap from Cellular to Macroscopic Scale. PhD Thesis, ETH Zurich, Zurich (2013)
130. Sjölund, J.: Effect of Cell Structure Geometric and Elastic Parameters on Wood Rigidity. PhD Thesis, University of Aalto, Aalto (2015)
131. Keunecke, D., Hering, S., Niemz, P.: Wood Sci. Technol. **42**, 633–647 (2008)
132. Koch, G., Oelker, M., Richter, H.: Macroholzdata: Illustrations, Identification, and Information Retrieval, 07–2018 ed. delta-intkey.com (2018)
133. Larsen, H.J., Leijten, A.J.M., van der Put, T.A.C.M.: The design rules in Eurocode 5 for compression perpendicular to the grain – continuous and semi continuous supported beams. In: Proceedings of CIB-W18, 41st meeting, St. Andrews, Canada, 24–28 August 2008, Paper 41-6-3, pp. 1–12 (2008)
134. Vorreiter, L.: Holztechnologisches Handbuch, vol. 1. Fromme, Vienna (1949)
135. Niemz, P., Schreiber, J., Naumann, J., Stockmann, M.: Holz Roh Werkst. **65**, 459–468 (2007)
136. Hänsel, A., Kühne, G.: Holzforsch. Holzverw. **40**, 1–5 (1988)
137. Schulte, M.: Zerstörungsfreie Prüfung elastomechanischer Eigenschaften von Holzwerkstoffplatten durch Auswertung des Eigenschwingverhaltens und Vergleich mit zerstörenden, statischen Prüfmethoden. PhD Thesis, Universität Hamburg, Hamburg (1997)
138. Niemz, P., Bauer, S.: Holzforsch. Holzverw. **43**, 68–70 (1991)
139. Kruse, K.: Untersuchungen verschiedener Einflussgrössen auf die zerstörungsfreie Werkstoffprüfung von Holzwerkstoffen mit Ultraschall. PhD Thesis, University of Hamburg, Hamburg (1993)
140. Niemz, P., Culik, M.: Holz Roh Werkst. **61**, 187–188 (2003)
141. Wagenführ, R.: Holzatlas, 6th edn. Fachbuchverlag Leipzig im Carl Hanser Verlag, Munich (2007)
142. Horvath, N., Molnar, S., Niemz, P.: Holztechnologie. **49**, 10–15 (2008)
143. Sonderegger, W., Martienssen, A., Nitsche, C., Ozyhar, T., Kaliske, M., Niemz, P.: Eur. J. Wood Prod. **71**, 91–99 (2013)
144. Chen, Z.: Torsional Fatigue of Wood. PhD Thesis, South Bank University, London (2002)
145. Chen, Z., Gabbitas, B., Hunt, D.: J. Mater. Sci. **41**, 7247–7259 (2006)
146. Neuhaus, F.: Elastizitätszahlen von Fichtenholz in Abhängigkeit von der Holzfeuchtigkeit. PhD Thesis, University of Bochum, Bochum (1981)
147. Nördlinger, H.: Die technischen Eigenschaften der Hölzer. Cottascher Verlag, Stuttgart (1860)
148. Mette, H.J.: Holzkundliche Grundlagen der Forstnutzung. Dt. Landwirtschaftsverlag, Berlin (1984)
149. Niemz, P., Bauer, S.: Holzforsch. Holzverw. **42**, 361–364 (1990)
150. Wimmer, R., Lucas, B.N., Oliver, W.C., Tsui, T.Y.: Wood Sci. Technol. **31**, 131–141 (1997)
151. Sonderegger, W., Niemz, P.: Holztechnologie. **50**, 11–16 (2009)
152. Schwab, E.: Holz Roh Werkst. **48**, 47–51 (1990)
153. Walter, F., Knitsch, H.W.: Holztechnologie. **11**, 32–36 (1970)
154. Görlacher, R.: Holz Roh Werkst. **45**, 273–278 (1987)
155. Niemz, P., Zürcher, E., Kucera, L.J., Bernatowicz, G.: Schweizer Ingenieur Architekt. **115**, 991–994 (1997)
156. Ishiguri, F., Matsui, R., Iizuka, K., Yokota, S., Yoshizawa, N.: Holz Roh Werkst. **66**, 275–280 (2008)
157. Llana, I., Hermoso, E., Bobadilla, I., Iniguez-Gonzalez, G.: Holzforschung. **72**, 549–555 (2018)
158. Niemz, P., Sonderegger, W.: Holz-Zentralblatt. **47**, 1327 (2007)
159. Schulz, H.: Holz Roh Werkst. **43**, 215–222 (1985)
160. Kollmann, F.: Die Esche und ihr Holz. Springer, Berlin (1941)
161. Kollmann, F., Krech, H.: Holz Roh Werkst. **19**, 113–118 (1961)

162. Mohr, B.: Zur Interaktion der Einflüsse aus Dauerstandbelastung und Ermüdungsbeanspruchung im Ingenieurholzbau Berichte aus dem konstruktiven Ingenieurbau. TU of Munich, Munich (2001)
163. Gillwald, W.: Holz Roh Werkst. **24**, 445–449 (1966)
164. Bachtiar, E., Clerc, G., Brunner, A., Kaliske, M., Niemz, P.: Holzforschung. **71**, 391–396 (2017)
165. Rose, O.: Holz Roh Werkst. **23**, 271–284 (1965)
166. Mark, H.: Cellulose: physical evidence regarding its constitution (Chap. 6). In: Wise, L.E., Jahn, E.C. (eds.) Wood Chemistry, vol. 1. Reinhold Publ. Corp., New York (1952)
167. Jayne, B.A.: Mechanical Properties of Wood Fibre, pp. 461–476. Technical Association of Pulp and Paper Ind. (1959)
168. Jayne, B.A.: For. Prod. J. **10**, 316–322 (1960)
169. Jayne, B.A.: Theory and Design of Wood and Fiber Composite Materials. Syracuse University Press, Syracuse (1972)
170. Tsuchikawa, S.: Appl. Spectrosc. Rev. **42**, 43–71 (2007)
171. Tsuchikawa, S., Schwanninger, M.: Appl. Spectrosc. Rev. **48**, 560–587 (2013)
172. Hofmeyer, P., Pederson, J.: Holz Roh Werkst. **53**, 165–170 (1995)
173. Meder, R., Thumm, A., Bier, H.: Holz Roh Werkst. **62**, 159–164 (2002)
174. Thumm, A., Meder, R.: J. Near Infrared Spec. **9**, 117–122 (2001)
175. Lichtenegger, K., Reiterer, A., Stanzl-Tscheg, S., Frantzl, P.: J. Struct. Biol. **128**, 257–269 (1999)
176. Keplinger, T.: Versatile Strategies for the Functionalization of Wood Cell Walls and Their Characterization. PhD Thesis, ETH Zurich, Zurich (2016)
177. Gierlinger, N., Schwanninger, M.: Plant Physiol. **140**, 1246–1254 (2006)
178. Kulasinski, K., Salmén, L., Derome, D., Carmeliet, J.: Cellulose. **23**, 1629–1637 (2016)
179. Salmén, L., Burgert, I.: Holzforschung. **63**, 121–129 (2009)
180. Trtik, P., Dual, J., Keunecke, D., Mannes, D., Niemz, P., Stähli, P., Kaestner, A., Groso, A., Stampanoni, M.: J. Struct. Biol. **159**, 49–55 (2007)
181. Rowell, R.M.: Handbook of Wood Chemistry and Wood Composites, 2nd edn. CRC Press, Boca Raton (2013)
182. Kulasinski, K.: Physical and Mechanical Aspects of Moisture Adsorption in Wood Biopolymers Investigated with Atomistic Simulations. PhD Thesis, ETH Zurich, Zurich (2015)
183. Derome, D., Kulasinski, K., Zhang, C., Chen, M., Carmeliet, J.: Using modeling to understand the hygromechanical and hysteretic behavior of the S2 cell wall layer of wood. In: Geitmann, A., Gril, J. (eds.) Plant Biomechanics: From Structure to Function at Multiple Scales, pp. 247–269. Springer International Publishing AG, Cham (2018)
184. Geitmann, A., Gril, J.: Plant Biomechanics. From Structure to Function at Multiple Scales. Springer International Publishing AG, Cham (2018)
185. Saint-Venant, A.J.C.B.d.: Bull. Soc. Philomathique Paris. **1**, 1–11 (1854)
186. Boussinesq, J.V.: Application des potentiels à l'étude de l'équilibre et du mouvement des solides élastiques: Principalement au calcul des déformations et des pressions que produisent, dans ces solides, des efforts quelconques exercés sur une petite partie de leur surface ou de leur intérieur: Mémoire suivi de notes étendues sur divers points de physique, mathematique et d'analyse, vol. 4 [Application of the Study of Potentials of Balance and Movement of Elastic-Solids: Mainly the Calculation of Deformities and Pressure That Is Produced, in These Solids, Any Efforts Exerted on a Small Part of Their Surface or Their Interior: Thesis Followed My Extended Notes on Physics, Mathematics and Analysis]. Gauthier-Villars (1885)
187. Rayleigh, J.W.S.: Lond. Edinb. Dublin Philos. Mag. J. Sci. **11**, 283–291 (1906)
188. Timoshenko, S.P.: Z. Angew. Math. Phys. **62**, 198–209 (1913)
189. Lee, E.H.: J. Appl. Mech. **7**, A-129–A-138 (1940)
190. Hoppmann Jr., W.H.: J. Appl. Mech. **15**, 125–136 (1948)
191. Barnhart Jr., K.E., Goldsmith, W.: J. Appl. Mech. **24**, 440–446 (1957)
192. Goldsmith, W.: Impact: The Theory and Physical Behaviour of Colliding Solids. Edward Arnold, London (1960)
193. Crafton, P.A.: Shock and Vibration in Linear Systems. Harper and Brothers, New York (1961)
194. Kolsky, H.: Stress Waves in Solids. Dover Publications, New York (1963)
195. Johnson, W.: Impact Strength of Materials. Arnold, London (1972)
196. Graff, K.F.: Wave Motion in Elastic Solids. Dover, New York (1975)
197. Ewins, D.J.: Modal Testing: Theory, Practice and Application, vol. 15, 2nd edn. Letchworth: Research Studies Press, Hertfordshire (1984)
198. Weaver Jr., W., Timoshenko, S.P., Young, D.H.: Vibration Problems in Engineering, 5th edn. Wiley, New York (1990)
199. Clough, R.W., Penzien, J.: Dynamics of Structures. McGraw-Hill, New York (1993)
200. Meyers, M.A.: Dynamic Behavior of Materials. Wiley-Interscience Publication, New York (1994)
201. Abrate, S.: Impact on Composite Structures. Cambridge University Press, Cambridge, UK (2009)
202. Jones, N.: Structural Impact. Cambridge University Press, Cambridge, UK (2010)
203. Stronge, W.J.: Impact Mechanics. Cambridge University Press, Cambridge, UK (2010)
204. Evans, A.G.: Int. J. Fract. **10**, 251–259 (1974)
205. Evans, A.G., Johnson, H.: J. Mater. Sci. **10**, 214–222 (1975)
206. Nadeau, J.S., Bennett, R., Fuller, E.R.: J. Mater. Sci. **17**, 2831–2840 (1982)
207. Keeton, J.R.: Dynamic Properties of Small, Clear Specimens of Structural-Grade Timber Tech. Rep. R-573. Y-F011-05-04-003. U. S. Navy Civ. Eng. Lab., Port Hueneme (1968)
208. Madsen, B.: Duration of Load Tests for Dry Lumber in Bending Structural research series report № 3. University of British Columbia, Vancouver (1971)
209. Madsen, B.: Duration of Load Tests for Dry Lumber Subjected to Shear Structural research series report № 6. University of British Columbia, Vancouver (1972)
210. Madsen, B.: Duration of Load Tests for Wood in Tension Perpendicular to Grain Structural research series report № 7. University of British Columbia, Vancouver (1972)
211. Madsen, B.: Duration of Load Tests for Wet Lumber in Bending Structural research series report № 4. University of British Columbia, Vancouver (1972)
212. Madsen, B.: Can. J. Civ. Eng. **2**, 270–279 (1975)
213. Spencer, R.: Rate of loading effect in bending for Douglas-Fir lumber. In: Proceedings of 1st International Conference on Wood Fracture (1978)
214. Polocoșer, T.: On the Dynamics of Wood Impact. PhD Thesis, Institute for Organic and Wood-Based Materials, Technische Universität Braunschweig, Braunschweig (2017)
215. Elmendorf, A.: J. Frankl. Inst. **182**, 771–790 (1916)
216. Wilson, T.R.C.: Impact tests of wood. In: Proceedings of Symposium on Impact Testing of Materials, 25th Annual Meeting, pp. 55–73. American Society for Testing Materials, Philadelphia (1922)
217. Wilson, T.R.C.: Strength–Moisture Relations for Wood Technical Bulletin No. 282. Unites States Department of Agriculture, Washington, DC (1932)
218. Liska, J.A.: Effect of Rapid Loading on the Compressive and Flexural Strength of Wood USDA For. Serv. Report No. 1767. USDA For. Serv. For. Prod. Lab., Madison (1950)

219. Brokaw, M.P., Foster, G.W.: Effect of Rapid Loading and Duration of Stress on the Strength Properties of Wood Tested in Compression and Flexure USDA For. Prod. Lab. Report No. 1518. USDA For. Serv. For. Prod. Lab., Madison (1958)
220. James, W.L.: For. Prod. J. **12**, 253–260 (1962)
221. James, W.L.: Wood Sci. **1**, 15–22 (1968)
222. Ylinen, A.: Eur. J. Wood Prod. **21**, 173–176 (1963)
223. Ylinen, A.: Eur. J. Wood Prod. **23**, 193–196 (1965)
224. Bocchio, N., Ronca, P., van de Kuilen, J.W.G.: Impact loading tests on timber beams. In: Proceedings of Innovative Wooden Structures and Bridges, pp. 349–354. International Association for Bridge and Structural Engineering (2001)
225. Widmann, R., Steiger, R.: Impact loaded structural timber elements made from Swiss Grown Norway Spruce. In: Proceedings of CIB-W18 Meeting 42, Dübendorf, Switzerland. Universität Karlsruhe (2009) paper 42-6-2
226. Jacques, E., Lloyd, A., Braimah, A., Saatcioglu, M., Doudak, G., Abdelalim, O.: Can. J. Civ. Eng. **41**, 56–64 (2014)
227. Lacroix, D.N., Viau, C., Doudak, G.: Flexural response of glued laminated (Glulam) beams subjected to blast loads. In: Proceedings of World Conference on Timber Engineering (2014)
228. Gatchell, C.J., Jarvis, D.M.: Pendulum Impact Tests of Wooden and Steel Highway Guardrail Posts USDA For. Serv. Research Paper NE-311. USDA Northeastern For. Expr. Station For. Serv., Upper Darby (1974)
229. Coon, B.A., Reid, J.D., Rohde, J.R.: Dynamic Impact Testing of Guardrail Posts Embedded in Soil Midwest Roadside Safety Facility: MwRSF Research Report No. TRP-03-77-98. Federal Highway Administration (FHWA), Turner-Fairbank Highway Research Center, McLean (1999)
230. Kubojima, Y., Ohsaki, H., Kato, H., Tonosaki, M.: J. Wood Sci. **52**, 202–207 (2006)
231. Hatt, W.K., Turner, W.P.: The Purdue University Impact Machine, Proceedings, pp. 462–475. American Society for Testing and Materials (1906)
232. Siewert, T.A., Manahan, M.P.: Pendulum Impact Testing: A Century of Progress STP 1380. American Society for Testing and Materials, West Conshohocken (2000)
233. ISO-17281: Plastics – Determination of Fracture Toughness (G_{IC} and K_{IC}) at Moderately High Loading Rates (1 m/s). International Organization for Standardization, Geneva (2002)
234. ASTM-E-2248-12: Test Method for Impact Testing of Miniaturized Charpy V-Notch Specimens. American Society for Testing and Materials International, West Conshohocken (2013)
235. Gerhards, C.C.: Effects of Type of Testing Equipment and Specimen Size on Toughness of Wood USDA For. Serv. Research Paper FPL 97. USDA For. Serv. For. Prod. Lab., Madison (1968)
236. Gerhards, C.C.: Effect of Duration and Rate of Loading on Strength of Wood and Wood-Based Materials USDA For. Serv. Research Paper FPL 283. USDA For. Serv. For. Prod. Lab., Madison (1977)
237. Drow, J.T., Markwadt, L.J., Youngquist, W.G.: Results of Impact Tests to Compare the Pendulum Impact and Toughness Test Methods USDA For. Serv. Report No. 2109. USDA For. Serv. For. Prod. Lab., Madison (1958)
238. DIN-52189: Prüfung von Holz: Schlagbiegeversuch, Bestimmung der Bruchschlagarbeit. Beuth, Berlin (1981)
239. ISO-3348: Wood – Determination of Impact Bending Strength. International Organization for Standardization, Geneva (1975)
240. ASTM-D-143-09: Test Methods for Small Clear Specimens of Timber. American Society for Testing and Materials International, West Conshohocken (2009)
241. Kollmann, F.F.P., Kuenzi, E., Stamm, A.: Principles of Wood Science and Technology Wood Based Materials, vol. 2. Springer, Berlin (1975)
242. Molnár, S., Bezerédi, Á., Vörös, G., Pukánszky, B.: Int. J. Fract. **109**, 153–168 (2001)
243. Schonberg, W., Keer, L., Woo, T.: Int. J. Solids Struct. **23**, 871–896 (1987)
244. Chou, P.C., Flis, W.: AIAA J. **15**, 455–456 (1977)
245. Christoforou, A.P., Yigit, A.S.: J. Sound Vib. **217**, 563–578 (1998)
246. Mindess, S., Madsen, B.: Mater. Struct. **19**, 49–53 (1986)
247. Sukontasukkul, P., Lam, F., Mindess, S.: Mater. Struct. **33**, 445–449 (2000)
248. Doyle, J.: The Hardness of Wood. PhD Thesis, University of Canterbury, Christchurch (1980)
249. Hertz, H.: J. Reine Angew. Math. **92**, 156–171 (1882)
250. Koehler, A.: Causes of Brashness in Wood USDA For. Serv. Technical Bulletin No. 342. United States Department of Agriculture, Washington, DC (1933)
251. Kollmann, F.F.P.: Preuss. Holzforschungsinst. **17**, 17–30 (1937)
252. Pettifor, C.B.: Aircr. Eng. Aerosp. Technol. **14**, 248–250 (1942)
253. Kloot, N.H.: Aust. J. Appl. Sci. **5**, 183–186 (1954)
254. Kollmann, F.F.P., Krech, H.: Holz Roh Werkst. **18**, 41–54 (1960)
255. Keith, C.T.: For. Prod. J. **14**, 285–289 (1964)
256. Keith, C.T.: J. Mater. **1**, 759–769 (1966)
257. Goens, E.: Ann. Phys. **11**, 649–678 (1931)
258. Venzi, S., Priest, A.H., May, M.J.: Influence of inertial load in instrumented impact tests. In: Impact Testing of Metals, ASTM STP 466, pp. 165–180. American Society of Testing and Materials International (1970)
259. Banthia, N., Mindess, S., Bentur, A., Pigeon, M.: Exp. Mech. **29**, 63–69 (1989)
260. Lagerhjelm, P.: Versuche zur Bestimmung der Dichtheit, Gleichartigkeit, Elasticität, Schmiedbarkeit und Stärke des gewalzten und geschmiedeten Stabeisens. Aus dem Schwedischen übersetzt von Dr. I. W. Pfaff [Experimental Determination of the Density, Homogeneity, Elasticity, Forgeability and Ultimate Strength of Rolled and Forged Rods. Translated from Swedish by Dr. I.W. Pfaff, 1889]. Johann Leonhard Schrag, Nürnberg (1828)
261. Hearmon, R.F.S.: Br. J. Appl. Phys. **9**, 381–388 (1958)
262. Hearmon, R.F.S.: Proc. Phys. Soc. **58**, 78–92 (1976)
263. Bell, E.R., Peck, E.C., Krueger, N.T.: Modulus of Elasticity of Wood Determined by Dynamic Methods USDA For. Serv. Report № 1977. USDA For. Serv. For. Prod. Lab., Madison (1954)
264. Burmester, A.: Holz Roh Werkst. **23**, 227–236 (1965)
265. Hardie, D., Parkins, R.N.: J. Phys. D. Appl. Phys. **2**, 77–85 (1968)
266. Kaiserlik, J.H.: Nondestructive Testing Methods to Predict Effect on Degradation of Wood: A Critical Assessment USDA For. Serv. Report No. FSGTR-FPL-19. USDA For. Serv. For. Prod. Lab., Madison (1978)
267. Yoshihara, H.: Holzforschung. **67**, 941–948 (2013)
268. Yoshihara, H., Yoshinobu, M.: Holzforschung. **69**, 493–499 (2015)
269. ISO-12680-1: Methods of Test for Refractory Products – Part 1: Determination of Dynamic Young's Modulus (MOE) by Impulse Excitation of Vibration. International Organization for Standardization, Geneva (2005)
270. ASTM-E-1876-09: Test Method for Dynamic Young's Modulus, Shear Modulus, and Poisson's Ratio by Impulse Excitation of Vibration. American Society for Testing and Materials International, West Conshohocken (2009)
271. ASTM-D-6874-12: Test Methods for Nondestructive Evaluation of Wood-Based Flexural Members Using Transverse Vibration. American Society for Testing and Materials, West Conshohocken (2012)
272. Jansson, B.: Impact Loading of Timber Beams. Masters Thesis, University of British Columbia, Vancouver (1992)
273. Wood, L.W.: Relation of Strength of Wood to Duration of Load, Information Reviewed and Reaffirmed from Original 1951 Report

USDA For. Serv. Report No. 1916. USDA For. Serv. For. Prod. Lab., Madison (1960)
274. Sekhar, A.C.: Eur. J. Wood Prod. **24**, 559–563 (1966)
275. Sekhar, A.C., Nagar, B.N.: Eur. J. Wood Prod. **23**, 3–6 (1965)
276. Pearson, R.G.: Holzforschung. **26**, 153–158 (1972)
277. Glos, P., Heimeshoff, B., Kelletshofer, W.: Holz Roh Werkst. **45**, 243–249 (1987)
278. State of the Art Report on Duration of Load Research for Lumber in North America: In: Karacabeyli, E., Soltis, L.A. (eds.) Proceedings of International Timber Engineering Conference. TRADA (1991)
279. Leijten, A.J.M.: Literature review of impact strength of timber and joints. In: Proceedings of World Conference on Timber Engineering (2000)
280. Buchar, J., Adamík, V.: Wood strength evaluation under impact loading. In: Proceedings of 39th International Conference on Experimental Stress Analysis (2001)
281. Botting, J.K.: Development of an FRP Reinforced Hardwood Glulam Guardrail. Masters Thesis, The University of Maine, Orono (2003)
282. Leijten, A.J.M.: Heron. **49**, 349–359 (2004)
283. Gutkowski, R.M., Shigidi, A., Peterson, M.: Dynamic Impact Load Tests of a Bridge Guardrail System MPC Report No. 07-188. Mountain-Plains Consortium, Fargo (2007)
284. Turnbull-Grimes, C., Charlie, W.A., Gutkowski, R.M., Balogh, J.: Bus-Stop Shelters – Improved Safety Report for North Dakota State University. Colorado State University, Fort Collins (2010)
285. Benthien, J.T., Georg, H., Maikowski, S., Ohlmeyer, M.: Landbauforsch. Appl. Agric. For. Res. **62**, 255–262 (2012)

Prof. Dr.-Ing.habil. Dr.h.c. Peter Niemz (Sects. 9.1–9.3, 9.5) studied at the Faculty of Mechanical Engineering of the TU Dresden. From 1972 onward he worked at the Institute of Wood Technology Dresden (IHD) and at the TU Dresden. From 1993 to 1996 he served as a Full Professor at the Universidad Austral de Chile in Valdivia before joining the Swiss Federal Institute of Technology (ETH Zurich) in 1997, where he has served as a Professor of Wood Physics since 2002. Until his retirement in 2015.

Dr. Walter Sonderegger (Sects. 9.1–9.3, 9.5) studied Forest Science at ETH Zurich. He worked as scientific assistant at the chair of Wood Science and in the Wood Physics Group at ETH Zurich, then at the Paul Scherrer Institute, Villigen (NIAG-Group) and at the chair of Wood Material Science (ETH Zurich and EMPA, Dübendorf). Now he is staff member of the company Swiss Wood Solutions, Altdorf, Switzerland.

Prof. Dr. Per Johan Gustafsson (1952–2020) (Sect. 9.4) obtained his PhD in Building Materials in 1985, with a thesis on the fracture behavior of non-yielding (softening) materials like concrete. Early after his PhD, he joined the Division of Structural Mechanics, where he later was promoted as Associate professor (1991) and Professor (2001). His research covered both basic and applied work and related to analysis and testing of strength and fracture. His work covered products, joints, and structural elements made of concrete, timber, and wood-based materials, adhesives, paper, fluff pulp, and corrugated board.

Prof. Dr. Bohumil Kasal (Sect. 9.6), PhD (Oregon State University), PE, is a Professor of Organic Construction Materials at Carolo-Wilhelmina University in Braunschweig, Germany and Director of the Fraunhofer Institute for Wood Research, WKI (2010-present). He holds professorships at the Czech Technical University in Prague and the University of Primorska, Slovenia. He held the Bernard and Henrietta Hankin Chair of Residential Building Construction at Penn State University (2005–2010) and was a Professor at North Carolina State University between 1993 and 2005. His research has been focused on timber structures under dynamic loads, in situ assessment of timber, and wood mechanics. Kasal is a Fulbright Scholar.

Dr. Tiberiu Polocoşer (Sect. 9.6) recently completed his doctoral degree (Dr.-Ing.) on the subject of the dynamic material properties of wood. The doctoral work emphasized the intermediate strain rates expected for structures under wind, seismic, and low-velocity impact loads. His interests are in structural dynamics behavior and structural mechanics.